POLITECNICO DI TORINO

DEPARTEMENT OF AEROSPACE AND MECHANICAL ENGINEERING

Master's Degree in Space Engineering

Escape maneuvers from Sun-Earth L_2 Lagrangian Point with electric propulsion

Supervisor:
Prof. Lorenzo Casalino

Candidate:
Ludovico Livrari
Matr. 267721

ACADEMIC YEAR 2020/2021

"Remember to look up at the stars
and not down at your feet.
Try to make sense of what you see
and wonder about
what makes the universe exist.
Be curious.
And however difficult life may seem,
there is always something you can do
and succeed at.
It matters that you don't just give up."

Stephen Hawking

Contents

List of Tables

List of Figures

Acknowlodgments

I would like to express my deepest and sincere gratitude to my supervisor, Prof. Lorenzo Casalino, for his incredible passion, and his continued support, which was essential for the success of the work.
I'm extremely grateful not only for what he did during the development of the thesis but also for all the stimulus he gave me during the courses and which will allow me to better face the world outside the Politecnico.

I'm extremely grateful to mum and my dad that always supported me in all the possible ways during this difficult chapter of my life.
I'm deeply indebted to my sister that that has always encouraged and endured me. Without them this achievement would not have been possible.

A special thanks to Andrea, Samuel, and Giorgio, who from strangers have become the friends I am most attached to, thanks for all the good times, the laughter, and the travels we have done in these five years, without you it would have been everything much more gray. I hope the future holds us many beautiful surprises always together.

Many thanks to Giovanni who adopted me during all the exam sessions from the third year onwards; to all the laughter, the discussions, and the demonstrations that did not come out on the first try. Thank you for encouraging me in the hardest moments and for always making me smile, in you I have not only found a friend but a brother.

Introduction

In recent years interest in space exploration is growing fast. The synergistic commitment between many nations is allowing an impressing growth in terms of technology, which expands the boundaries of what humankind can achieve.
With the ISS, humans have set a fundamental step for the understanding and study of how the human body reacts to low gravity and therefore has set an important step towards the possibility of long period mission in space.
A new space run has begun to make space more accessible for all the people, thanks to the development of suborbital flights, but also less expensive, thanks to the progress in terms of rocket reusable first stage. Furthermore, with NASA's mission Artemis, what seemed science fiction a few years ago is now becoming reality. A new human outpost will be settled on the Moon and a Lunar Orbital Platform-Gateway (LOP-G) will be placed on L_2 of the Moon-Earth system.
The interest in L_2 has therefore increased again, not only in the Earth-Moon system but also in the Sun-Earth system.
The second Lagrangian point is expected to be the most suitable point where to place the new Comet Interceptor mission. This mission is an ESA-JAXA collaboration, that aims to leave a spacecraft at L_2 of Sun-Earth system, where it will wait for a suitable target. Once the target will be found, then the spacecraft will travel to the objective until the three modules, which composed the Comet Interceptor spacecraft, separate a few weeks prior to intercepting the comet. This mission is very ambitious and will help to explore how comet-like bodies form and evolve in other star systems.
The study of evasion maneuver from L_2 became fundamental for future missions, L_2 is also ideal for astronomy because a spacecraft is close enough to readily communicate with Earth; can keep Sun, Earth and Moon behind the spacecraft for solar power and provides a clear view of deep space. A small-sat could be left at the Lagrangian point as a piggyback of a larger primary spacecraft and then can perform the evasion maneuver that will be investigated in this thesis.
This thesis aims to describe the numerical and physical aspects of the optimization of the Escape maneuver from the Sun-Earth collinear Lagrangian point L_2. The method utilized for the optimization process is an indirect method, based on the Optimal Control Theory, that aims to the maximization of the payload fraction through the minimization of the propellant consumption.
At the beginning an overview of past and future mission from L_2 will be carried out. Secondly, a brief outline of orbital mechanics and space propulsion will be given, in order to furnish all the information necessary for a full understanding of the problem. Thirdly, the general characteristics of indirect methods of space trajectory optimization are described, with a focus on the Optimal Control Theory (OCT). Then, the model adopted will be introduced, with the presentation of the main perturbations present and the specification of the boundary conditions of the problem considered. In the end, the results are reported.

Chapter 1

Mission from L_2 Sun-Earth system

There are five special points where a small mass can orbit in a constant pattern with two lager masses, these points are known as Lagrange Points. The Lagrange Points are ≪Positions where the gravitational pull of two large masses precisely equals the centripetal force required for a small object to move with them≫. This is what stated Joseph-Louis Lagrange in his *Essai sur le Problème des Trois Corps, 1772* where, for the first time, the solution of the "*Three body problem*" was found.
Lagrange was an Italian astronomer and mathematician, who was later naturalized French. Of the five Lagrange points, is possible to identify two stable points, known as Equilateral points, and three unstable points, known as Collinear points. The mathematical problem will be discussed later in Chapter 2. Between all the Lagrangian points, one is extremely interesting, and is the L_2 point. This point is situated 1.5 million kilometres directly 'behind' the Earth as viewed from the Sun. It is about four times further away from the Earth than the Moon and orbits around the Sun at the same rate as the Earth. Considering a spacecraft placed in this point, it is more distant from Sun than Earth and so its orbital velocity should be lower than Earth's one. Despite that, the extra pull of our planet added to the Sun's one, allows the spacecraft to move faster and so permit to maintain the alignment between Sun, Earth and L_2. This point is ideal for the observation of the large universe and for astronomy in general. A spacecraft ubicated in this point can readily communicate with Earth, can provide a clear view of deep space and can keep Earth, Moon and Sun behind itself. This position is also very favourable because a spacecraft in this position would not have to make constant orbits around Earth, and thus it is not affected by the heat up and cool down caused by the passing in and out of the Earth's shadow which distort its view and therefore provides a much more stable viewpoint.
In this chapter a brief overview of some missions that occupy L_2 point is given. Initially past mission will be considered, secondly present and future mission will be exhibited.

1.1 Past missions

Chang'e 2

Chang'e 2 is a CNSA mission that was launched in 2010. This probe belongs to the first phase of the Chinese Lunar Exploration Program. It conducted research from a 100 km high lunar orbit. After the success in its primary objective, the probe was moved to the L_2 Earth-Sun Lagrangian point in order to test its tracking and control network. In 2012 it has been decided to extend its mission, redirecting the probe toward the asteroid 4179 Toutatis. The probe is expected to return close to Earth in 2029 after the contact with the probe was lost in 2014 due to distance.

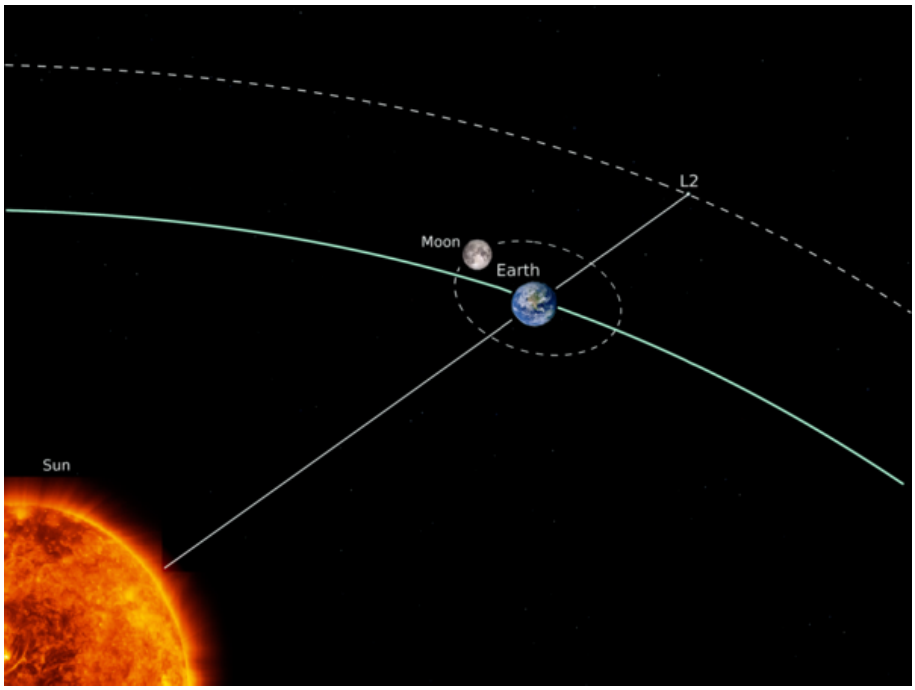

Figure 1.1: Graphic representation of the position of L_2 of Sun-Earth system. (Not in scale)

Herschel Space Observatory

The Herschel Space Observatory was a space observatory built and operated by the European Space Agency (ESA). It was the largest infra-red telescope ever launched and it operated from 2009 to 2013. L_2 Earth-Sun Lagrangian point was reached two months later than its insertion in orbit in May 2009. The life of the mission was governed by the amount of coolant available for its instrument. Once the coolant has run out the instruments would stop functioning in the correct way.
The main task for this mission was to investigate about life-forming molecules, such as water, form into star-forming clouds. In 2013, one year later than the expected, Herschel probe run out of liquid helium, that was used to cool the instruments. In order to place the probe on a known trajectory, the probe was placed into an heliocentric orbit where it would not encounter Earth for at least several hundred years.

Wilkinson Microwave Anisotropy Probe (WMAP)

Wilkinson Microwave Anisotropy Probe was a spacecraft operated by NASA. Its main purpose was to measure temperature differences across the sky in the cosmic microwave background (CMB). The duration of this mission was of about 9 years, its last signal was transmitted on August 2010. On October 2010 the spacecraft was placed into an heliocentric graveyard orbit. During its 9 years long measurements, WMAP has obtained lots of important results like the oval images that present the CMB temperature differences distribution. Thanks the observations through the telescope during the mission these results are obtained by the WMAP team. The results are a picture of the universe around 375,000 years after the Big Bang, that happened about 13.8 billion years ago.

Planck

Planck was a space observatory operated by ESA. Its main purpose was to map the anisotropies of the cosmic microwave background (CMB) at microwave and infra-red fre-

quencies. This mission is an improvement of the results obtained by WMAP mission. It searched for information about early Universe and the origin of cosmic structure. Most of the data obtained are defined as *the most precise measurements*, thanks the very high sensitivity and small angular resolution of the payloads, of several key cosmological parameters, like the average density of ordinary matter and dark matter in the universe and also the age of universe. On March 2013 was released the first all-sky map of the cosmic microwave background.
The mission last three years more than the expected. On October 2013, at the end of the mission, the probe was put into an heliocentric orbit and passivated in order to minimize the probability of endangering any future missions.

1.2 Present missions

Gaia

Gaia is a space observatory of the European Space Agency (ESA). It was launched in 2013 and is expected it will operate since 2022, it is placed into a Lissajous orbit around L_2 of the Sun-Earth system. This orbit permit Gaia to avoid almost entirely to fall into Earth's shadow. The main objective of this mission is to create the most precise 3D space catalogue ever made of the Milky Way. This is possible thanks to the incredibly precision with which Gaia can measure position, distances and motion of stars but also planets, comets and asteroids. The extreme precision with which the measurements are made are linked with the fact that Gaia will monitor each of its objects for more than 70 times during the first 5 year of the mission and it will continue doing so also after this period. In addition Gaia mission is expected to detect Exoplanets beyond the solar system with the size similar to Jupiter and also thousands of new asteroids.

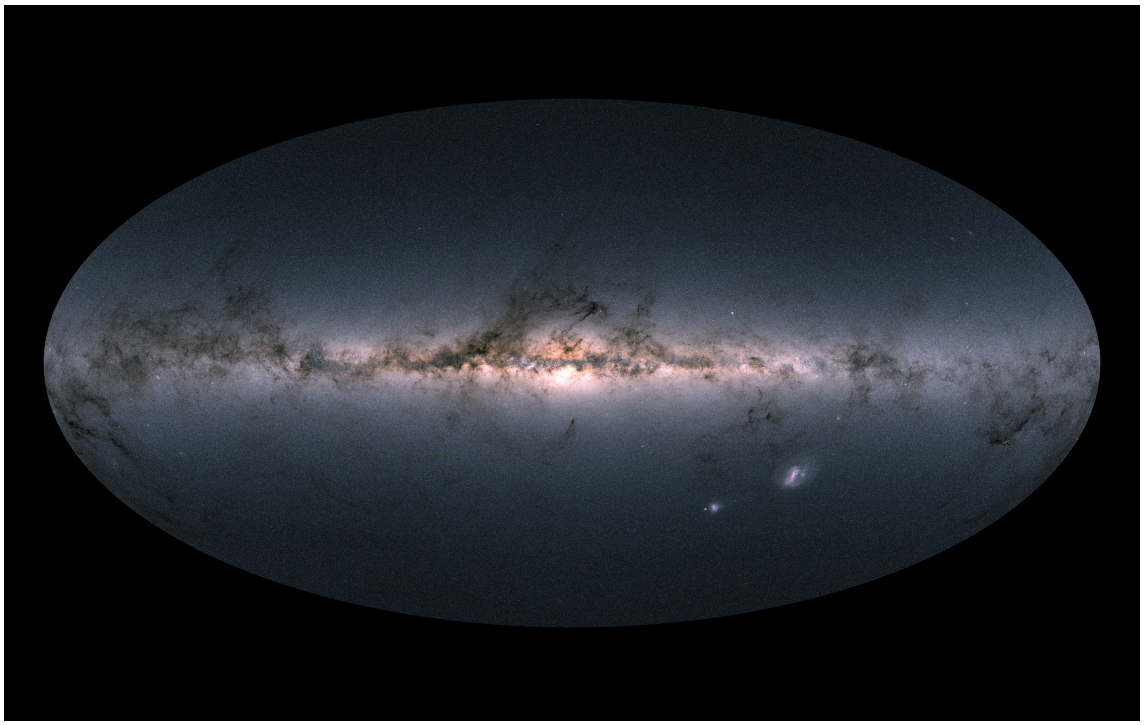

Figure 1.2: Gaia's map of the sky by star density

1.3 Future missions

Comet Interceptor

Comet Interceptor is a robotic spacecraft mission led by the European Space Agency in collaboration with JAXA. The spacecraft will be placed in L_2 Sun-Earth and will wait there for three years for a long-period comet to flyby. Its mission has the goal of visiting an interstellar object or a distant comet making its its first journey into the inner solar system. This mission has no a determined target yet, the planned spacecraft is meant to be as a sentinel in space, awaiting a rendezvous opportunity.
In 2017 the so called asteroid 'Oumuamua was discovered. This object was classified as the first interstellar asteroids known, before 'Oumuamua their existence were only on the theoretical level. Now, the 1I/2017 U1 asteroid, is too far and too fast for any current spacecraft to ever reach it and therefore a great occasion to investigate about interstellar objects was lost. Considering that, the only way to encounter in a dynamic way new comets or interstellar objects is to discover them inbound with enough warning to direct a spacecraft to them. The main problem is that the time between the discovery, perihelion, departure from the inner solar system is in terms of months or a year and therefore there is no time to prepare a launch of a spacecraft. From this comes the idea of Comet Interceptor: a spacecraft that orbits around L_2 of the Sun-Earth system, ready to perform the rendezvous of a comet. From 2023, with the Large Synoptic Survey Telescope, that is now under construction in Chile, will be possible to discover Long Period Comets much further away and provide a true revolution in the understanding of their populations, making this mission possible.
Comet Interceptor will target a comet visiting the inner Solar System for the first time, maybe coming from the vast Oort cloud. The Oort cloud is a theoretical cloud, hypothesized for the first time from the Dutch astronomer Jan Oort, that is thought to surround the outer reaches of the Sun's realm. The comet will contain material that has not experienced much processing since the dawn of the Sun and planets. The mission will therefore offer new information about the evolution of comets and as they migrate towards the centre of the Solar System from the periphery. Another example of a potential target is an interstellar interloper coming from another star system, like 'Oumuamua as introduced before.
Comet Interceptor will be launched with ARIEL spacecraft, it also belongs to ESA's mission, in 2029 and will be delivered to the Second Lagrangian point of Sun-Earth system where it will wait for the spot of a notable target. Once the target has been found, a few

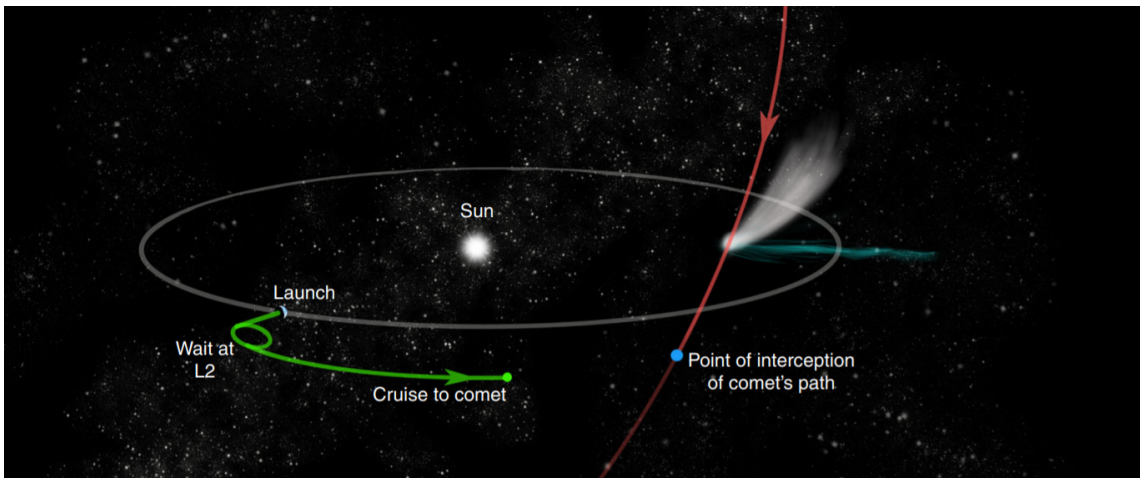

Figure 1.3: Sketch of mission phases of Comet Interceptor mission

weeks or days before the flyby, the spacecraft will release two small sub-spacecraft. For very active comets, separation will be earlier in order to optimize the separation of the spacecraft elements, whereas for low activity targets separation will occur only a few days before the encounter takes place. The spacecrafts will not land on its destination, instead they will conduct a fast flyby, observing its target. The main craft will pass between the Sun and the Comet, far from the major dust hazard, and will be used as a communication relay and will do remote sensing. The other two small spacecrafts will travel closer to collect more detailed data without risking to damage the main vehicle. The incoming data from the three spacecrafts will allow to create a 3D profile of the object and characterize its surface, composition, shape and structure.
The Launch mass of the mission is approximately 850 Kg, in this thesis the same mass will be considered.

James Webb Space Telescope (JWST)

The James Webb Space Telescope is a space telescope developed under the collaboration of NASA-ESA-CSA. This telescope is planned to succeed the Hubble Space Telescope as main astrophysics mission lead by NASA.
The Webb telescope will be placed near the second Lagrange point L_2 of the Sun-Earth system, it will circle around this point into a Halo orbit, inclined with respect to the ecliptic. This orbit, and thus position, will provide a much more stable viewpoint because the shadow of Earth will be avoided and so the distortion caused by the transition from a hot case to a cold case are bypassed. Due to the instability of this Lagrangian point, station keeping maneuvers are required. The main objective of James Webb Telescope is the investigation about the origins of the universe by observing infra-red light from young galaxy and possibly first stars. It will allow a better understandings of how stars and planetary systems form. In order to have an unprecedent view of the universe in the mid-infrared wavelengths, it will operates a very low temperatures (-230 $^{\circ}C$). The Webb telescope is required to work for a minimum of five years, but it is planned for ten.
The launch of JWST is expected to be on 31 October 2021.

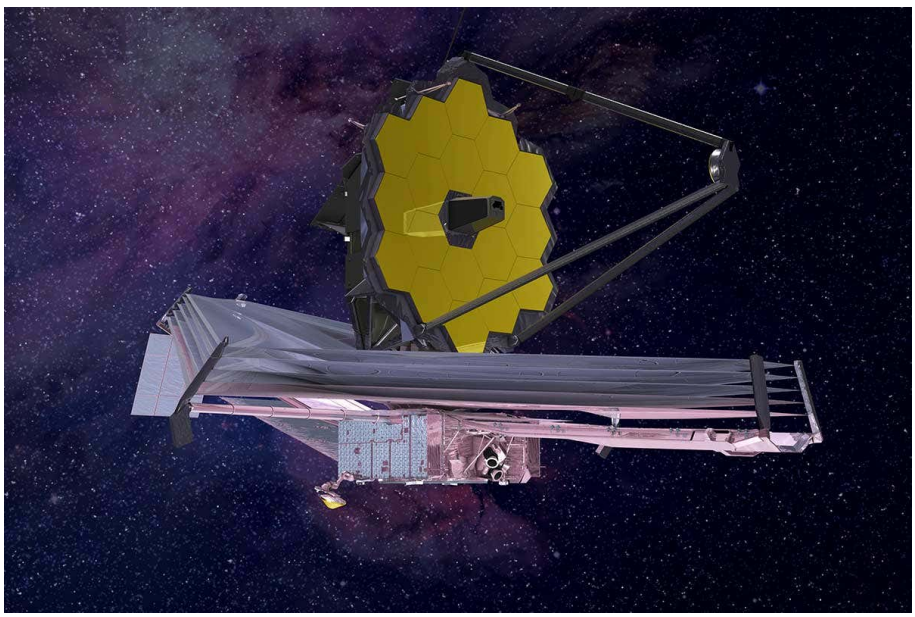

Figure 1.4: 3D render of James Webb Telescope

Advanced Telescope for High-ENergy Astrophysics (ATHENA)

Athena is an X-ray observatory mission operated by ESA. This mission belongs to its Cosmic Vision Program. Its main goal is to map hot gas structures, determine their physical properties and look for supermassive black holes. This mission is expected to be launched in the early 2030s, a large amplitude Halo orbit around L_2 is the chosen orbit where the probe will be placed. This orbit allow a very stable thermal environment but also a good sky visibility and mostly, a high observing efficiency. Athena's mission is expected to last more than 4 year.

PLAnetary Transits and Oscillations of stars (PLATO)

PLATO is a space telescope which is under the development of ESA. The main goal of this mission is to discover and characterize rocky extrasolar planets around yellow and red dwarf stars or subgiant stars. Obviously the main target of the research are Earth-like planets situated in the habitable zone around Sun-like stars. If these conditions are satisfied, is possible that water can exist in liquid state. A secondary goal is to study stellar oscillation in order to measure stellar masses and to define the characteristic of the planet host star, including its age. The launch is planned for 2026.

Euclid

Euclid is a space telescope under development from ESA. The main goal of the mission is to improve the knowledge about the dark matter and the dark energy by measuring the acceleration of the universe. This spacecraft is expected to be placed on a Lissajous orbit of large amplitude, of about 1 million kilometres, around thee Sun-Earth L_2 point. During the mission Euclid will observe almost one third of the sky, with a special focus on the extragalactic sky. The launch is expected to be on the window between July and December 2022 and is expected to last at least 6 years.

Chapter 2

Fundamentals of Orbital Mechanics

Before dealing with the main topic of the thesis is important to give an overview of the basis of space flight mechanics. In this chapter, in fact, are introduced the basics knowledge and the physical aspect of the space flight mechanics.
The main topics covered will be the Two-Body Problem, the Three-Body Circular Problem with a focus on the Lagrangian points and then an overview of interplanetary mission will be given with a focus on the evasion maneuver.

2.1 Two-Body Problem - 2BP

As a starting point of every orbital mechanics problem, there is the Two-Body Problem. The 2BP describes the motion between two bodies that interact one to each other only thanks to the gravitational force.
The gravitational force is a central and attractive interaction, indirectly proportional to the square of the distance of the two bodies and proportional to the product of the two masses.

$$\boldsymbol{F} = G\frac{Mm}{r^2}\frac{\boldsymbol{r}}{r} \tag{2.1}$$

Where $G = 6.67 \cdot 10^{-11}\,\frac{m^3}{kg\,s}$ is the gravitational constant and $\boldsymbol{r}$ is the distance vector from the mass of the primary body M and the mass of the secondary body m.
It is possible to simplify this problem by the introduction of five hypotheses, this new formulation is known as the Restricted Two-Body Problem (R2BP). It is possible to apply the R2BP where one of the mass is negligible compared to the other one, to systems like Earth-Satellite or Sun-Earth. R2BP's hypothesis can be summarized as follows:

1. M $\gg$ m
2. Gravitational forces are the only present in this system
3. Spherical Symmetry of the mass distribution
4. Homogeneity of the mass distribution
5. Punctiform bodies, masses are concentrated in the centers of mass of the bodies

Thanks to these hypotheses, is possible to obtain the equation of motion:

$$\ddot{\boldsymbol{r}} = -\frac{\mu}{r^2}\frac{\boldsymbol{r}}{r} \tag{2.2}$$

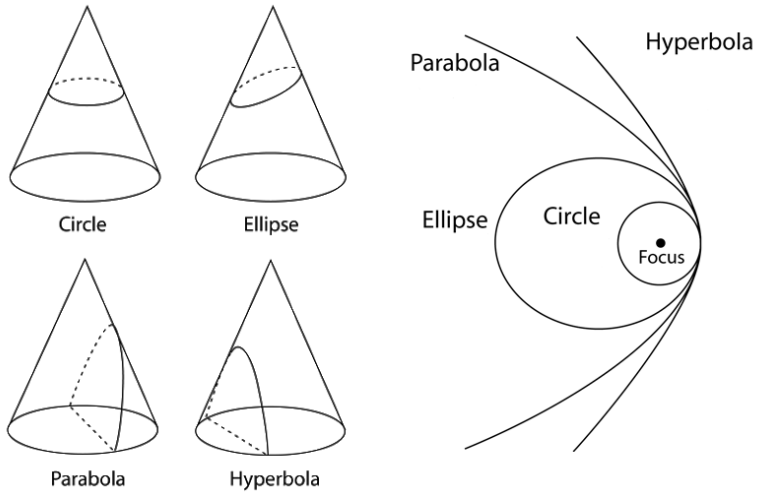

Figure 2.1: Conic section

where $\mu = GM$ is given by the product between the gravitational constant and the bigger mass and is the gravitational parameter of the principal body. Solving this equation is possible to obtain the equation that expresses the distance between the two bodies:

$$r = \frac{\frac{h^2}{\mu}}{1 + e\,cos(\nu)} \tag{2.3}$$

where e is the eccentricity and ν is the true anomaly, these quantities will be defined and explained in the next section.
Eq. (2.3) is important because generates trajectories that follow the shape of conic sections, that are represented in Figure 2.1.
It is also important to highlight that some physical quantities are constant during all the motion, if only gravitational forces are present, and so considering R2BP.
The constant are two:

- Angular Momentum
$$\boldsymbol{h} = \boldsymbol{r} \wedge \dot{\boldsymbol{r}} \tag{2.4}$$
Since the angular momentum is constant both in module and orientation, the motion followed by the smaller body around the primary one in the R2BP is a planar trajectory.

- Mechanical Energy
$$E = \frac{v^2}{2} - \frac{\mu}{r} \tag{2.5}$$
where the first term is the kinetic energy while the second term is the potential energy.

2.2 Orbital parameters

In this section, six orbital parameters will be introduced. The orbital elements introduced later are only one of the possibilities and are called classical orbital parameters.
These parameters are extremely important because, thanks to them, is possible to identify univocally the position of a body in the R2BP. The orbital elements are the following:

1. Eccentricity **e**
   Is connected to the form of the orbit. In particular, it can be demonstrated through the analysis of the conic sections' geometry. Figure 2.1 describes the families of trajectories divided by the value of their eccentricity. In fact, if $e = 0$ the trajectory is circular, if $0 < e < 1$ the trajectory is elliptic, if $e = 1$ the trajectory is parabolic and finally if $e > 0$ the trajectory is hyperbolic.

2. Major Semi-axis **a**
   Is connected to the dimension of the orbit and the energy of the orbit. It can be demonstrated that, unifying the energetic analysis to the geometric one:
   $$E = -\frac{\mu}{2a} \tag{2.6}$$

3. Right Ascension of Ascending Node **Ω**
   The RAAN gives the position of the ascending node of the trajectory that is the point where the secondary body enters the region of the positive values of the coordinate z.

4. Argument of Periapsis **ω**
   Defines the position of the periapsis, which is the closest point of the trajectory to the principal body.

5. Inclination **i**
   It is the inclination of the orbit's perifocal plane, with respect to a fixed direction.

6. True Anomaly **ν**
   Is the angular position of the secondary body, along the orbit, from the periapsis. In the R2BP, this is the only variable element, while all the others are constant.

In Figure 2.2 are shown the classical orbital elements, the pic allows a better understanding of the orbital parameters, this specific case is defined for a satellite orbiting around Earth. Despite that, their definition can be broadened to any secondary body in revolution around a primary one much bigger. Obviously these parameters are not the only can be used but are only one of the choices possible.
Depending on the trajectory assumed for the mission, the orbital parameters will change, in Table 2.1 is possible to understand better the relationship between eccentricity, semi-major axis, energy, and the form of the orbit.

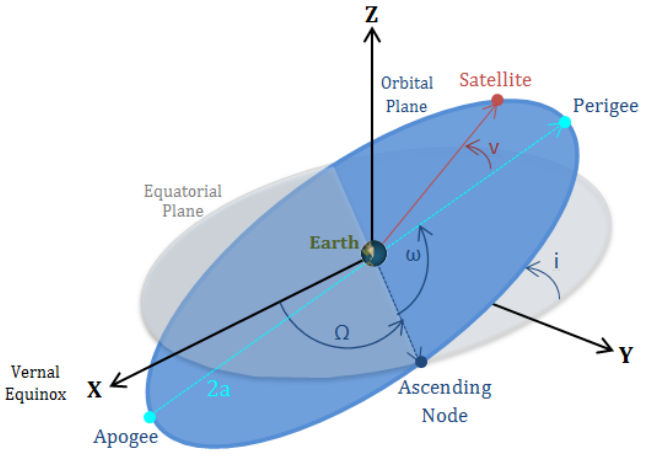

Figure 2.2: Classical orbital elements

Trajectory	Eccentricity	Semi Major Axis	Energy	V_∞
Circular	e = 0	a > 0	E < 0	
Elliptical	0 < e < 1	a > 0	E < 0	
Parabolic	e = 1	a $\longrightarrow \infty$	E = 0	$V_\infty = 0$
Hyperbolical	e > 1	a < 0	E > 0	$V_\infty > 0$

Table 2.1: Features of different kind of orbits and trajectories

2.3 Restricted Three-Body Circular Problem - R3BCP

To explain what is the L_2 point, that is the initial point of the trajectory studied in this thesis, is crucial to define what is a Lagrangian point. Thus, is necessary to introduce the Restricted Three-Body Circular Problem. This is based on two main hypotheses:

- Three bodies: two are the principal bodies, while one is negligible in terms of mass. The third body, the one who has a negligible mass, does not affect the other two with its gravitational interaction.
- Circularity: the principal bodies are characterized by circular orbits around the center of mass of the system.

Various systems can be modelled and studied under the hypotheses of R3BCP, for example, the Moon-Earth-Spacecraft system or, as in the case of study, the Sun-Earth-Spacecraft system.
Two constants can be defined:

$$M = m_1 m_2$$

$$\mu = \frac{m_2}{M}$$

The positions of the principal bodies, with respect to the center of mass of the system, can be easily derived:

$$m_1 = \begin{bmatrix} -\mu\, r_{12} \\ 0 \\ 0 \end{bmatrix} \tag{2.7}$$

$$m_2 = \begin{bmatrix} (1-\mu)\, r_{12} \\ 0 \\ 0 \end{bmatrix} \tag{2.8}$$

considering as reference scheme Figure 2.3.
The position of the secondary body, with respect to the primary ones, can be defined as:

$$\boldsymbol{r_1} = \begin{bmatrix} (x\ +\ \mu) r_{12} \\ y \\ z \end{bmatrix} \tag{2.9}$$

$$\boldsymbol{r_2} = \begin{bmatrix} (x\ -(1\ -\ \mu) r_{12} \\ y \\ z \end{bmatrix} \tag{2.10}$$

The reference frame is not inertial but is a rotating frame. The system rotate with the angular velocity ω that is defined as follow:

$$\omega = \sqrt{\frac{GM^3}{r_{12}}} \tag{2.11}$$

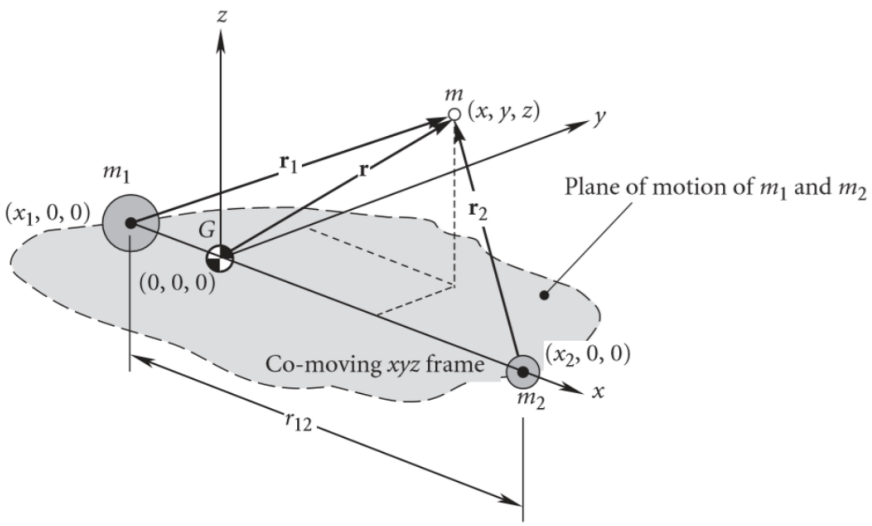

Figure 2.3: Three Body Problem (TBP) frame

Writing down the vectorial form of the equations of motion:

$$\ddot{\boldsymbol{r}} + \boldsymbol{\omega} \wedge (\boldsymbol{\omega} \wedge \boldsymbol{r}) + 2\boldsymbol{\omega} \wedge \dot{\boldsymbol{r}} = \frac{1}{m}(\boldsymbol{F_1} + \boldsymbol{F_2}) \tag{2.12}$$

where:

$$\boldsymbol{F_1} = -G\frac{(1-\mu)Mm}{{r_1}^3}\boldsymbol{r_1} \tag{2.13}$$

$$\boldsymbol{F_2} = -G\frac{\mu Mm}{{r_2}^3}\boldsymbol{r_2} \tag{2.14}$$

Expliciting the components along the three coordinates, the Equation of Motion can be written as:

$$\ddot{x} - \omega^2 x - 2\omega\dot{y} = -GM\frac{1-\mu}{{r_1}^3}(x + \mu r_{12}) - GM\frac{\mu}{{r_2}^3}[x + (1-\mu)r_{12}] \tag{2.15}$$

$$\ddot{y} - \omega^2 y - 2\omega\dot{x} = -GM\frac{1-\mu}{{r_1}^3}y - GM\frac{\mu}{{r_2}^3}y \tag{2.16}$$

$$\ddot{z} = -GM\frac{1-\mu}{{r_1}^3}z - GM\frac{\mu}{{r_2}^3}z \tag{2.17}$$

motion equation can be also written in a dimensionless form where, some substitution has to be done. In fact is possible to write:

$$\boldsymbol{\rho} = \frac{\boldsymbol{r}}{r_{12}} \quad \rightarrow \quad \xi = \frac{x}{r_{12}} \quad \eta = \frac{y}{r_{12}} \quad \zeta = \frac{z}{r_{12}} \tag{2.18}$$

$$\tau = t\omega \quad \rightarrow \quad \frac{d}{dt} = \omega\frac{d}{d\tau} \tag{2.19}$$

Substituting the previous relations into the Eq. (2.15) Eq. (2.16) Eq. (2.17) is possible to obtain:

$$\xi'' - \xi - 2\eta' = -(1-\mu)\frac{\xi + \mu}{{\rho_1}^3} - \mu\frac{\xi - (1-\mu)}{{\rho_2}^3} \tag{2.20}$$

$$\eta'' - \eta - 2\xi' = -(1-\mu)\frac{\eta}{{\rho_1}^3} - \mu\frac{\eta}{{\rho_2}^3} \tag{2.21}$$

$$\zeta'' = -(1-\mu)\frac{\zeta}{{\rho_1}^3} - \mu\frac{\zeta}{{\rho_2}^3} \tag{2.22}$$

$$\tag{2.23}$$

Is important to introduce the definition of the gravitational potential function in the Three-Body Circular Problem. It is defined as:

$$U = G\frac{m_1}{r_1} + G\frac{m_2}{r_2} + \frac{1}{2}\left(x^2 + y^2\right) \tag{2.24}$$

that, in the dimensionless form can be written as:

$$u = \frac{(1-\mu)}{\rho_1} + \frac{\mu}{\rho_2} + \frac{1}{2}\left(\xi^2 + \eta^2\right) \tag{2.25}$$

From the derivation of the potential function with respect to the dimensionless coordinates and the substitution into the system of the equation of motion, a new set of equation can be derived:

$$\xi'' - 2\eta' = \frac{\partial u}{\partial \xi} \tag{2.26}$$

$$\eta'' + 2\xi' = \frac{\partial u}{\partial \eta} \tag{2.27}$$

$$\zeta'' = \frac{\partial u}{\partial \zeta} \tag{2.28}$$

2.3.1 Lagrangian Points

From the derivation of the Three-Body Circular Problem, is possible to identify five particular positions in space where gravitational interactions and inertial forces are at equilibrium. These points are known as the Lagrangian points. They are characterized by the following set of equalities:

$$\begin{aligned} \xi' &= 0 \qquad \xi'' = 0 \\ \eta' &= 0 \qquad \eta'' = 0 \\ \zeta' &= 0 \qquad \zeta'' = 0 \end{aligned}$$

Lagrangian points are extremely important because, if a spacecraft is in one of them, it rotates solidly with the system.
Given the definition of Lagrangian point, the equation of motion in these points become:

$$\frac{\partial u}{\partial \xi} = 0 \tag{2.29}$$

$$\frac{\partial u}{\partial \eta} = 0 \tag{2.30}$$

$$\frac{\partial u}{\partial \zeta} = 0 \tag{2.31}$$

this means that, the Lagrangian points are the minimum of the potential function of the Three-Body System.
In order to satisfy Eq. (2.31):

$$\zeta = 0 \tag{2.32}$$

This means that all the Lagrangian points lie in the same plane. Lagrangian points can be divided into two families, the first one includes the collinear points, which have the peculiarity of being unstable points, the other one includes the equilateral points that are characterized by stability. The following discussion will explain in a better way the differences between these two different families of Lagrangian points.

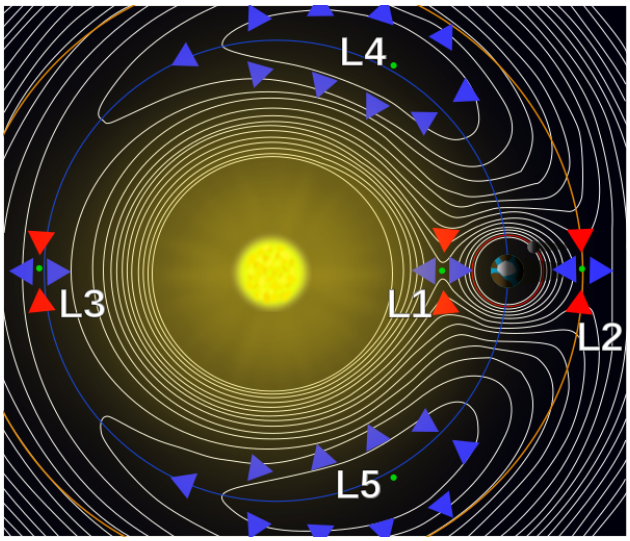

Figure 2.4: Earth-Sun system Lagrangian points

Collinear Points

The conditions under these points are obtained are:

$$\zeta = 0 \tag{2.33}$$

$$\eta = 0 \tag{2.34}$$

These points are spots of unstable equilibrium. Thus, if an external disturbance tends to shift the satellite from one of these points, it continues to move away from the Lagrangian point itself. If the goal of the mission is to maintain a spacecraft in one of these Lagrangian points, station keeping maneuvers are needed. The name of these points results from the peculiarity that they lie on the same line, which correspond to the x axis and are three:

- *Lagrangian Point* L_1

  It is found imposing:

  $$-\mu < \xi < (1-\mu) \tag{2.35}$$

  solving the system:

  $$\begin{cases} \xi - (1-\mu)\frac{\xi+\mu}{{\rho_1}^3} - \mu\frac{\xi-(1-\mu)}{{\rho_2}^3} = 0 \\ \rho_1 + \rho_2 = 1 \end{cases}$$

  That is characterized by:

  $$\rho = \sqrt[3]{\frac{\mu}{3}} \tag{2.36}$$

- *Lagrangian point* L_2

  It is found imposing:

  $$\xi > (1-\mu) \tag{2.37}$$

  solving the system:

  $$\begin{cases} \xi - (1-\mu)\frac{\xi+\mu}{{\rho_1}^3} - \mu\frac{\xi-(1-\mu)}{{\rho_2}^3} = 0 \\ \rho_1 - \rho_2 = 1 \end{cases}$$

That is characterized by:

$$\rho = \sqrt[3]{\frac{\mu}{3}} \tag{2.38}$$

obviously in the opposite direction with respect to L_1

- *Lagrangian point* L_3

  It is found imposing:

  $$\xi > -\mu \tag{2.39}$$

  solving the system:

  $$\begin{cases} \xi - (1-\mu)\frac{\xi+\mu}{{\rho_1}^3} - \mu\frac{\xi-(1-\mu)}{{\rho_2}^3} = 0 \\ \rho_2 - \rho_1 = 1 \end{cases}$$

  That is characterized by:

  $$\rho_1 = 1 \tag{2.40}$$

  $$\rho_2 = 2 \tag{2.41}$$

Equilateral Points

These points are obtained under the following conditions:

$$\zeta = 0 \tag{2.42}$$

$$\rho_1 = \rho_2 = 0 \tag{2.43}$$

As can be deduced by their definition, these points have the same distance from the two masses. They can be retrieved, solving the system:

$$\begin{cases} \xi - (1-\mu)(\xi+\mu) - \mu[\xi-(1-\mu)] = 0 \\ \eta - (1-\mu)\eta - \eta\mu = 0 \end{cases}$$

The equilater points are:

- *Lagrangian point* L_4

  $$\begin{cases} \xi = \frac{1}{2} - \mu \\ \eta = \frac{\sqrt{3}}{2} \end{cases} \tag{2.44}$$

- *Lagrangian point* L_5

  $$\begin{cases} \xi = \frac{1}{2} - \mu \\ \eta = -\frac{\sqrt{3}}{2} \end{cases} \tag{2.45}$$

The two equilateral points lies on the vertices of two equilateral triangles formed between the two principal masses and the Lagrangian points. The two points rotates on the same orbit of the mass m_2 around m_1. In particular L_4 anticipate the second mass of 60° while L_5 follows m_2 of the same angular distance. The equilateral points are spots of stable equilibrium. If a disturbance arises, the spacecraft moves back to its position, in fact is not necessary any maneuver in order to maintain the orbit.
Considering the three-body system Moon-Earth-Satellite is possible to identify:

- L_1: Lies between Earth and the Moon.

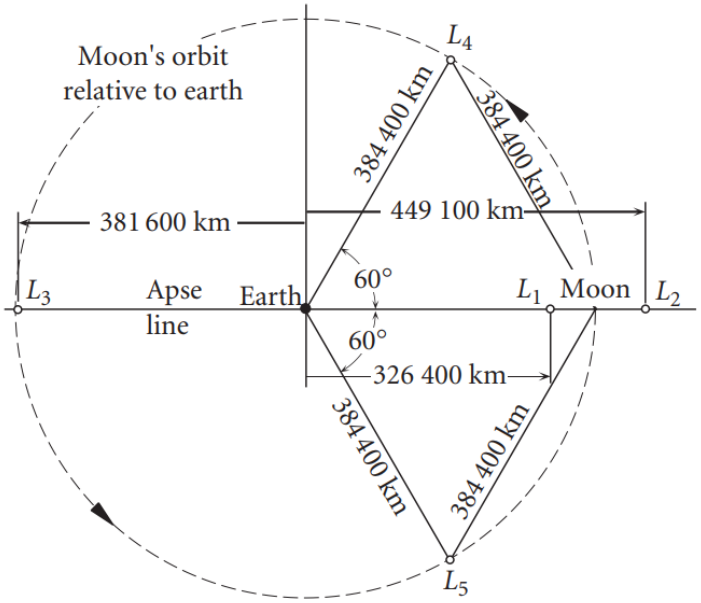

Figure 2.5: Location of the five Lagrange points of the Earth–Moon system.

- L_2: Lies at the same distance ol L_1 but it is opposite of his position, in fact it lies in an orbit external to the Moon one.
- L_3: Is simmetrycal to the position of the Moon with respect to the Earth.
- L_4: Precedes the Moon of 60° on its orbit.
- L_5: Chases the Moon of 60° on its orbit.

The position of these points are easier to understand and looking at the Figure 2.5 where distances and angles are explicated.
Obviously in a real system, where no hypothesis are present, the Lagrangian points are not punctiform. In fact they represent an area in which the third body is at equilibrium.

2.4 Interplanetary Missions

In order to describe the mission is necessary to introduce some fundamentals about interplanetary missions. For a better understanding is necessary to introduce the Patched Conics Method (PCM). This method is based on the hypothesis that space can be divided into different zones called sphere of influence. The sphere of influence of a body is the portion of space around it where the spacecraft can be supposed to interact only with the body itself. Conics derive from the fact that Keplerian orbits are conic sections with the focus at the attracting body, which means that in every sphere of influence there will be a different trajectory derived from the conic section.
Is possible to divide the interplanetary trajectory into three different part:

1. Escape from the sphere of influence of the departure body
2. Heliocentric trajectory
3. Arrival in the sphere of influence of the target body

During the Heliocentric trajectory, the spacecraft is outside the sphere of influence of any planet, thanks to this, is possible to consider the Sun as the principal body, and the spacecraft is only under its gravitational interaction. It is impossible to describe in a general way the Heliocentric trajectory insofar it is strongly affected by the maneuver effectuated during its duration. Most of the time, in literature, the heliocentric trajectory is studied like a coasting arc of a Hohmann Transfert between the two bodies but this description only fits with the concept of impulsive maneuver, that is not considered in this work. Considering the Sun as the principal body and the Earth as the second body is possible to calculate the Earth's sphere of influence as follow:

$$r \simeq \left(\frac{m_\oplus}{m_\odot}\right)^{\frac{2}{5}} r_{\oplus-\odot} \simeq 10^6 km \tag{2.46}$$

where $r_{\oplus-\odot}$ is the mean distance between the Sun and the Earth and $m_\oplus$ and $m_\odot$ are respectively the masses of the Earth and of the Sun.
Whereas when the spacecraft is inside the sphere of influence of the planet is possible to identify a planetocentric trajectory. One of the most important trajectories in an interplanetary mission is the escape maneuver that will be studied in the following subsection.

2.4.1 Escape maneuvre

In order to escape to the sphere of influence of a planet, and thus to its gravitational pull, is necessary a trajectory that allow the spacecraft to have a relative velocity v_∞ greater than zero, where v_∞ is the hyperbolic excess velocity. If the hyperbolic excess of velocity is equal to zero the spacecraft will not leave the sphere of influence, in fact it stays in the same orbit of the planet and does not embark upon a heliocentric elliptical path. Is possible to write the hyperbolic excess speed as follow:

$$v_\infty = \sqrt{\frac{\mu_\odot}{R_1}}\left(\sqrt{\frac{2\,R_2}{R_1+R_2}-1}\right) \tag{2.47}$$

Usually the starting point of an escape maneuver is a circular parking orbit around the the departure body. The radius of the parking orbit is equal to the periapse radius r_p of the departure hyperbola.
Writing the angular momentum as:

$$h = \frac{\mu_1\sqrt{e^2-1}}{v_\infty} \tag{2.48}$$

and substituting into the definition of the periapse radius:

$$r_p = \frac{h^2}{\mu_\oplus}\frac{1}{1+e} \tag{2.49}$$

is possible to obtain the eccentricity in function of r_p and v_∞.

$$e = 1 + \frac{r_p {v_\infty}^2}{\mu_\oplus} \tag{2.50}$$

Substituting into Eq (2.48) is possible to explicit the angular momentum:

$$h = r_p\sqrt{{v_\infty}^2 + \frac{2\mu_\oplus}{r_p}} \tag{2.51}$$

Given the hyperbolic excess speed, that is specified by the mission requirements, choosing

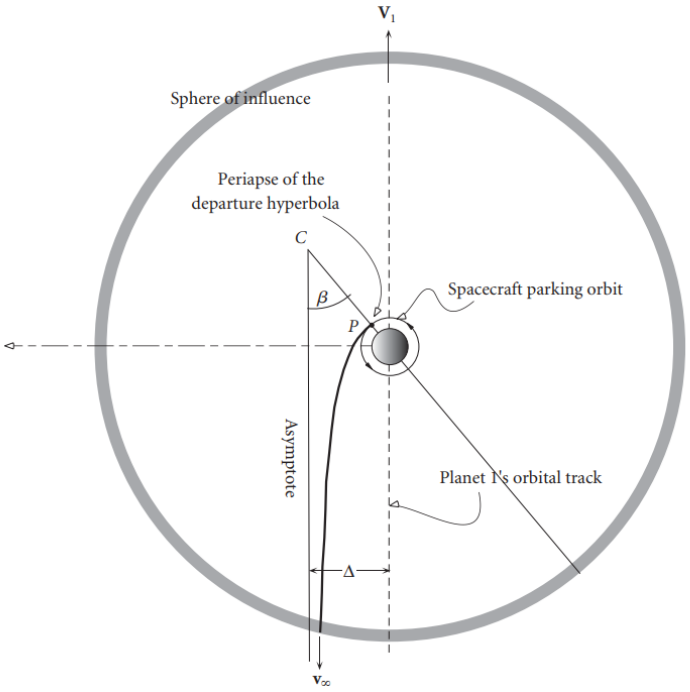

Figure 2.6: Departure of a spacecraft on a trajectory from an outer planet to an inner planet.

the correct r_p is fundamental to the definitions of the eccentricity and the angular momentum of the departure trajectory. In order to calculate the Δv necessary to perform the escape maneuver, the periapse speed and the speed of the circular parking orbit are needed, and they can be written as follows:

$$v_p = \frac{h}{r_p} = \sqrt{{v_\infty}^2 + \frac{2\mu_\oplus}{r_p}} \tag{2.52}$$

$$v_c = \frac{\mu_\oplus}{r_p} \tag{2.53}$$

Now can be easily calculated the Δv necessary to accomplish the escape maneuver as follow:

$$\Delta v = v_p - v_c = v_c \left(\sqrt{2 + \left(\frac{v_\infty}{v_c} \right)^2} - 1 \right) \tag{2.54}$$

In addition of the magnitude of Δv is important where the Δv is given and so where the position of the periapse is. Thus is necessary to introduce a new parameter that gives the orientation of the apse line of the hyperbola to the planet's heliocentric velocity vector, this is β and can be calculated as:

$$\beta = cos^{-1}\left(\frac{1}{e}\right) = cos^{-1}\left(\frac{1}{1 + \frac{r_p {v_\infty}^2}{\mu_\oplus}}\right) \tag{2.55}$$

Is important to underline how the evasion maneuver change depending on the position of the planet. If the mission is to send a spacecraft from an outer planet to an inner planet, the evasion trajectory has to emerge from the back side of the sphere of influence of the planet with the velocity v_∞ that points opposite to the $V_\oplus$. This is necessary because the

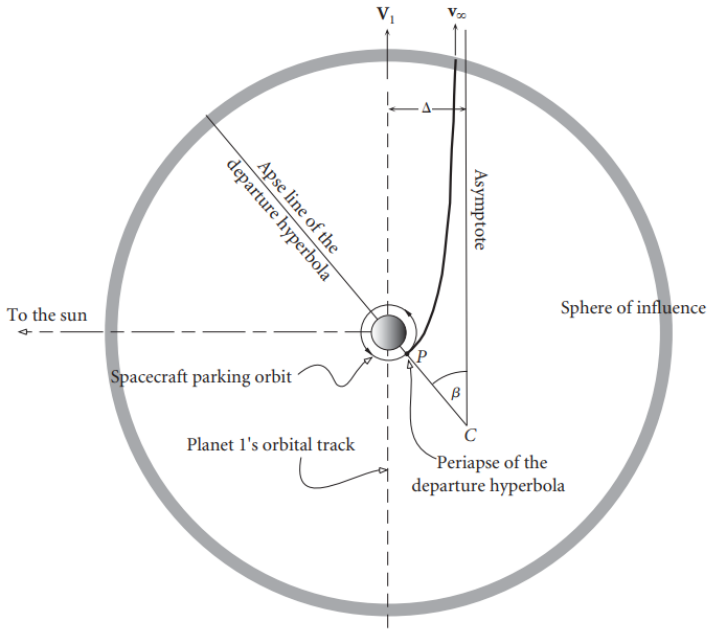

Figure 2.7: Departure of a spacecraft on a trajectory from an inner planet to an outer planet.

heliocentric speed of the spacecraft V_D has to be lower that the circular velocity of the departure planet $V_\oplus$ as shown in Figure 2.6.
On the other hand if the mission has as target an outer planet the spacecraft has to emerge from the front side of the sphere of influence because the v_∞ has to point in the same direction of $V_\oplus$ in order to reach the higher heliocentric speed V_D needed to reach an outer planet as shown in Figure 2.7.

2.4.2 Two impulses escape maneuvre - Oberth Maneuvre

Is important to underline that there is not only the one impulse evasion maneuver but there is also a two impulses escape maneuver that is also known as Oberth Transfert. Oberth's transfert is a two impulses maneuver where the first impulse is given in order to

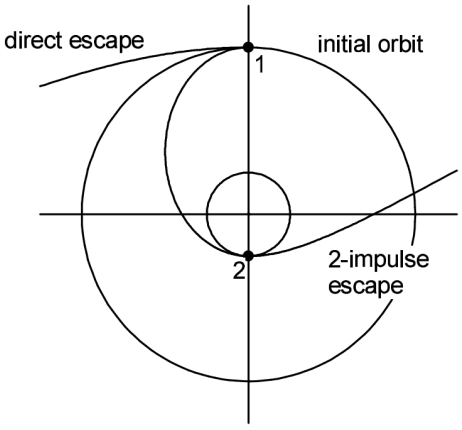

Figure 2.8: Schematic representation of Oberth's maneuver.

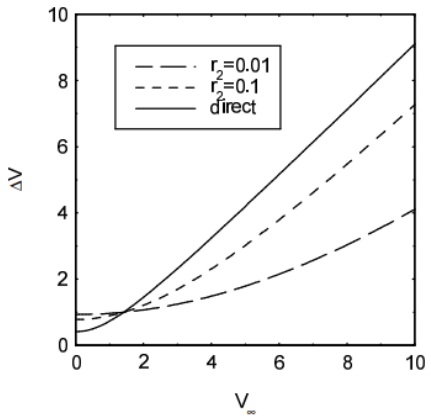

Figure 2.9: ΔV necessary for Oberth's maneuver in function of v_∞ ad r_2.

bring the spacecraft into a less energetic orbit, is a braking impulse, moving the perigee of the trajectory closer to the departure body and, once it has reached the perigee, the second impulse is given to complete the evasion maneuver, accelerating the spacecraft (Figure 2.8). The second impulse is given when the distance to the departure body is smaller than the initial one, this lead to a more efficent burn and reduce the gravity losses because minimize the time under the influence of gravity of the planet.
Oberth's maneuver is not always advantageous, in fact in case of $v_\infty < \sqrt{2}V_{c1}$ one impulse maneuver is less expensive and therefore convenient (Figure 2.9).

Chapter 3

Space Propulsion Foundamentals

In this chapter will be collected all the fundamentals of space propulsion, which are essential for a better understanding of the mission. In the beginning, a global overview of the principles that rule all the propulsion systems will be given, then a brief examination of the basics of electric propulsion will be carried out. Propulsion can be defined as the capability to generate a force to change the velocity of the spacecraft and, as a consequence, allow to modify or maintain the trajectory.

3.1 Introduction to Space Propulsion

> *"When one body exerts a force on a second body, the second body simultaneously exerts a force equal in magnitude and opposite in direction on the first body"*

This is what state the third Newton law of motion or action-reaction principle, propulsion system to generate thrust lay on this concept. In order to generate thrust in space, considering that space is a vacuum, is necessary to carry onboard something to exchange momentum with: the propellant. There are other possibilities to generate thrust that does not rely on the propellant, like the magnetic sails and the solar sails, but they will not be specifically discussed in this thesis. The presence of propellant affects the capability of motion in space since the spacecraft can carry only a limited amount of propellant. Once it has run out there is no chance for the spacecraft to modify his orbit.
There are different methods to categorize the different kinds of space propulsion. One of the most common is based on the purpose of the propulsor itself:

- *Primary propulsion*: it is designed and used in order to change the trajectory of the spacecraft.
- *Secondary or Auxiliary propulsion*: it is designed and used in order to maintain the desired trajectory and contrasting external disturbance actions.

Another way to classify the propulsor is based on what kind of propellant is used to generate thrust. In this case propulsion can be divided into three different classes:

- *Chemical propulsion*: in order to create thrust are needed two propellant, the fuel and the oxidizer, the reaction between this two elements generate the product of the reaction which will be accelerated into a nozzle.
  Chemical propulsion can be further divided into solid propellants, liquid propellants and hybrid propellants.
- *Electrical propulsion*: the propellant is accelerated thanks to electromagnetic phenomena. Also in this group are identifiable different kind of electrical propulsion,

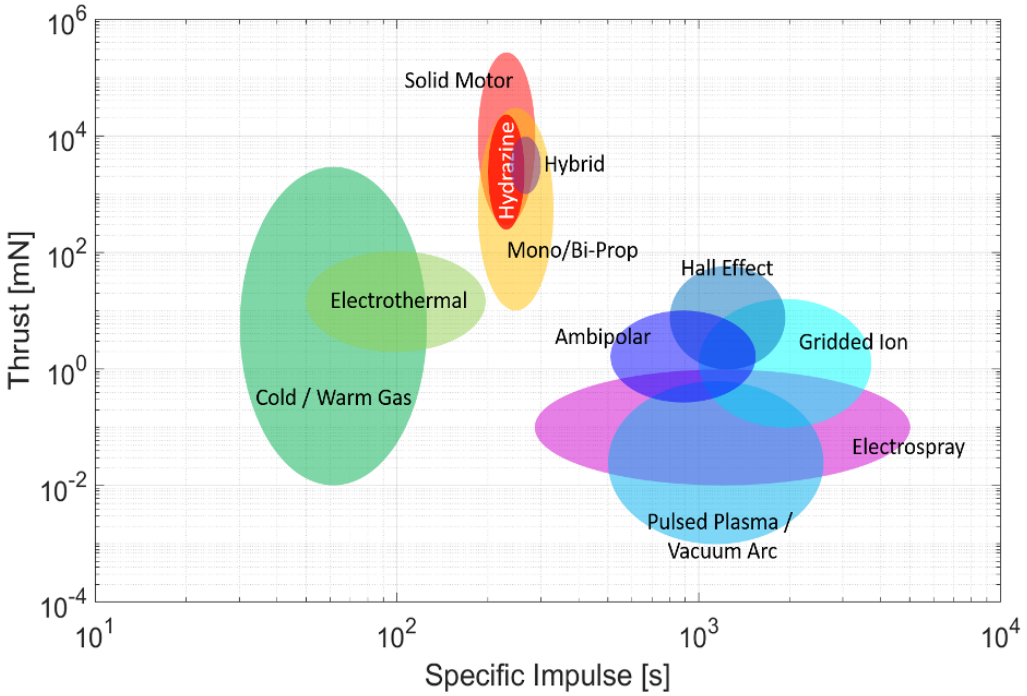

Figure 3.1: Typical small spacecraft in-space propulsion trade space

for example electrothermal propulsion, electrostatic propulsion and electromagnetic propulsion.

- *Nuclear propulsion*: it exploits nuclear power to generate thrust.

Considering that all the propulsion system introduced are based on the action-reaction principle, is possible to define some parameters and some concepts which are common in all the categories.
A system can be considered as a "closed system" if no external forces are applied on itself, if this assumption is true, the global momentum is constant over time. Assuming a body with mass m and velocity v at the initial instant, after an infinitesimal amount of time, the body has ejected an infinitesimal part of his mass that correspond with the propellant mass dm_P. Thanks to the expulsion of the infinitesimal mass there is an increment of the speed of the body that is related to the ejection velocity of the infinitesimal mass, the velocity c is known as the effective discharge velocity. Is important to underline that c is a velocity with respect to the spacecraft, accordingly with that, the global velocity of the propellant is $c - v$
In order to describe how the electric propulsors work, is important to introduce some variables that describe the performances.
Imposing the conservation of the total momentum of the system

$$mv = (m - dm_p)(v + dv) - dm_p(c - v) \tag{3.1}$$

where the first term on the right is the total momentum of the body while the second term is the total momentum of the mass of propellant ejected. Neglecting the second order terms resulting from the Eq. (3.1) is possible to obtain:

$$m\ dv = dm_p\ c$$

It is possible to define the propellant flow as:

$$\dot{m}_p = \frac{dm_p}{dt} \tag{3.2}$$

and thus:

$$m\frac{dv}{dt} = \dot{m}_p\, c \tag{3.3}$$

Considering that the term on the left is a force given by the product of the mass with the acceleration, the term on the right has to be a force too. Accordingly to Newton's second law of motion this force has to be applied on the body itself, the result of this consideration is that the force examined is nothing more than the thrust, it follows that:

$$T = \dot{m}_p\, c \tag{3.4}$$

Is possible to introduce also the thrust power, that is the power necessary to accelerate the propellant at the velocity that generate the thrust T and it can be expressed as:

$$P_T = \frac{1}{2}Tc = \frac{1}{2}\dot{m}_p c^2 \tag{3.5}$$

After this brief overview is now possible to introduce four important variables for the description of the performances of the propulsor.
For space propulsor, in general, the exit velocity is almost the same of the effective exhaust velocity c that is defined as follow:

$$c = \frac{T}{\dot{m}_p} \tag{3.6}$$

Integrating the thrust is possible to obtain the total impulse:

$$I_{TOT} = \int_{t_0}^{t_f} T dt \tag{3.7}$$

that indicates the total propulsive power of the system. Obviously, with the increase of total impulse also the propulsive cost of the mission, that the spacecraft can afford, increase. Defined the total impulse is possible to obtain the specific impulse that is defined as:

$$I_{sp} = \frac{I_{TOT}}{m_p\, g_0} \tag{3.8}$$

where g_0 is the gravity acceleration on Earth's surface while m_p is the total mass of the propellant onboard. In order to explicit the relation between c and the I_{sp} is necessary to introduce two more hypothesis, in fact if the thrust is constant is possible to write down:

$$I_{TOT} = T\Delta t$$

with Δt is the working time of the propulsor. If also c is constant also the propellant flow is constant and it is equal to:

$$m_p = \dot{m}_p\, \Delta t$$

Substituting now the expression of I_{TOT} and m_p in case of T and c constant into the Eq. (3.8) is possible to obtain:

$$I_{sp} = \frac{c}{g_0} \tag{3.9}$$

As can be easily seen from Eq. (3.9) the specific impulse have the same value of the effective exhaust velocity, neglecting a constant term. Both the variables are a measure of the efficiency with which the propellant is used to generate thrust. Obviously to increase the performances is better have an higher value of specific impulse and effective exhaust velocity. Considering a case study where the specific impulse of the spacecraft is high, it can functioning for the same time of one spacecraft with lower I_{sp} but with a higher thrust or can generate the same thrust but can be used for a longer time, thus lead to the fact that having an higher specific impulse is advantageous.

Tsiolkovsky Equation

Every mission is characterized by an unique ΔV and it is linked to the propulsive effort needed to reach the target. The most important equation utilized to calculate the ΔV as a first approssimation is the Tsiolkovsky Equation, also known as the Rocket Equation. This relation is fundamental because it relates the ideal propulsive cost of a maneuver with the associated mass of propellant needed to reach the target orbit. It is important to underline that this relation do not take into account any kind of external disturbances, in fact is possible to refer to it with the term ideal.
Introducing the definition of propulsive cost that is the variation of velocity of the body during the maneuver:

$$\Delta V = \int_{t_0}^{t_f} \frac{T}{m} dt \tag{3.10}$$

Substituting the definition of Thrust is possible to obtain:

$$\Delta V = \int_{t_0}^{t_f} \frac{c\, \dot{m}_p}{m} dt \tag{3.11}$$

In order to express the relation with respect to the variation of the mass, is fundamental to underline that $\dot{m}_p = -\dot{m}$ because the spacecraft's mass decrease with the increase of the propellant expelled.

$$\Delta V = -\int_{t_0}^{t_f} \frac{c\, \dot{m}}{m} dt \tag{3.12}$$

The integral can be easily solved if the assumption of $c = cost$ is adopted, but this is not always possible, in this case is possible to use an average value of the effective exhaust velocity.
By the integration is possible to obtain:

$$\Delta V = c\, ln\left(\frac{m_0}{m_f}\right) \tag{3.13}$$

and now from inverting the equation just calculated is possible to express the final mass in function of the initial mass and the ΔV as follow:

$$m_f = m_0\, e^{-\frac{\Delta V}{c}} \tag{3.14}$$

Thanks to the equation is possible to obtain important considerations. First of all there is an exponential relation between the propellant consumption and the propulsive cost, this means that during the acceleration of a payload, the propulsor is not only accelerating the payload but it is also accelerating the propellant that is required to accelerate that payload. So, if the payload increase, also the propellant mass increase but not following a linear law but an exponential one. As a consequence the propulsor has not only to accelerate the additional payload but also the additional propellant. Also in this equation is possible to notice the importance of having an high specific impulse, the higher the specific impulse the higher will be the final mass considering the same initial mass.

3.2 Electric Propulsion

Electric Propulsion is a class of space propulsion that count on the electrical power to accelerate the propellant thanks to the electrical or magnetic properties of itself. The use of electrical propulsion is the state of art for the unmanned mission and will be very challenging, in the following years, to understand if this kind of propulsion can be a valid alternative to chemical propulsion in manned mission. The use of electrical power increase

the propulsive performances of electric thruster compared to chemical thruster, in fact electric propulsion is not limited in energy but is only limited by the available electrical power on board. Furthermore, electric propulsion requires a very little mass to accelerate the spacecraft and can eject the propellant faster than from a classical chemical thruster, this leads to an increased efficiency. The initial thrust is quite low but it can continue accelerating for months or even years and it can also slow down and change direction and this is one of the most important benefit of electrical propulsion. There are different way to generate electrical power, the most common is using solar array.
Is possible to identify different categories of electrical propulsor, in this case the will be classified considering how the energy to create thrust is generated. There are three main categories:

- Electrothermal propulsion: Electrical power is used to heat the propellant that is then expanded through a nozzle. During the expansion in the nozzle the thermal energy is converted into kinetic energy and thanks to this thrust is generated. Is important to consider that during the expansion there are losses and non ideal effects to take into account.

- Electrostatic propulsion: The electrical power is used to ionize and accelerate the propellant. Once the gas is ionized, the ions are accelerates trough an electric field. In order to maintain a neutral charge on the spacecraft, an electron flow is used to neutralize the flux at the exit of the propulsor

- Electromagnetic propulsion: Electrical power is used to generate the electric and magnetic field. Thanks to the forces generated by the fields the propellant can be accelerated, creating thrust.

It is important to underline that not all the propulsor can be used for all the missions, in fact is important to categorize the propulsor on the basis of the characteristic power of the thruster. They can be divided into:

- Microthruster: they are mainly used for precision control

- 1 kW propulsor: mainly used for station keeping (SK) or orbit/deorbit injection of CubeSat or small satellites but also for small robotic interplanetary missions.

- 5 - 10 kW: mainly used for the deorbit operations of big satellites or for the GEO insertion.

- 100+ kW: this class of thruster is not available yet but is under development, they will be mainly used for human exploration and development of human presence in space.

System	Specific Impulse [s]	Thurst [N]
Resistojet	200 - 350	0.2 - 0.3
Arcjets	400 - 1500	0.2 - 1
Ion thruster	2000 - 5000	< 0.2
Hall thrusters	1500 - 2000	< 2
Pulsed Plasma thruster	600 - 2000	< 0.01
MPD thruster	2000 - 5000	< 2

Table 3.1: Characteristics of electric propulsion system

All the electrical thruster convert the electrical power into the useful effect that is the thrust. Thus lead to some consideration that are common to all the electrical thruster. Is possible to introduce the global efficiency that is how the conversion form electrical power to thrust is close to the ideal process of conversion. The value of the global efficiency can not be neglected and is important to know that can vary form one kind of propulsor to the other.
Given:

$$\eta P_E = \frac{1}{2} T c \tag{3.15}$$

where η is the global efficiency, P_E is the electrical power consuption and the term on the right is the thrust power. By the inversion of Eq. (3.15) is possible to write explicitly the effective discharge velocity as follow:

$$c = \frac{2\eta P_E}{T} \tag{3.16}$$

From Eq. (3.16) is possible to extrapolate one of the most important concept of the electrical propulsion, the effective exhaust velocity is strictly linked with the electrical power consumption and the magnitude of thrust. In order to have an high c and as a consequence an high specific impulse is possible to use or small thrust or having high electric power consumption and as a consequence high power source's mass. Making a comparison to chemical thruster, is possible to understand why electrical propulsors, has an higher specific impulse than the chemical ones. Low thrust ($10\mu N - 1N$) or heavy power generation system can be identified as the cause of the higher specific impulse of the electrical propulsor.

3.2.1 Ion Thruster

One of the most diffused category of electrical propulsor are, for sure, the Ion Thruster. This kind of propulsors belongs to the Electrostatic propulsors and, as can be deduced by the name, utilize a ionized propellant to create thrust thanks of the acceleration of the ion themselves. The acceleration of the ion is possible thanks to the electric field that is generated into the propulsor, also a magnetic field is present but it is not used for this purpose. Is possible to identify three main steps to accomplish in order to permit the correct operation of the propulsor:

- Ionization of the propellant
- Acceleration of the ion
- Neutralization of the accelerated ion beam

Thus the first step to create thrust is necessary to ionize the propellant. This is possible thanks to the ionization process.
The ionization of a propellant is the process thanks to which is possible to separate electrons from their initial atoms and therefore creating an ion. In order to create an ion is necessary to provide an amount of energy that is higher to the first ionization energy ε_I, that is unique and different for each element of the periodic table.
The ionization reaction usually happens as follows

$$A \ + \varepsilon_I \leftrightarrows A^+ + e^- \tag{3.17}$$

where e^- is the free electron and A^+ and A are the ion of the propellant and the atom of propellant itself. Even if the first ionization energy is given to an atom of the propellant, only a fraction of the whole propellant will be ionized, because not all the atoms receives

enough energy to lose an electron. As a consequence, if a ionization ratio is defined, this will not be equal to one but it will be lower. In addition is necessary to consider that electrical power is not only used to accelerate the ion but also to create themselves. As a consequence, also in the more ideal case, the process has not efficiency equal to 100%, and is therefore necessary to introduce an ideal efficiency defined as:

$$\eta_{id} = \frac{\frac{1}{2} m_+ {u_+}^2}{\frac{1}{2} m_+ {u_+}^2 + \varepsilon_B} \tag{3.18}$$

In this category of propulsion, ionization can be performed in two different ways:

- Electron Bombardment
- Radiofrequency

Considering the first method, an electron gun injects electron at high energy in the chamber where is contained also the propellant. The electrons, once they are inside the chamber, are subjected to an electric field and a magnetic field. The first accelerate the electrons, the second one tends to confine them inside the chamber, increasing the permanence time and protecting the chamber itself from the collision of high energy electrons. The movement of the electrons from the cathode to the anode permit the collision of the electrons with the propellant atoms. These collision lower the velocity of the electrons and may ionize the atoms of the propellant. The second method is different from the first only for the way in which the electrons are accelerated. In this case in fact the electrons are provided with energy thanks to electromagnetic waves created by a radiofrequency coil.
In both cases the process is not ideal and thus not all the atoms are ionized.
Once ions are created, in order to generate thrust, is necessary to separate them from electrons, otherwise if both are accelerated the net thrust will be null. This happens because electrons and ion have the same charge, considering the module, but different sign. In fact, explicating the force applied to a charge under the effect of an electric field is possible to write:

$$\boldsymbol{F} = q\boldsymbol{E} \tag{3.19}$$

How forces act on the different type of particles is shown in Figure 3.2 and thanks to the representation can be easily seen that electrons and ions are subjected to the same but opposite force.
In order to separate the charge, in this specific type of propulsion, a magnetic field is

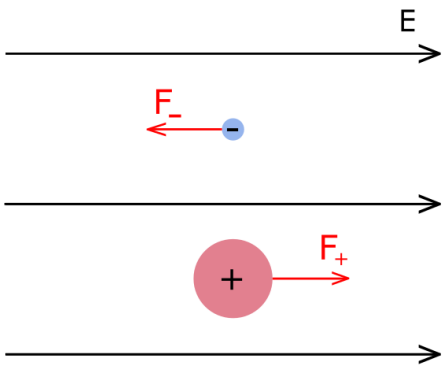

Figure 3.2: Schematic representation of electric forces acting on different species

introduced, this allows the ion to be accelerated through an acceleration grid, while the electrons are confined in the ionization chamber.
Once the ion are created and then separated from the electrons, they have to be accelerated, this is possible thanks to an acceleration grid. Before explaining how the grid works an overview of the physics of the grid is needed.
The acceleration of the ion is generated thanks to the application of an electric field on the ion themselves. The electric field, is a conservative field and thus, can be connected to the electrical potential, in fact is possible to identify the Net Accelerating Potential, defined as V_N, as the potential connected to the acceleration. Ions entering inside the acceleration zone convert their potential energy into kinetic energy, thus lead to an increase of their velocity. Mathematically, imposing the conservation of the total energy and neglecting the efficiency of the conversion process between kinetic and potential energy is possible to write:

$$qV_N = \frac{1}{2} m_+ {u_+}^2 \tag{3.20}$$

where the left term is referred to the chamber, where propellant is static. Considering that the only motion present in the chamber is due to the chaotic thermal motion, the velocity is globally null. On the other hand the right term is only composed to the kinetic term of the energy, m_+ is the mass of the ion and u_+ is the velocity at the exit section.
Considering that, the exit velocity can be considered almost equal to the effective exhaust velocity, is possible to obtain :

$$u_+ = \sqrt{\frac{2qV_N}{m_+}} \tag{3.21}$$

by this equation is possible to understand that the only two parameters modifiable are V_N and m_+.
Thus, in the propulsor is present a zone where ions are accelerated, this zone is between two grids, the first is an higher potential grad and has the name of *screen grid* while the second is with a lower potential value and is know as *acceleration grid*. Both of the grids are curved and not flat in order to avoid buckling due to thermal expansion, molybdenum is most common material used for their production because of its easiness in manipulation. Grids are designed with millimetric holes in them, this choice is made in order to have a more focused beam. Is important to design accurately the grid and the distance between holes, otherwise is possible that ion beam interact one to the other causing the divergence of the beam and the degradation of the propulsor itself caused bu the interaction of high velocity ion with the walls of the propulsor. Fundamental is also the distance between the two grids, they are posed at a millimetric distance but is important not to place the grids too close one to the other and not with an high potential difference. If this happens, the proximity of the two grids and the high potential difference could lead to the insurgence of sparks but, in order to avoid this possibility is common to respect the relation:

$$\frac{V_G}{d} < 2\frac{kV}{mm} \tag{3.22}$$

where V_G is the potential difference and d is the distance. Also their dimension has to be limited, in fact in general:

$$\frac{D}{d} < 600 \tag{3.23}$$

where D is the diameter of the grids.
Once the ion are created from the ionization and accelerated between the two grid they are ejected into the void in order to create thrust.
If only ion are expelled from the propulsor it will become partially charged negatively, and that is not positive for the spacecraft. Thus, is necessary to neutralize the ion beam

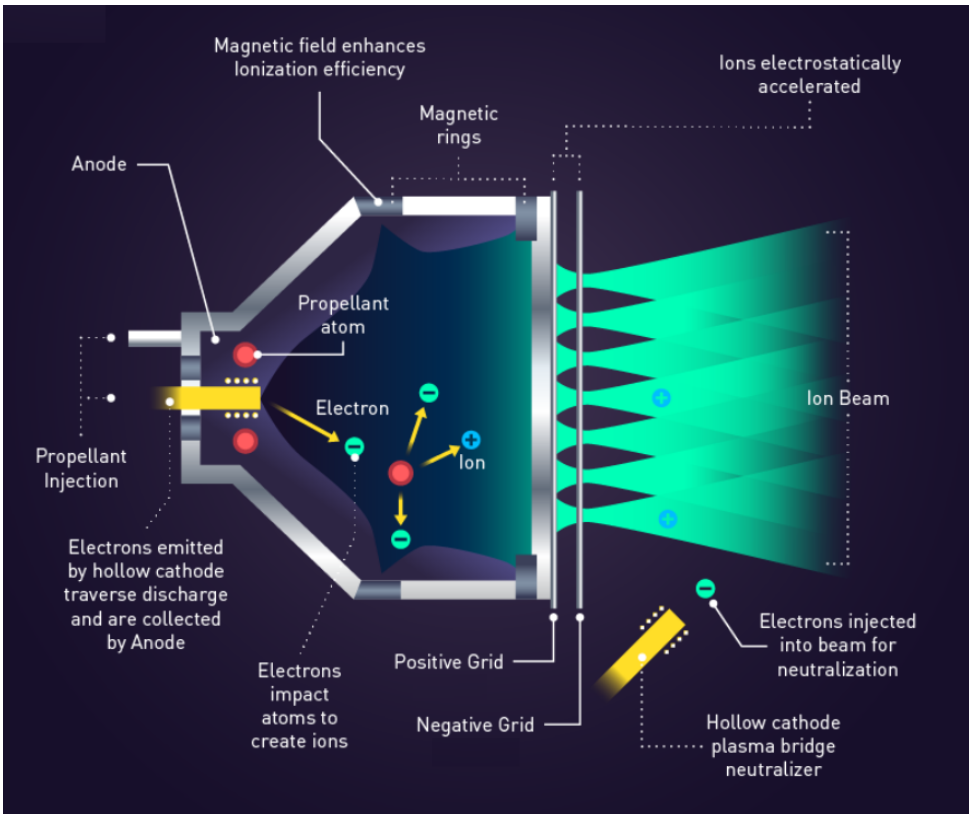

Figure 3.3: Schematic representation of an Ion thruster

and restabilishing the global neutrality of the propulsor, this is possible thanks to the neutralization. To avoid the insurgence of this unwanted event is necessary to neutralize the ion beam with the same number of electrons. Thanks to an hollow cathode, that extracts electrons from a fraction of the propellant flow, a sort of cloud of electron is created at a certain distance from the exit section of the propulsor, the neutralizing current is not accelerated because it is not utilized to produce thrust. Once the ion is ejected at high velocity it passes through the cloud and interact with the electrons bringing with itself one of the electrons and getting neutralized. It follows that, extending this process to all the ions, a neutral beam of atoms is what exits from the propulsor. The process that brings to the extraction of electrons for the neutralization brings with itself a loss. Is possible in fact to define the efficiency of the propellant utilization as follows:

$$\eta_u = \frac{\dot{m}_+}{\dot{m}_P} \tag{3.24}$$

where $\dot{m}_P$ is the sum of the flow of the ion plus two losses, the first is $\dot{m}_A$ that is the non-ionized fraction and the second is $\dot{m}_C$ that is the fraction that goes to the hollow cathode for the neutralization beam.

$$\dot{m}_P = \dot{m}_+ + \dot{m}_A + \dot{m}_C \tag{3.25}$$

In Figure 3.3 is possible to observe a schematic representation of how is made an Ion thruster. Is possible to easily notice the three different zones of the propulsor, fundamental for the correct working of the propulsive system.
Finally is possible to explicit the fraction of the electrical power that is converted in thrust power.
Considering that: if no electrical power losses are taken into account, and this lead the

present tractation to an almost ideal case, is possible to define the global efficiency as:

$$\eta_g = \eta_u \eta_{id} \tag{3.26}$$

and thus:

$$P_T = \frac{1}{2} T c = \eta_g P_E \tag{3.27}$$

Chapter 4

Optimal Control Theory - OCT

The optimal control theory is based on variational calculus and will be explained, during this chapter, choosing the most suitable form for the optimization of spatial trajectories and to the method adopted for the solution of the differential problem within the limits that arises from its application. The optimal control theory is applied to a generic system that is described by a vector of state variables x, the differential equations that describe the evolution of the system between the initial time and the final time are in function of x, u (control vector) and the time t (independent variable). The generic form is:

$$\frac{d\mathbf{x}}{dt} = \mathbf{f}(\mathbf{x}, \mathbf{u}, t) \tag{4.1}$$

It is useful to divide the trajectory into n arc, o sub-ranges, within each of which the variable are continuous but discontinuities can be present at the arcs' interfaces. The j-th interval starts at time $t_{(j-1)+}$ and finish at time t_{j-} and values that the variables assume at its extremes are $x_{(j-1)+}$ and x_{j-} where the signs - and + indicate respectively the values assumed immediately before or after the point considered. Thanks to this strategy is possible to take into account any discontinuities of the variables and time that apply to the junction points between the various intervals, such as discontinuities in mass or velocity related to impulsive maneuver or time discontinuities. It is also possible, thanks to this formulation, to make the second member of Eq. (4.1) assume a different value depending on the sub-range considered, that will result, as will be shown later, very convenient. The boundary conditions are, in general, both mixed and non-linear. Thus, they involve non-linear relations between the state and time variables at the external and internal boundaries. In the generic form, they can be expressed as following:

$$\boldsymbol{\chi}\left(\mathbf{x}_{(j-1)+}\ ,\ \mathbf{x}_{j-}\ ,\ t_{(j-1)+}\ ,t_{j-}\right) = 0 \qquad j = 1, ..., n \tag{4.2}$$

Other kind of boundary conditions could involve the control vector u. The optimum problem consist in the research of the extremal values of the functional, maximum or minimum depends on the goal to reach. The functional can be expressed as follow:

$$J = \phi\left(\mathbf{x}_{(j-1)+}\ ,\ \mathbf{x}_{j-}\ ,\ t_{(j-1)+}\ ,t_{j-}\right) + \sum_{j} \int_{t(j-1)+}^{t_{j-}} \mathbf{\Phi}(\mathbf{x}(t), \mathbf{u}(t), t)dt \qquad j = 1, ..., n \tag{4.3}$$

The functional J is formed of two components:

- ϕ: a function depending on the values of the variables vector and on the values of the independent variable at the boundaries
- Integral of Φ function: depends on the time and on the values assumed by the state and the controls in each instant

It is possible to formulate the functional's expression in order to present:

- $\varphi = 0$: Lagrange's formulation
- $\Phi = 0$: Mayer's formulation

This is possible thanks to the introduction of particular auxiliary variables, that allows to reformulate the functional. Introducing:

- μ : adjoint constant, related to the boundary conditions
- $\boldsymbol{\lambda}$: adjoint variables, related to the state equations

Thus the modified functional can be written as follow:

$$J^* = \phi + \boldsymbol{\mu}^T \boldsymbol{\chi} + \sum_j \int_{t(j-1)+}^{t_{j-}} (\boldsymbol{\Phi} + \boldsymbol{\lambda}^T (\boldsymbol{f} - \dot{\boldsymbol{x}}))dt \qquad j = 1, ..., n \tag{4.4}$$

where $\dot{\boldsymbol{x}}$ is the state vector derivative with respect to time.
Both functional J and modified functional J^* depend on the time, the state vector, its derivative and the control vector $\boldsymbol{u}$. The values of time and state variables which affect the functionals, are the ones related to each arch's edges. In fact, if the boundary conditions and the state equations are satisfied, the two functionals and thus their extremal values coincide.
Integrating by parts is possible to eliminate the dependence of the modified functional J^* from the derivatives of the state vector:

$$\begin{aligned} J^* = \phi + \boldsymbol{\mu}^T \boldsymbol{\chi} + \sum_j ({\boldsymbol{\lambda}^T}_{(j-1)+} \boldsymbol{x}_{(j-1)+} - {\boldsymbol{\lambda}^T}_{(j-)} \boldsymbol{x}_{j-} + \\ + \sum_j \int_{t(j-1)+}^{t_{j-}} (\boldsymbol{\Phi} + \boldsymbol{\lambda}^T (\boldsymbol{f} - \dot{\boldsymbol{\lambda}}^T \boldsymbol{x}))dt \qquad j = 1, ..., n \end{aligned} \tag{4.5}$$

Differentiating the previous expression is possible to obtain the differential of the functional itself:

$$\begin{aligned} \delta J^* = & \left(-H_{(j-1)+} + \frac{\partial \varphi}{\partial t_{(j-1)+}} + \boldsymbol{\mu}^T \frac{\partial \boldsymbol{\chi}}{\partial t_{(j-1)+}} \right) \delta t_{(j-1)+} + \\ & + \left(-H_{j-} + \frac{\partial \varphi}{\partial t_{j-}} + \boldsymbol{\mu}^T \frac{\partial \boldsymbol{\chi}}{\partial t_{j-}} \right) \delta t_{j-} + \\ & + \left({\boldsymbol{\lambda}^T}_{(j-1)+} + \frac{\partial \varphi}{\partial \boldsymbol{x}_{(j-1)+}} + \boldsymbol{\mu}^T \left[\frac{\partial \boldsymbol{\chi}}{\partial \boldsymbol{x}_{(j-1)+}} \right] \right) \delta \boldsymbol{x}_{(j-1)+} + \\ & + \left({\boldsymbol{\lambda}^T}_{j-} + \frac{\partial \varphi}{\partial \boldsymbol{x}_{j-}} + \boldsymbol{\mu}^T \left[\frac{\partial \boldsymbol{\chi}}{\partial \boldsymbol{x}_{j-}} \right] \right) \delta \boldsymbol{x}_{j-} + \\ & + \sum_j \int_{t(j-1)+}^{t_{j-}} \left(\left(\frac{\partial H}{\partial \boldsymbol{x}} + \dot{\boldsymbol{\lambda}}^T \right) \delta \boldsymbol{x} + \frac{\partial H}{\partial \boldsymbol{u}} \delta \boldsymbol{u} \right) dt \qquad j = 1, ..., n \end{aligned} \tag{4.6}$$

Where H is the Hamiltonian of the system:

$$H = \Phi + \boldsymbol{\lambda}^T \boldsymbol{f} \tag{4.7}$$

In order to find the optimal condition, it is necessary to impose the stationariness of the functional. The derivative of the functional with respect to any possible variation has to be null and has to be compatible with the differential equations and boundary

conditions. With a convenient choice of the adjoint variables and constants, is possible to contemporarily cancel the coefficient of each variation in equation (4.6), thus assuring the stationariness of the functional expressed by the condition $\delta J^* = 0$.
In particular, cancelling the coefficient of $\delta \boldsymbol{x}$ and $\delta \boldsymbol{u}$, are possible to derive two important relations:

- For the adjoint variables: Euler Lagrange differential equations

$$\frac{d\boldsymbol{\lambda}}{dt} = -\left(\frac{\partial H}{\partial \boldsymbol{x}}\right)^T \tag{4.8}$$

- For the controls: Algebraic equations

$$\left(\frac{\partial H}{\partial \boldsymbol{x}}\right)^T = 0 \tag{4.9}$$

The control laws have an interesting property, these laws are formal independent from the stationary point searched, in fact seeking maximum or minimum of the functional J does not affect the algebraic equations (4.9).
It is important to underline the importance of dealing with constrained controls infact controls could be limited to a particular admissible domain.
For instance, the thrust provided by a propulsor has to be positive and can not exceed a certain value, that is T_{max}, peculiar of the thruster category. In this analysis, will not be considered controls' constraints variable with time or dependent from the state vector variables. Thus, any boundary condition on the controls is constant and explicit. If such a constraint is present, the optimal value of the bound control in any point of the trajectory is the one that, belonging to the admissibility domain, maximizes (if maximum is seeked) or vice versa minimizes the Hamiltonian in that point. This concept is explained in the Pontryagin Maximum Principle (PMP).
There are two different possibilities:

- The optimal value for control is the one derived from Eq. (4.9) if it belongs to the admissibility domain. In that point the constraint does not affect the system, resulting in a locally non-constrained control

- The optimal value for control is at the domain extremes. Thus, if the optimal control that derived from Eq. (4.9) falls outside the domain, the control assumes its maximum or minimum value. In this case, the control is constrained

If the Hamiltonian is linear respect to one of the constrained controls, the system present a peculiarity. Infact in the Eq. (4.9) the contrlo does not appear directly, so it can not be determined. If this happen there are two different possibilities:

- The constrained control coefficient in equation (4.7) is not null. That means that the Hamiltonian is maximized assuming the maximum value for the control if it is positive or the minimum if it is negative. This derived from the PMP and it is often referred to it as bang-bang control

- The constrained control coefficient in equation (4.7) is null within a singular arc. It is necessary to impose the cancellation of every derivative of the coefficient itself, with respect to the time, until one of them does not explicitly contain the control. The optimal control is then determined by imposing the last derivative equal to null. It is established that the derivative degree necessary is always even. Naming the derivative's degree n, the order of the singular arch is n/2

In case the boundary conditions are missing it is convenient to refer o the j-th extreme. It is possible to write down, for the considered boundary, the conditions deriving from considering it as the final edge of the (j-1)-th sub-interval or as the initial point of the j-th sub-interval. Different condition can be considered in this case by cancelling the coefficient of $\delta\mathbf{x}_{j+}, \delta\boldsymbol{x}_{j-}, \delta t_{j+}, \delta t_{j-}$ in equation (4.6), they can be written as follows:

$$\left(-\boldsymbol{\lambda}^T{}_{j-} + \frac{\partial\varphi}{\partial\boldsymbol{x}_{j-}} + \boldsymbol{\mu}^T\left[\frac{\partial\boldsymbol{\chi}}{\partial\boldsymbol{x}_{j-}}\right]\right) = 0 \qquad j = 1, ..., n \tag{4.10}$$

$$\left(-\boldsymbol{\lambda}^T{}_{j+} + \frac{\partial\varphi}{\partial\boldsymbol{x}_{j+}} + \boldsymbol{\mu}^T\left[\frac{\partial\boldsymbol{\chi}}{\partial\boldsymbol{x}_{j+}}\right]\right) = 0 \qquad j = 1, ..., n-1 \tag{4.11}$$

$$H_{j-} + \frac{\partial\varphi}{\partial t_{j-}} + \boldsymbol{\mu}^T\frac{\partial\boldsymbol{\chi}}{\partial t_{j-}} = 0 \qquad j = 1, ..., n \tag{4.12}$$

$$-H_{j+} + \frac{\partial\varphi}{\partial t_{j+}} + \boldsymbol{\mu}^T\frac{\partial\boldsymbol{\chi}}{\partial t_{j+}} = 0 \qquad j = 1, ..., n-1 \tag{4.13}$$

where j_- and j_+ are the values assumed right before and right after the point j. As already introduced, it is important to distinguish the two instants, as a discontinuity could happen at the arcs' conjunction points. Clearly, Eq. (4.10) and Eq. (4.12) can not be considered for the starting point of the trajectory (j = 0), and Eq. (4.11) and Eq. (4.13) are not significant at the end (j = n). Eliminating the adjoint constants μ from the set of equations above, the Optimum Boundary Conditions can be defined as follow:

$$\boldsymbol{\sigma}\left(\mathbf{x}_{(j-1)+}, \mathbf{x}_{j-}, \boldsymbol{\lambda}_{(j-1)+}, \boldsymbol{\lambda}_{j-}, t_{(j-1)+}, t_{j-}\right) = 0 \qquad j = 1, ..., n \tag{4.14}$$

The final system of differential equation is composed by Eq. (4.1), Eq. (4.2), Eq. (4.8). Considering a generic state variable x, if subjected to particular boundary conditions, Eq. (4.10) and Eq. (4.11) give particular optimal values for the relative adjoint variable λ_x. In particular:

- If the state variable x value is known at the initial instant, which means that the imposed boundary conditions vector $\boldsymbol{\chi}$ contains the equation $x_0 - a = 0$, with a explicit value, on the corresponding adjoint variable λ_x there are no conditions. Thus, the adjoint variable's initial value λ_{x0} is free, this also applies for the final instant if the state variable is explicitly defined in that point.

- If the initial value of the state variable x_0 does not appear either in the function φ or in the boundary conditions, the relative adjoint variable is null at the initial instant: λ_{x0}. Also in this case, the consideration can be extended to the final instant.

- If a state variable is continuous but not explicitly defined at an internal point j (which means that the vector $\boldsymbol{\chi}$ contains $x_{j+} = x_{j-}$), the corresponding adjoint variable is continuous in that point: $\lambda_{x_{j+}} = \lambda_{x_{j-}}$

- If a state variable is continuous and known at a defined internal interface, which means that the equations $x_{j+} = a$ and $x_{j-} = a$ are contained in $\boldsymbol{\chi}$ vector, the corresponding adjoint variable in that point presents a free discontinuity. This means that its value after the point j is independent from the value it assumed before, and has to be determined through the optimization algorithm.

Is possible writing down mathematically, what just explained, as follow:

$$\begin{array}{lccc} if & x_0 - a = 0 & \longrightarrow & \lambda_{x0} \quad is \quad free \\ if & \varphi \neq f(x_0) \quad \wedge \quad \boldsymbol{\chi} \neq f(x_0) & \longrightarrow & \lambda_{x0} \quad = \quad 0 \\ if & x_{j+} = x_{j-} & \longrightarrow & \lambda_{xj+} = \lambda_{x_{j-}} \\ if & x_{j+} = x_{j-} = a & \longrightarrow & \lambda_{xj+} \neq f(\lambda_{x_{j-}}) \end{array}$$

Same consideration can be done with the Hamiltonian, infact if the Hamiltonian does not explicitly depends on the time, also Eq. (4.12) and Eq. (4.13) give some peculiar boundary conditions. In particular:

- If the initial time t_0 does not explicitly appear in the boundary conditions or in the function φ, the Hamiltonian of the system is null at the initial point: $H_0 = 0$. As always, the same conclusions can be extended to the final instant of the trajectory.
- If the internal time t_j does not explicitly appear in the function φ, which means that the only condition in which it is involved is the continuity of the time at the internal boundary $t_{j+} = t_{j-}$, the Hamltonian of the system is continuous in j: $H_{j+} = H_{j-}$
- If the internal time tj is explicitly defined, which means that in χ appears the equations $t_{j+} = a$ and $t_{j-} = a$, the Hamiltonian of the system in that point has a free discontinuity

4.1 Boundary Value Problem - BVP

The indirect method, that is used mainly to optimize orbital transferts and space missions in general, relies on the application of the Optimal Control Theory at the system of differential equations. The Optimal Control Theory, as explained in Section 4.1, formulates the optimization problem as a mathematical problem subjected to both differential and algebraic bounds. OCT can be studied as a BVP made up of the following systems:

$$\frac{d\mathbf{x}}{dt} = \mathbf{f}(\mathbf{x}, \mathbf{u}, t) \qquad \text{State Differential Equations}$$

$$\frac{d\boldsymbol{\lambda}}{dt} = -\left(\frac{\partial H}{\partial \boldsymbol{x}}\right)^T \qquad \text{Euler Lagrange Equations}$$

$$\boldsymbol{\chi}\left(\mathbf{x}_{(j-1)+}\ ,\ \mathbf{x}_{j-}\ ,\ t_{(j-1)+}\ ,t_{j-}\right) = 0 \qquad \text{Imposed Boundary Conditions}$$

$$\boldsymbol{\sigma}\left(\mathbf{x}_{(j-1)+}, \mathbf{x}_{j-}, \boldsymbol{\lambda}_{(j-1)+}, \boldsymbol{\lambda}_{j-}, t_{(j-1)+}, t_{j-}\right) = 0 \qquad \text{Optimum Boundary Conditions}$$

$$\left(\frac{\partial H}{\partial \boldsymbol{x}}\right)^T = 0 \qquad \text{Controls Algebraic Equations}$$

Some of the variables' initial value of the BVP are unknown, the solution of BVP consist in finding the initial values which satisfy contemporarily all the boundary conditions: both imposed and optimal. Such method relies on the numerical integration of the system of differential equations.
The introduced problem is marked by some singular characteristic:

- The integration domain is divided into sub-intervals called arcs. Within each arc the formulation of the differential equations is constant, but may be different from one arc to another
- The duration of each arc, or sub-interval, is in general unknown
- The variables may be discontinuous at the internal boundaries and their values after such singularity might be unknown
- The boundary conditions may be non-linear, as well they can involve the values of the variables both at the external boundaries and the external

A method for the solution of the BVP is a indispensable tool for the resolution of one of the main difficulties of the indirect optimization technique that is the solution of the boundary value problem.
The solution is achieved by reducing the BVP to a sequence of sub-problems, which is then taken to convergence exploiting the Newton method.
In order to solve the problem related to indefiniteness of the duration of the arcs, the independent variable t is replaced, only for the integration, with a new variable ε, that is defined as follow:

$$\varepsilon = j - 1 + \frac{t - t_{j-1}}{t_j - t_{j-1}} = j - 1 + \frac{t - t_{j-1}}{\tau_j}$$

with τ_j is the duration of the arc. As a consequence internal and external boundaries are fixed, in fact, thanks to the introduction of the unknown parameters τ_j, the interface points are represented by the natural values of the new independent variable ε.
In order to describe the method, the differential equations are reformulated introducing the new variables vector which include both the state variables and the adjoint variables, $\boldsymbol{y} = (\boldsymbol{x}, \boldsymbol{\lambda})$

$$\frac{d\boldsymbol{y}}{dt} = \boldsymbol{f}^*(\boldsymbol{y}, t) \tag{4.15}$$

It is important to highlight that in the considered problem, some parameters are constant, such as the duration of the arcs τ. It is therefore important to introduce a new vector $\boldsymbol{z} = (\boldsymbol{y}, \boldsymbol{c}$ where $\boldsymbol{z}$ include state variables, adjoint variables and constant parameters.
Thus, the system of differential equations can be expressed as follow:

$$\frac{d\boldsymbol{z}}{d\varepsilon} = \boldsymbol{f}(\boldsymbol{z}, \varepsilon) \tag{4.16}$$

The second member of the Eq. (4.17), considering the state variables and the adjoint variables, can be written in the following form:

$$\frac{d\boldsymbol{y}}{d\varepsilon} = \tau_y \frac{d\boldsymbol{y}}{dt} \tag{4.17}$$

while the constants' vector che be easily derived:

$$\frac{d\boldsymbol{c}}{d\varepsilon} = 0 \tag{4.18}$$

The boundary conditions can be grouped in a single vector that takes into account both the imposed ones and the optimal ones.

$$\boldsymbol{\Psi}(s) = 0 \tag{4.19}$$

where $\boldsymbol{s}$ is a new vector that includes the values of the variables at every boundary, external and internal, and the unknown constant parameters. Thus it can be written as:

$$\boldsymbol{s} = (\boldsymbol{y}_0, \boldsymbol{y}_1, ..., \boldsymbol{y}_n, \boldsymbol{c}) \tag{4.20}$$

The initial values of some variables are usually unknown, thus the research of the solution coincides with the determination, through an iterative process, of the values they have to assume to satisfy the boundary conditions in Eq. (4.19). The methodology here described is the one which consider all of the initial values as unknown. If one or more are explicitly defined, the method is simplified. The r-th iteration starts with the integration of Eq. (4.16) using as initial values $\boldsymbol{p}^r$ the ones found at the end of the previous iteration. This means that the following equality is imposed:

$$\boldsymbol{z}(0) = \boldsymbol{p}^r \tag{4.21}$$

then, the differential equations are integrated throughout the whole trajectory, taking into account the discontinuities at the internal boundaries. In order to run the process it is necessary to choose the values of the first attempt vector: $\boldsymbol{p}^1$. At each internal boundary is determined the values of the state variables and, at the end of the integration process, the error on the boundary conditions is computed. The error at the r-th is $\boldsymbol{\Psi}^r$. The variation $\Delta\boldsymbol{p}$ brings changes to the error on the boundary conditions. Considering only the first order terms, the error $\Delta\boldsymbol{\Psi}$ can be expressed as:

$$\Delta\boldsymbol{\Psi} = \left[\frac{\partial\boldsymbol{\Psi}}{\partial\boldsymbol{p}}\right]\Delta\boldsymbol{p} \tag{4.22}$$

The error has to be null in order to fulfil the boundary conditions Eq. (4.19), it is therefore necessary that $\Delta\boldsymbol{\Psi} = -\boldsymbol{\Psi}^r$. Thus result in a modification of the initial values at each iteration of:

$$\Delta\boldsymbol{p} = \boldsymbol{p}^{r+1} - \boldsymbol{p}^r = \left[\frac{\partial\boldsymbol{\Psi}}{\partial\boldsymbol{p}}\right]^{-1}\boldsymbol{\Psi}^r \tag{4.23}$$

this correction is applied until the boundary conditions are respected with the desired accuracy. The matrix present in the second term of Eq. (4.23) can be calculated as a product of two matrices:

$$\left[\frac{\partial\boldsymbol{\Psi}}{\partial\boldsymbol{p}}\right] = \left[\frac{\partial\boldsymbol{\Psi}}{\partial\boldsymbol{s}}\right]\left[\frac{\partial\boldsymbol{s}}{\partial\boldsymbol{p}}\right] \tag{4.24}$$

where the first matrix can be easily obtained derivating the boundary conditions with respect to the variables they depend on while, the second matrix, takes into account the derivative of the variables at the boundaries with respect to their initial values. Hence, the second matrix represents the values assumed by the matrix at the boundaries:

$$\left[\frac{\partial\boldsymbol{z}}{\partial\boldsymbol{p}}\right] = [\boldsymbol{g}(\varepsilon)] \tag{4.25}$$

which is obtained from the integration of the main system of differential equations (4.16) with respect to each of the initial values:

$$[\dot{\boldsymbol{g}}] = \frac{d}{d\varepsilon}\left[\frac{\partial\boldsymbol{z}}{\partial\boldsymbol{p}}\right] = \left[\frac{\partial}{\partial\boldsymbol{p}}\left(\frac{d\boldsymbol{z}}{d\varepsilon}\right)\right] = \left[\frac{\partial\boldsymbol{f}}{\partial\boldsymbol{p}}\right] \tag{4.26}$$

where the $\dot{}$ represents the derivative with respect to the new independent variable ε. The Jacobian of the principal system (1.16) can be expressed, finding the following form for Eq. (4.26):

$$[\dot{\boldsymbol{g}}] = \left[\frac{\partial\boldsymbol{f}}{\partial\boldsymbol{z}}\right]\left[\frac{\partial\boldsymbol{z}}{\partial\boldsymbol{p}}\right] = \left[\frac{\partial\boldsymbol{f}}{\partial\boldsymbol{z}}\right][\boldsymbol{g}] \tag{4.27}$$

One of the peculiarities of the described method, for the solution of indirect optimization problems, is the symmetry of some terms of the Jacobian. These properties are not

described here. The initial values of the homogeneous system (4.27) can be retrieved through the derivative of Eq. (4.22) so, the identity matrix, can be found:

$$[\boldsymbol{g}(0)] = \left[\frac{\partial \boldsymbol{z}(0)}{\partial \boldsymbol{p}}\right] = [\boldsymbol{I}] \tag{4.28}$$

It is important to underline that this method allows to deal also with discontinuities in the variables. In order to take into account a discontinuity at point i, is sufficient to update both the vector of variable $\boldsymbol{z}$ and the matrix $\boldsymbol{g}$. This operation can be realized through the relation $\boldsymbol{h}$ which connects the values of the variables before and after the discontinuity:

$$\boldsymbol{z}_{i+} = \quad \boldsymbol{h}(\boldsymbol{z}_{i+}) \tag{4.29}$$

$$[\boldsymbol{g}_{i+}] = \left[\frac{\partial \boldsymbol{h}}{\partial \boldsymbol{z}}\right] \boldsymbol{g}_{i+}] \tag{4.30}$$

This is the explanation of why the vector $\boldsymbol{s}$ has been defined without a clear distinction between y_{i+} and y_{i-}. In fact, one is a known function of the other and of the vector $\mathbf{c}$, through the relation $\mathbf{h}$. The vector $\mathbf{p}$ is reduced to the estimate only of the unknown components of the vector z(0) and the vector Φ consists only of the boundary conditions which are unknown at the initial instant so, if some of the initial values are known, the problem is simpler.
The matrix in the left term of equation (1.23) can be calculated numerically instead than analytically. In fact, its i-th row can be obtained lightly changing the i-th component of the vector $\mathbf{p}$, through the addiction of a certain Δp but keeping the other components fixed during the integration. Thus, it is possible to calculate the related change in the boundary conditions $\Delta\Psi = (\Delta p)$ and, through linearization, to obtain the corresponding row with the expression: $\Delta\Psi = (\Delta p)$. One benefit of using this method is that some times it allows to cut down the computational times but on the other hand, the convergence is not always reached. As a matter of fact, the numerical determination of the matrix in equation (1.23) is way less precise than its calculation through the solution of the system (1.27). Considering the sensibility of the problem, even adopting the most suitable value of Δp, that is usually between 10^{-7} and 10^{-6}, the introduced numerical approximation can compromise the convergence of the solution.
The numerical procedure is adopted in this work in order to calculate the Jacobian of the system and the matrix $\left[\frac{\partial \boldsymbol{\Psi}}{\partial \boldsymbol{s}}\right]$, this method is chosen in order to reduce the computational times even if is less precise than the analytical method.
The linearization, introduced in order to calculate the correction Δp of the first attempt initial values, brings to errors that can invalidate the method's convergence. In fact, the linearization can bring the error on the boundary conditions to grow instead then decreasing. In order to solve this problem, the following strategy is carried out:

- In order to prevent the method from distancing too much from the solution of the problem, the correction applied is only a fraction of the one determined using equation (1.23). In particular:

  $$\boldsymbol{p}^{r+1} = \boldsymbol{p}^{r} + K_1 \Delta p \tag{4.31}$$

  where $K_1 \in [0.1, 1]$ and his value iis determined empirically during the first implementation of the , and depend on the distance of the first solution from the one searched.

- Each iteration follow the same logic process.

  1. Through the equation (1.31) the vector of the attemp initial values $\boldsymbol{p}^{r+1}$ is determined.

2. The motion differential equation are integrated.
3. The error on the boundary conditions ${E_{max}}^{r+1}$ is compared to the one calculated from the previous iteration step ${E_{max}}^{r}$. At this point if:

$$ {E_{max}}^{r+1} < K_2 {E_{max}}^{r} $$

next iteration can be performed. The error on the boundary conditions may grow in the first iterations. Thus, the value of K_2 shall be greater than one. In particular, a value $K_2 \in [2, 3]$ brings satisfying results.

- If the error that concern to the latest iteration is too high respect to the previous, the method proceeds with the bisection of the correction. That is, the equations of motion are integrated with the attempt values:

$$ \boldsymbol{p}^{r+1} = \boldsymbol{p}^{r} + K_1 \frac{\Delta p}{2} \tag{4.32} $$

The new error is then compared to the one of the previous iteration step. If necessary, the bisection can be applied to the correction value up to 5 times. If even after such a procedure the new iteration determines an error greater than the previous one, the computation is stopped. This means that the chosen attempt solution is not compatible with the convergence of the method and has to be modified.

Chapter 5

Dynamic Problem

In this chapter the equations that describe the analysed problem will be introduced. Optimal control theory will be applied to these equations that will be specialized for the case study. Then a description of the model will be given.
Is possible to study the problem adopting the two body problem. In order to describe the motion of the satellite is necessary to introduce the vectorial differential equations:

$$\frac{d\boldsymbol{r}}{dt} = \boldsymbol{v} \tag{5.1}$$

$$\frac{d\boldsymbol{v}}{dt} = -\frac{\mu \boldsymbol{r}}{r^3} + \frac{T}{m} + \boldsymbol{a}_p \tag{5.2}$$

$$\frac{dm}{dt} = -\frac{T}{c} \tag{5.3}$$

where r is the position vector, v is the velocity vector of the spacecraft and T is the thrust vector. The trajectory of the spacecraft is controlled by the thrust vector T and the effective exhaust velocity c is assumed constant. The term a_p on the right side of Eq 5.2 is the perturbing acceleration and is composed from three contributes,

$$\boldsymbol{a}_p = \boldsymbol{a}_J + \boldsymbol{a}_{lsg} + \boldsymbol{a}_{srp} \tag{5.4}$$

where $\boldsymbol{a}_J$ is the is the perturbation due to the Earth asphericity, $\boldsymbol{a}_{lsp}$ is the perturbation due to the luni-solar gravity while $\boldsymbol{a}_{srp}$ is due to the solar radiation pressure. These perturbing acceleration will be explained better in the following section.
From the Optimal Control Theory is known that:

$$H = \Phi + \boldsymbol{\lambda}^T \boldsymbol{f}$$

that combined with the vectorial expression of the State Equation leads to:

$$H = \boldsymbol{\lambda}_{\boldsymbol{r}}^T \boldsymbol{V} + \boldsymbol{\lambda}_{\boldsymbol{V}}^T \left(-\frac{\mu}{r^2}\frac{\boldsymbol{r}}{r} + \frac{\boldsymbol{T}}{m} \right) - \lambda_m \frac{T}{c} + \mathbf{a}_P \tag{5.5}$$

Introducing the definition of Switching function:

$$S_F = \frac{\boldsymbol{\lambda}_{\boldsymbol{V}}^T \boldsymbol{T}}{mT} - \frac{\lambda_m}{c} \tag{5.6}$$

and substituting into Eq.(5.5) brings to the definition of the Hamiltonian as:

$$H = \boldsymbol{\lambda}_{\boldsymbol{r}}^T \boldsymbol{V} + \boldsymbol{\lambda}_{\boldsymbol{V}}^T \left(-\frac{\mu}{r^2}\frac{\boldsymbol{r}}{r} \right) - T\, S_F + \mathbf{a}_P \tag{5.7}$$

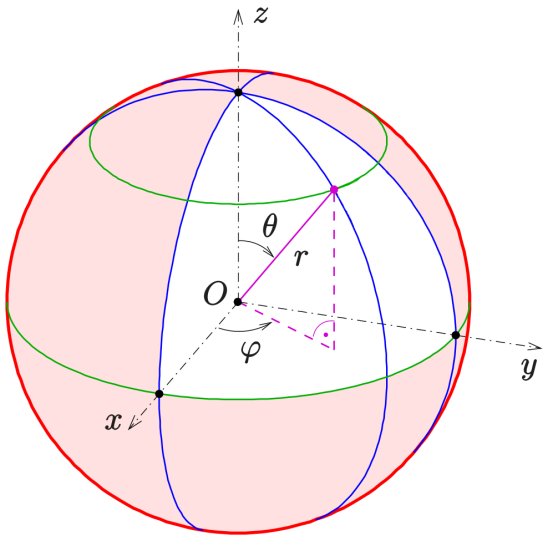

Figure 5.1: Spherical coordinates frame

The maximization of the Hamiltonian is imposed by the optimal Control Theory in order to obtain the optimal solution, thus lead to have the thrust parallel to the primer vector λ_v, as a consequence is possible to define the switching function as:

$$S_F = \frac{\lambda_V}{m} - \frac{\lambda_m}{c} \tag{5.8}$$

The definition of the switching function and therefore its sign, define the strategy that permit to maximise the Hamiltonian.

$$S_F < 0 \Rightarrow T = 0 \tag{5.9}$$

$$S_F > 0 \Rightarrow T = T_{max} \tag{5.10}$$

In order to have all the quantities on a convenient reference frame, the set of vectorial equation that describes the trajectory of the spacecraft has to be projected. The optimal frame is an inertial frame where Coriolis and inertial accelerations are not taken into account. In particular the reference frame adopted is The Earth Mean Equator and Equinox of Epoch J2000 reference frame where **I**, **J**, **K** are the unity vector along the axes of EME2000. In the model adopted precession and nutation are neglected.
Is possible to define the position vector in spherical coordinates in function of the radius r, the right ascension ϑ and the declination angle φ as follow:

$$\boldsymbol{r} = rcos\vartheta cos\varphi \boldsymbol{I} + rsin\vartheta cos\varphi \boldsymbol{J} + rsin\varphi \boldsymbol{K} \tag{5.11}$$

Topocentric reference frame is introduced, with i is the unit vector in the radial direction, j is in the eastward direction and k is in the northward direction. Is therefore possible to write the position vector with respect to the topocentric frame thanks to the rotational matrix. Starting from the Eq. 5.11, it follows that $\boldsymbol{r} = r\boldsymbol{i}$ and the velocity vector can be written as:

$$\boldsymbol{v} = \dot{\boldsymbol{r}} = u\boldsymbol{i} + v\boldsymbol{j} + w\boldsymbol{k} \tag{5.12}$$

where u, v, w are the components of the velocity radial, eastward and northward respectively.

5.1 State Variables and Adjoint Variables

By the projection of the State Equation into the chosen reference frame is possible to obtain the following relations:

$$\frac{dr}{dt} = u \tag{5.13}$$

$$\frac{d\vartheta}{dt} = \frac{v}{r cos\varphi} \tag{5.14}$$

$$\frac{d\varphi}{dt} = \frac{w}{r} \tag{5.15}$$

$$\frac{du}{dt} = -\frac{\mu}{r^2} + \frac{v^2 + w^2}{r} + \frac{T_u}{m} + (a_p)_u \tag{5.16}$$

$$\frac{dv}{dt} = \frac{-uv + vwtan\varphi}{r} + \frac{T_v}{m} + (a_p)_v \tag{5.17}$$

$$\frac{dw}{dt} = \frac{-uv - v^2 tan\varphi}{r} + \frac{T_w}{m} + (a_p)_w \tag{5.18}$$

$$\frac{dm}{dt} = -\frac{T}{m} \tag{5.19}$$

where the initial state vector is $\boldsymbol{x} = [r\ \vartheta\ \varphi\ u\ v\ w\ m]$, the component of thrust are defined as $T_u = T\ sin\gamma_T$, $T_v = T\ cos\gamma_T\ cos\psi_T$, $T_w = T\ cos\gamma_T\ sin\psi_T$ where ψ_T is the heading angle and γ_T is the elevation angle of the thrust.
The simpliness of these equation with this set of variables will facilitate the analytical derivation of the necessary condition for optimality.
It is therefore possible to formulate the expression of the Hamiltonian as follow:

$$\begin{aligned} H = {} & \lambda_r u + \lambda_\vartheta \frac{v}{r cos\varphi} + \lambda_\varphi \frac{w}{r} + \\ & + \lambda_u \left(-\frac{\mu}{r^2} + \frac{v^2}{r} + \frac{w^2}{r} + \frac{T}{m} sin\gamma_T \right) + \\ & + \lambda_v \left(\frac{uv}{r} + \frac{vw}{r} tan\varphi + \frac{T}{m} cos\gamma_T cos\psi_T \right) + \\ & + \lambda_w \left(-\frac{uw}{r} - \frac{v^2}{r} tan\varphi + \frac{T}{m} cos\gamma_T sin\psi_T \right) + \\ & - \lambda_m \frac{T}{c} \end{aligned} \tag{5.20}$$

Imposing equal to null the partial derivatives of the Hamiltonian, argument addressed in Chapter 4, is possible to obtain the optimal values of γ_T and ψ_T which are the control that define the direction of thrust.
Mathematically is possible to write:

$$\left(\frac{\partial H}{\partial \boldsymbol{u}} \right)^T = 0 \tag{5.21}$$

with $\boldsymbol{u} = [\gamma_T\ \psi_T]$ the control vector. This yields to the Algebraic Equations of Control:

$$sin\gamma_T = \frac{\lambda_u}{\lambda_V} \tag{5.22}$$

$$cos\psi_T cos\gamma_T = \frac{\lambda_v}{\lambda_V} \tag{5.23}$$

$$sin\psi_T cos\gamma_T = \frac{\lambda_w}{\lambda_V} \tag{5.24}$$

$$\tag{5.25}$$

where λ_V is the primer vector's module and can be expressed as:

$$\lambda_V = \sqrt{{\lambda_u}^2 + {\lambda_v}^2 + {\lambda_w}^2} \tag{5.26}$$

Is important to underline that the prime vector is parallel to the optimal direction of thrust.
The Euler-Lagrange equations are used in order to define the only set of equation left that is the differential equations for the adjont variables $\boldsymbol{\lambda} = [\lambda_r\ \lambda_\vartheta\ \lambda_\varphi\ \lambda_u\ \lambda_v\ \lambda_w\ \lambda_m]$ For the problem taken into account the Euler Lagrange Equations

$$\frac{d\boldsymbol{\lambda}}{dt} = -\left(\frac{\partial H}{\partial \boldsymbol{x}}\right)^T \tag{5.27}$$

becomes:

$$\begin{aligned}\dot{\lambda_r} = \frac{1}{r^2}\Bigg[\lambda_\vartheta \frac{v}{cos\varphi} + \lambda_\varphi w + \lambda_u\left(-\frac{2}{r} + v^2 + w^2\right) + \\ + \lambda_v\left(-uv + vwtan\varphi\right) + \lambda_w\left(-uw - v^2 tan\varphi\right)\Bigg] + \frac{dH}{da_p}\frac{da_p}{dr}\end{aligned} \tag{5.28}$$

$$\dot{\lambda_\vartheta} = 0 \tag{5.29}$$

$$\dot{\lambda_\varphi} = \frac{1}{r cos^2\varphi}\left(\lambda_\vartheta v sin\varphi - \lambda_v vw + \lambda_w v^2\right) + \frac{dH}{da_p}\frac{da_p}{d\varphi} \tag{5.30}$$

$$\dot{\lambda_u} = \frac{1}{r}(-\lambda_r r + \lambda_v v + \lambda_w w) + \frac{dH}{da_p}\frac{da_p}{du} \tag{5.31}$$

$$\dot{\lambda_v} = \frac{1}{r}\left[-\lambda_\vartheta \frac{1}{cos\vartheta} - 2\lambda_u v - \lambda_v(u - wtan\varphi) + 2\lambda_w vtan\varphi\right] + \frac{dH}{da_p}\frac{da_p}{dv} \tag{5.32}$$

$$\dot{\lambda_w} = \frac{1}{r}(-\lambda_\varphi - 2\lambda_u w - \lambda_v(vtan\varphi + \lambda_w u) + \frac{dH}{da_p}\frac{da_p}{dw} \tag{5.33}$$

$$\dot{\lambda_m} = \frac{T}{m^2}\lambda_V + \frac{dH}{da_p}\frac{da_p}{dm} \tag{5.34}$$

5.2 Perturbations

In order to describe in a better way the environment in which the spacecraft will work and the forces to which the spacecraft is subjected, is necessary a wider view over the three different perturbation presents into the model adopted. Common perturbations of two-body motion include a nonspherical central body, atmospheric drag, solar radiation pressure, and gravitational interactions with celestial objects like the Moon and the Sun or a third body in general. In this thesis only three of these perturbations are taken into account. In particular they will be explained in the following order: the first perturbation considered is the perturbation due to the Earth asphericity $\boldsymbol{a}_J$ then the perturbation due to the luni-solar gravity $\boldsymbol{a}_{lsp}$ and finally the solar radiation pressure $\boldsymbol{a}_{srp}$.

5.2.1 Earth Potential Model

The simplified gravitational potential of the Earth $\frac{\mu}{r}$, is due to a symmetric mass body and results in conic orbits. However, the Earth is not a spherically symmetric body but is bulged at the equator, flattened at the poles and is generically asymmetric. The

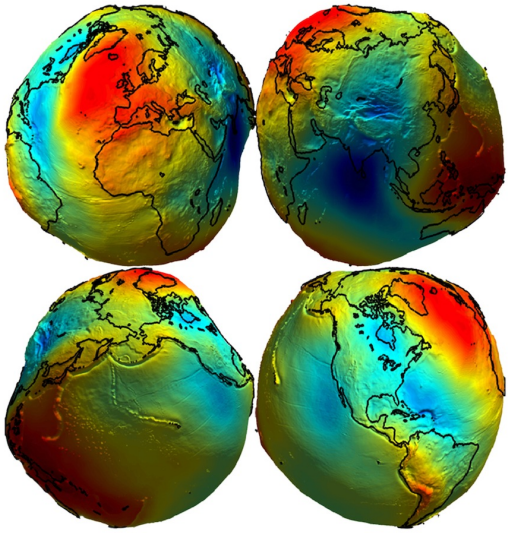

Figure 5.2: 3D representation of Earth Gravitational Model EGM2008

Earth Gravitational Model EGM2008 is utilized as description of the Earth potential and provides the normalized harmonic coefficients for the Earth gravitational potential. The "Tide Free" system is used in this thesis, but in case of the need of higher-degree terms the code can be modified in order to implement the "Zero Tide" system. The "Zero Tide" system is provided in order to minimize any chance of error that may occur while converting from one tide system to another.
Is possible to express the potential correspond to the Earth asphericity, according to EGM2008 as follow:

$$\Phi = -\frac{\mu}{r}\sum_{n=2}^{N}\left(\frac{r_E}{r}\right)^n\sum_{m=0}^{n}(C_{nm}cosm\lambda + S_{nm}sinm\lambda)P_{mn}(sin\varphi) \tag{5.35}$$

where μ is the Earth gravitational parameter, r_E is the semimajor axis of the Earth ellipsoid and N is set as equal to 8.

Normalized quantities would allow a greater accuracy but are not necessary for the present application, in fact unnormalized form is utilized using the associated Legendre functions $P_{nm}sin\varphi$ and the spherical harmonic coefficients C_{nm} and S_{nm} in order to reduce the computational time.
Since the nutation is meglected, the terrestrial latitude coincides with the declination angle φ while the longitude $\lambda = \vartheta - \vartheta_{Gref} - \omega_E(t - t_{ref})$ where ϑ_{Gref} is the position of the Greenwich right ascension at the reference time t_{ref} that coincides with 51544.5 MJD and ω_E is the rotational speed of Earth evaluated on the sidereal day, neglecting the precession of the Earth.
In order to find the perturbing acceleration due to the Earth asphericity is necessary to do the gradient of $-\Phi$. Considering the components along the topocentric frame is possible to write:

$$(a_j)_u = -\frac{\partial\Phi}{\partial r} \tag{5.36}$$

$$(a_j)_v = -\frac{\partial\Phi/\partial\vartheta}{\partial r cos\varphi} \tag{5.37}$$

$$(a_j)_w = -\frac{\partial\Phi/\partial\phi}{r} \tag{5.38}$$

Particular attenction has to be paid to the derivatives with respect to φ, in fact requires the derivative of the associated Legendre functions, which are obtained recursively using the properties of the Legendre polynomials, on the other hand the differentiation with respect to r and ϑ is easy to accomplish.

5.2.2 Luni-Solar Perturbation

Luni-Solar perturbation takes into account the effect of the gravitational attraction of the Sun and the Moon over an orbiting spacecraft. Moon and Sun position are evaluated considering DE405 JPL ephemeris, that directly provide the body position in rectangular coordinates x_b, y_b, z_b, with respect to the Earth in the International Celestial Reference Frame and therefore in the EME2000 frame. The differences between these two reference frame are vary small so they can be neglected in this problem. In order to explicit the perturbing acceleration on the spacecraft caused by a body with μ_b as gravitational parameter and $\boldsymbol{r}_b = x_b\boldsymbol{I} + y_b\boldsymbol{J} + z_b\boldsymbol{K}$ as position vector with respect to Earth (where b is $b = l$ if Moon is considered while $b = s$ in case of Sun is considered) is necessary to do the difference between the gravitational acceleration that the third body causes on the spacecraft and the one caused by Earth. It follows that the perturbing acceleration is :

$$\boldsymbol{a}_{bg} = -\left(\frac{\mu_b}{R^3}\right)\boldsymbol{R} - \left(\frac{\mu_b}{{r_b}^3}\right) r_b \tag{5.39}$$

where $\boldsymbol{R} = \boldsymbol{r} - \boldsymbol{r}_b$ is the vector that represent the relative position with respect to the perturbing body. In Fig. 5.1 is possible to see the schematic representation of the problem's geometry.
Projecting the acceleration into the topocentric reference frame is possible to obtain:

$$(a_{bg})_u = -\left(\frac{\mu_b}{R^3}\right)[(r_b)_u - r] - \left(\frac{\mu_b}{{r_b}^3}\right)(r_b)_u \tag{5.40}$$

$$(a_{bg})_v = -\left(\frac{\mu_b}{R^3}\right)(r_b)_v - \left(\frac{\mu_b}{{r_b}^3}\right)(r_b)_v \tag{5.41}$$

$$(a_{bg})_w = -\left(\frac{\mu_b}{R^3}\right)(r_b)_w - \left(\frac{\mu_b}{{r_b}^3}\right)(r_b)_w \tag{5.42}$$

where $R = \sqrt{[r - (r_b)_u]^2 + {(r_b)_v}^2 + {(r_b)_w}^2}$.

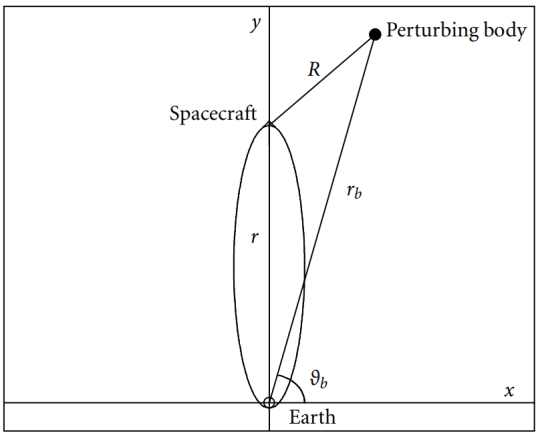

Figure 5.3: Schematic geometry of gravitational perturbation

Expliciting the position's components of the perturbing body in the topocentric reference frame, is possible to notice how the perturbing acceleration is only in function of time and state variables, in fact is possible to write:

$$(r_b)_u = \quad x_b cos\vartheta cos\varphi + y_b sin\vartheta cos\varphi + z_b sin\varphi \tag{5.43}$$

$$(r_b)_v = -x_b sin\vartheta + y_b cos\vartheta \tag{5.44}$$

$$(r_b)_w = -x_b cos\vartheta sin\varphi - y_b sin\vartheta sin\varphi + z_b cos\varphi \tag{5.45}$$

5.2.3 Solar Radiation Pressure

The Solar Radiation Pressure is a perturbing acceleration caused by the emission from the Sun of Photons. In fact the photons in light emitted from the Sun move at the speed of light and have momentum, because of that when they hit objects, and in this particular case the spacecraft, transfert momentum to that object causing an increase of the velocity in the Sun - Spacecraft direction.
Considering that the photon pressure at a distance R from the Sun is given by the relation:

$$p = \frac{L_s}{4\pi R^2 c_{light}} \tag{5.46}$$

where L_s is the total power radiated by the Sun and c_{light} is the speed of light. Assuming a reflectivity of $\eta = 0.7$ the perturbing acceleration on a spherical body with mass m and cross-section S is:

$$\boldsymbol{a}_{sp} = (1+\eta)p^* \left(\frac{R^*}{R}\right)^2 \left(\frac{S}{m}\right) \frac{\boldsymbol{R}}{R} = \frac{\Gamma \boldsymbol{R}}{mR^3} \tag{5.47}$$

where $p^* = 4.55682$ is the photon pressure at $R^* = 1$ AU.

Projecting the acceleration into the topocentric reference frame is possible to obtain:

$$(a_{srp})_u = \left[\frac{\Gamma}{mR^3}\right][(r_s)_u - r] \tag{5.48}$$

$$(a_{srp})_v = \left[\frac{\Gamma}{mR^3}\right][(r_s)_v] \tag{5.49}$$

$$(a_{srp})_w = \left[\frac{\Gamma}{mR^3}\right][(r_s)_w] \tag{5.50}$$

The solar radiation is therefore inversely proportional to the squared distance of the two bodies and caused an acceleration on the Sun spacecraft direction, the same happens

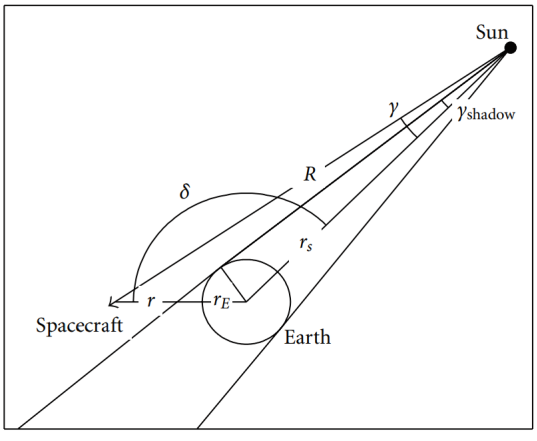

Figure 5.4: Schematic geometry of Earth's shadow for solar radiation pressure perturbation

with the solar accelerations but with opposite directions. These two perturbations can be treated simultaneously due to the similarity of the right term of Eq. (5.40), Eq. (5.41), Eq. (5.42) with Eq. (5.48), Eq. (5.49), Eq. (5.50).
In order to take into consideration the eclipses period, when spacecraft is obscured by the presence of the Earth between itself and the Sun, a conical shadow of Earth is considered; when $(r_s)_u < 0$ Sun and spacecraft are on opposite sides with respect to the Earth.
The conic shadow determined by the presence of Earth has a semi angle $\gamma_{shadow} = arcsin(r_E/r_s)$ where r_E is the Earth radius and r_s is the distance between Sun and Earth. On the other hand, the spacecraft is on a surface of a cone with semi-angle $\gamma = arcsin(rsin\delta/R)$ where δ is the angle between the Earth centered vector that points towards the Sun and the Earth centered vector that points towards the spacecraft and can be evaluated as $\delta = arcos[(r_s)_u/r_s]$.
It conveys that the spacecraft is in the Earth shadow when $\gamma < \gamma_{shadow}$ and $(r_s)_u < 0$ and thus, the spacecraft is behind the Earth from Sun's point of view.

5.3 Dimensionless Quantities

In order to formulate the problem in a more general form, dimensionless quantities are taken into account and will be described below.

5.3.1 Dimensionless Distance

Instead of using distances in kilometres to define spatial variables all the distances are expressed in a dimensionless form. If a geocentric trajectory is considered, the distance is seen as a multiple of the Earth's ellipsoid semimajor axis.

$$a_\oplus = 6378.1363 \;\; km \tag{5.51}$$

On the other hand if a heliocentric trajectory is considered, the distance is seen as a multiple of the mean Sun-Earth distance which is also know as Astronomical Unit (AU)

$$1 \; AU = 149597870.7 \; km = r_{conv} \tag{5.52}$$

The adoption of the dimensionless distance is important in order to operate with smaller and more accessible numbers, the quantities in fact are in the orders of units instead of several millions.

5.3.2 Dimensionless Velocity

As already seen for the distance, also the velocity is expressed in a dimensionless form. Also in this case if a geocentric trajectory is considered, the velocity is referred to a characteristic velocity, the first cosmic velocity.

$$v_1 = \sqrt{\frac{G \, m_\oplus}{R_\oplus}} = 7.9054 \; Km/s \tag{5.53}$$

On the other hand if a heliocentric trajectory is considered, the velocity is seen as a multiple of the circular velocity of the Earth around the Sun

$$V = \sqrt{\frac{\mu_\odot}{r_{conv}}} = 29.7847 \; Km/s \tag{5.54}$$

5.3.3 Dimensionless Time

Also time is expressed in a dimensionless form and also in this case there is a differentiation between a geocentric or heliocentric trajectory. In the first case, time become dimensionless using the reference time

$$t = \frac{a_{\oplus}}{v_1} = 806.811\ s \tag{5.55}$$

In the second case time is related to the revolution of the Earth around the Sun. Thus, radians are used to measure time instead years. Considering that in one year Earth complete a revolution around the Sun is possible to write:

$$1\ \ year = 2\pi\ rad \tag{5.56}$$

As a consequence is possible to write the reference time as follow:

$$t_{conv} = \frac{365\ days}{2\pi} = 58.1324209\ days \tag{5.57}$$

In order to define univocally the date take into account is necessary to define a date from which time is measured. As in most space mission analysis J2000 is the most used reference date, that correspond to the 12 UT 1/1/2000.

5.3.4 Dimensionless Acceleration and Dimensionless mass

It is possible to refer to the Earth's orbit to find the reference acceleration as already done with the velocity in the case of heliocentric phase. This is

$$a_{conv} = \frac{\mu_{\odot}}{{r_{conv}}^2} = 5.930083517 \cdot 10^6\ Km/s^2 \tag{5.58}$$

Also for the mass is possible to use a dimensionless form, in this case the final mass is related to the initial mass in order to have at the beginning of the mission the ratio equal to 1 while with the progression of the mission it decreases with value minor of 1.

$$m_{ratio} = \frac{m_{final}}{m_{initial}} \tag{5.59}$$

5.4 Definition of the case study

Once the set of equations that define the problem are set and the dimensionless parameters are introduced, is necessary to introduce the boundary conditions that characterize the case study. As previously introduced, the starting point of the evasion maneuver will be the Lagrangian point L_2. As a consequence:

$$\boldsymbol{r}(t_0) = \boldsymbol{r}_{\oplus}(t_0 + 0.01\ \text{AU})$$

$$\boldsymbol{V}(t_0) = \boldsymbol{V}_{\oplus}(t_0 + 0.01\ \text{AU})$$

and the angle ϑ defined as $\vartheta = \vartheta_{\odot} - \vartheta_{SC}$:

$$\vartheta(t_0) = -180\ \text{deg}$$

considering that L_2, and thus where the spacecraft is initially situated, is in opposition with respect to the Sun.
At the end of the escape maneuver the spacecraft has to reach the end of the Earth's sphere of influence and thus the distance at final time has to be fixed:

$$\boldsymbol{r}(t_F) = 0.929\ \times 10^6\ \text{Km}$$

In addition to the final position of the spacecraft, also the length of the evasion maneuver is fixed to a defined value, but it will vary from one case to the other.
After the simulations carried out maintaining the value of the characteristic energy c_3 free to vary, also c_3 will be fixed to a defined value.
In the case study considered, the trajectory is controlled by the thrust, this happens modifying itself in magnitude and direction. The direction is fixed to be parallel to the primer vector while the module follow the "Bang Bang" control law. As a consequence the magnitude of the thrust will change in function of the value that the switching function assume, in fact:

$$S_F < 0 \Rightarrow T = 0$$
$$S_F > 0 \Rightarrow T = T_{max}$$

All of the trajectories considered in this thesis are divided into two arcs, the first one is a propelled arc where the $SF > 0$ and thus the thrust assume the maximum value in magnitude; the second one is a coasting arc where the $SF < 0$ this mean that $T = 0$ and thus no thrust is present. In all the result presented in the next chapter, are visible both the arcs, the length of these arches will define in almost the cases the amount of propellant mass carriable in order to achieve the mission, this will be treaty deeper in Chapter 6.

Chapter 6

Results

In this chapter the results of the escape maneuver from the sphere of influence of Earth will be discussed. The initial point of the trajectory is the Lagrangian Point L2 of the Sun-Earth system. Initially only the departure date and the length of the mission will be varied leaving c_3 free to vary. In a second moment c_3 will be fixed to a defined value, also in this case the length of the mission and the departure date will be varied.

6.1 Evasion maneuvre from L2 Sun-Earth system, C_3 free

Before entering the particulars of the solutions, it is necessary to describe some aspects of the methodology followed. Different solutions in terms of duration of the mission and departure date are taken into account. To understand better how the results vary, the values of the dimensionless time (t_0) and the period of the mission will change. As initial values are chosen: $t_0 = 176$, duration of the mission = 80 days, subsequently t_0 will vary with steps of 0.1 from 176 to 176.5 while the period of the mission will change from 80 days to 100 days with 5 days step each time. It is chosen to vary t0 within this range because of the synodic period of the moon, in fact is almost 29 days long, that correspond with 0.5 of the dimensionless time. This means that there should be a periodicity in the results for each 0.5 of the dimensionless time so, results from t_0=176 should be almost the same as $t_0 = 176.5$. In Table 5.1 are shown the date considered as departure date in the dimensionless form, in the standard format (dd/mm/yyyy) and the angle between the Moon and Earth in the day chosen.

The results obtained considering the free case, where c_3 is not fixed to a defined value, will be divided into two parts, the first part will show the results obtained for mission longer than 80 days while the second part will show the results obtained for mission shorter than

Departure Date (Dimensionless)	Departure Date (dd/mm/yyyy)	Right Ascension Angle (deg)
176,0	05/01/2028	13,5
176,1	11/01/2028	96,1
176,2	16/01/2028	179,8
176,3	22/01/2028	257,5
176,4	28/01/2028	329,9
176,5	03/02/2028	34,5

Table 6.1: Conversion between the dimensionless form and the standard format for the departure date with the corresponding Right Ascension Angle between the Moon and Earth in that day.

Departure Data (dd/mm/yyyy)	Duration (Days)	Propelled Arc Length (Days)	Propellant Mass Utilized (Kg)
05/01/2028	100	2,79	1,208
11/01/2028	100	2,86	1,238
16/01/2028	100	1,76	0,762
22/01/2028	100	1,30	0,563
28/01/2028	100	1,89	0,820
03/02/2028	100	2,90	1,254
05/01/2028	95	3,18	1,377
11/01/2028	95	3,26	1,410
16/01/2028	95	2,15	0,930
22/01/2028	95	1,68	0,728
28/01/2028	95	2,28	0,987
03/02/2028	95	3,29	1,424
05/01/2028	90	3,67	1,591
11/01/2028	90	3,74	1,622
16/01/2028	90	2,62	1,135
22/01/2028	90	2,15	0,932
28/01/2028	90	2,76	1,196
03/02/2028	90	3,78	1,639
05/01/2028	85	4,30	1,862
11/01/2028	85	4,36	1,889
16/01/2028	85	3,20	1,388
22/01/2028	85	2,73	1,181
28/01/2028	85	3,36	1,456
03/02/2028	85	4,41	1,911
05/01/2028	80	5,08	2,200
11/01/2028	80	5,15	2,230
16/01/2028	80	3,94	1,707
22/01/2028	80	3,44	1,489
28/01/2028	80	4,10	1,774
03/02/2028	80	5,19	2,250

Table 6.2: Escape maneuver data for mission's duration over 80 days

75 days.
As can be seen in Table 5.2 the same mission can be carried out in different period and with different durations, resulting in non-identical durations of the propelled arc and final mass. Comparing the mission with the same duration but different departure date is possible to note that there is an oscillation of the length of the propelled arc and thus of the final mass. In fact, is possible to identify a minimum in the length of the propelled arc when $t_0 = 176.3$, corresponding to a minimum of the propellant mass utilized and thus a maximum of the final mass. This means that to reach the evasion from the sphere of influence of the Earth is required less propellant because the propulsor have to work for a shorter time and thus more payload can be allocated on the spacecraft. On the other hand the longer is the propelled arc the lower will be the available mass for the payload due to increased mass of propellant needed.
The causes that brings to the oscillation visible in the results is the lunisolar perturbation. Is possible to observe that the maximum correspond to a precise departure date and thus to a defined value of the right ascension angle between Moon and Earth at the initial time,

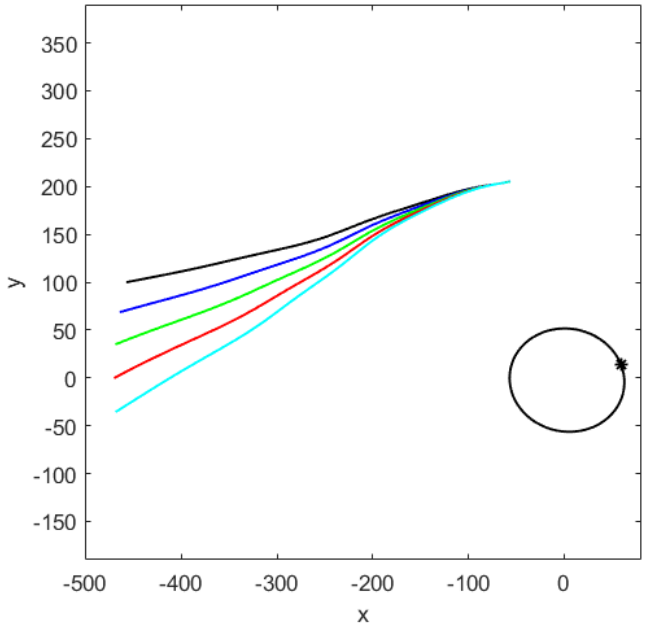

Figure 6.1: Evasion maneuver from L2 Sun-Earth, t_0=176; duration 80 days (black), 85 days (blue), 90 days (green), 95 days (red), 100 days (cyan)

that is $\theta_b \simeq 257^\circ$.
Considering now the missions with different duration but the same departure date is possible to note that leaving L_2 in $t_0 = 176.3$ is favourable in terms of final mass in almost the cases. Comparing mission with length of 100 days and 80 days is possible to note that the differences are mainly on the length of the propelled arc, in fact in the first case the thrust effort has to be lower than in the second case. The first case has to be carried out in a longer time and thus a smaller propellant output is needed, since relying on much time achieve the mission there is a lower use of thrust and a higher final mass. The second case, on the other hand, is linked to a broader use of thrust, resulting in a higher need of propellant. Considering Figure 6.1 is possible to notice that the evasion maneuver is not a perfect hyperbola because of the influence of Sun, in fact, when the distance from Earth is wide, the influence of Sun tend to modify the trajectory. Considering Figure 6.2 that represent the missions with the same length but different departure date is possible to identify how the starting point move, L_2 in fact rotate at the same angular speed of the Sun-Earth system, thus modifying t_0 also the position of L_2 with respect to the Earth will change. On the other hand, by maintaining the same departure date but modifying the length of the mission, can be easily seen that L_2 do not vary his position but the trajectory is different. If the mission has to be accomplished in 80 days the propelled arc last more than in the case of 100 days, this place the spacecraft in a more energetic trajectory as it can be seen from Figure 6.1.
From Figure 6.3 to Figure 6.8 are shown the position of the Moon, the spacecraft, and the Sun during the escape maneuver. In order to make the figure more understandable, Sun's position vector has been scaled by 100. For a fully understanding of the result it is proved necessary to decrease the duration of the mission varying, in the same way done previously, the duration of the mission. The following result will take into consideration mission with duration between 75 days and 45 days with 5 days step and t_0 which vary from 176 and 176.5 with 0.1 step. Simulation with duration of the mission lower than 45 days are not taken into account because the length of the propelled arc lasted more than

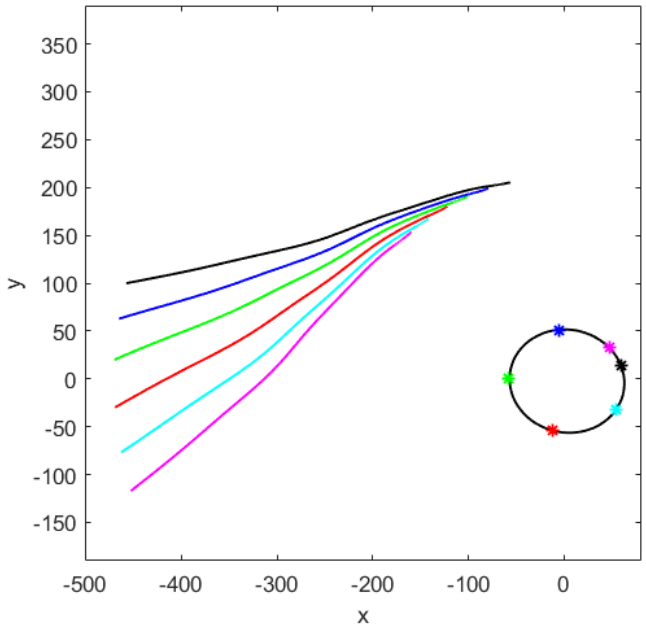

Figure 6.2: Evasion maneuver from L2 Sun-Earth, t_0 =176 (black),t_0 =176.1 (blue), t_0 =176.2 (green), t_0 =176.3 (red), t_0 =176.4 (cyan), t_0 = 176.5 (magenta); duration 80 days; moon orbit (black) with asterisk indicating the moon position at the initial time

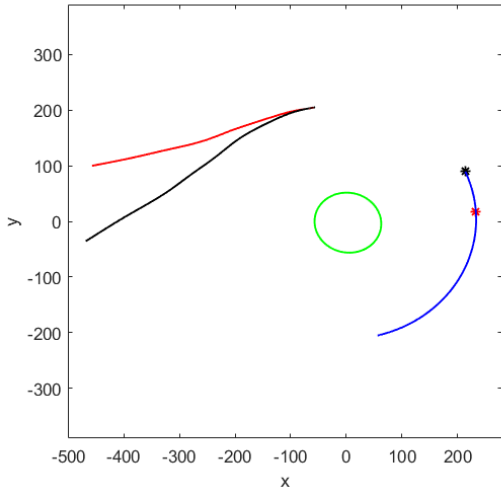

Figure 6.3: Escape maneuver from L2 Sun-Earth; Sun orbit (blue), Moon orbit (green), SC trajectory (80 days red, 100 days black), t0 = 176. The asterisk indicate the final position of the Sun.

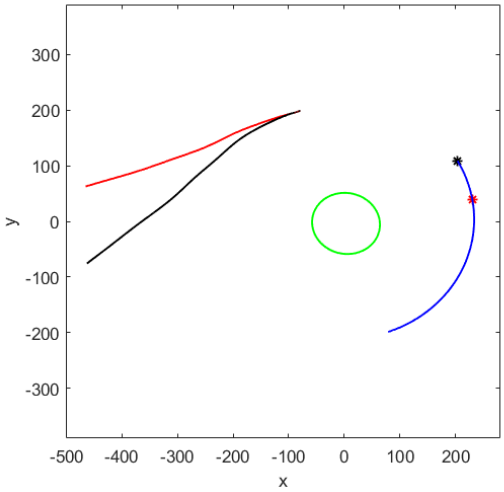

Figure 6.4: Escape maneuver from L2 Sun-Earth; Sun orbit (blue), Moon orbit (green), SC trajectory (80 days red, 100 days black), t0 = 176.1. The asterisk indicate the final position of the Sun.

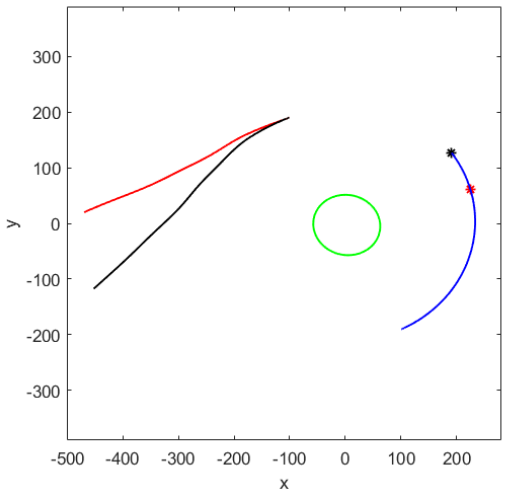

Figure 6.5: Escape maneuver from L2 Sun-Earth; Sun orbit (blue), Moon orbit (green), SC trajectory (80 days red, 100 days black), t0 = 176.2. The asterisk indicate the final position of the Sun.

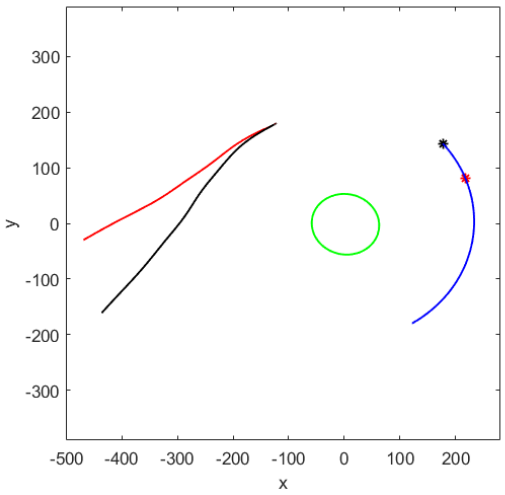

Figure 6.6: Escape maneuver from L2 Sun-Earth; Sun orbit (blue), Moon orbit (green), SC trajectory (80 days red, 100 days black), t0 = 176.3. The asterisk indicate the final position of the Sun.

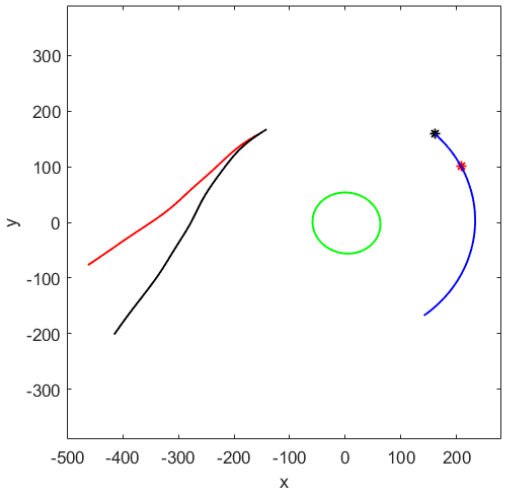

Figure 6.7: Escape maneuver from L2 Sun-Earth; Sun orbit (blue), Moon orbit (green), SC trajectory (80 days red, 100 days black), t0 = 176.4. The asterisk indicate the final position of the Sun.

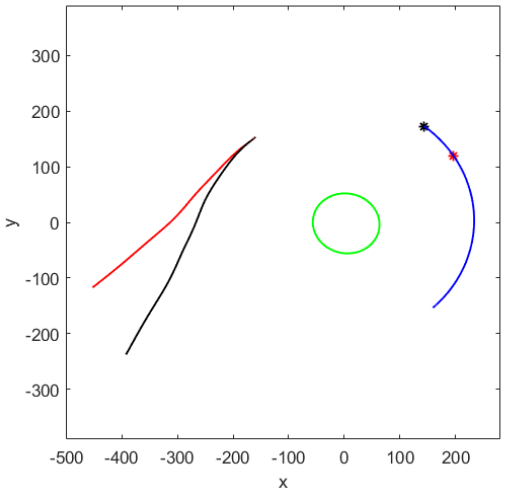

Figure 6.8: Escape maneuver from L2 Sun-Earth; Sun orbit (blue), Moon orbit (green), SC trajectory (80 days red, 100 days black), t0 = 176.5. The asterisk indicate the final position of the Sun.

the escape maneuver itself.
Is possible to notice from Figure 6.9 that the fold caused on the trajectory by the increase influence of the Sun is much more closer to the initial point with the decreasing length of the mission, this because the shorter is the mission the faster the spacecraft reach the limit of Earth's sphere of influence due to the increasing length of the propelled arch.
Considering Table 6.3 is possible to notice that the trend of the quantities, given the same duration of the mission and varying t_0 is the same of the Table 6.2. There is still a minimum on the length of the propelled arc for $t_0 = 176.3$ thus lead to a minimum on the propellant mass utilized as can be easily seen in Table 6.3.
On the other hand if is considered the same t_0 but the duration of the mission is varied, is possible to notice that the final mass decrease due to the longer duration of the propelled arc, in addition is possible to underline that, the shorter is the mission the longer is the propelled arc and compared to the duration of the mission it gains of importance, in fact in the case of: $t_0 = 176$, Duration 45 days, the propelled arc last more than the half of the total duration of the escape maneuver while in the case of $t_0 = 176$, Duration 75 days it is less than 1/10th of the total time of the mission. This lead to a great decrease of the final mass compared to the results obtained for mission longer than 80 days.
Comparing the results obtained for missions with $duration = 70, 75$ days; $t_0 = 176$ and $duration = 50, 45$ days; $t_0 = 176$ is possible to notice that the differences of the final mass between $75 - 70$ days is almost 0.5 Kg while between 50 - 45 is around 3.5 Kg, this means that the shorter is the mission the higher will be the loss in terms of payload's mass, in fact is necessary to take into account that the propellant mass needed for spacecraft to perform the maneuver will rise due to the increase of the duration of the propelled arc. The length of the propelled arc is not only linked to the duration of the mission itself but also to other factors that will be introduced and discussed in the following pages.

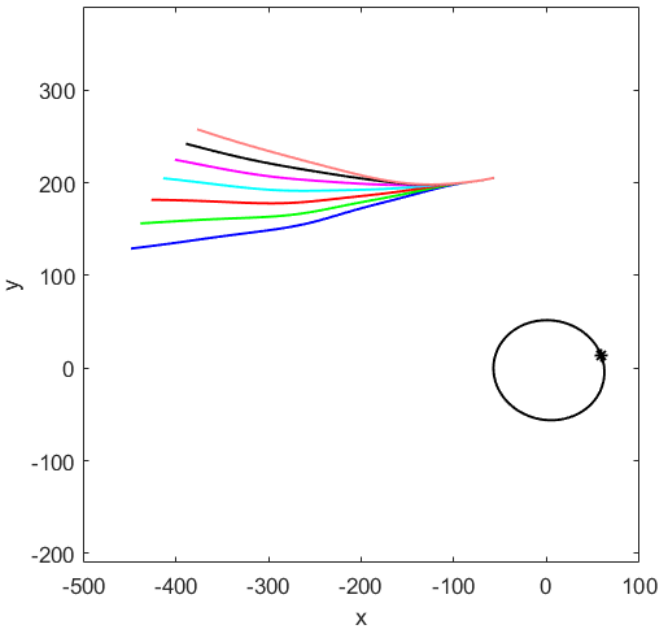

Figure 6.9: Evasion maneuver from L2 Sun-Earth, t_0=176; duration 75 days (blue), 70 days (green), 65 days (red), 60 days (cyan), 55 days (magenta), 50 days (black), 45 days (orange); moon orbit (black) with asterisk indicating the moon position at the initial time

Departure Data (dd/mm/yyyy)	Duration (Days)	Propelled Arc Length (Days)	Propellant Mass Utilized (Kg)
05/01/2028	75	6,05	2,620
11/01/2028	75	6,14	2,659
16/01/2028	75	4,88	2,116
22/01/2028	75	4,34	1,881
28/01/2028	75	5,01	2,171
03/02/2028	75	6,16	2,669
05/01/2028	70	7,27	3,149
11/01/2028	70	7,38	3,197
16/01/2028	70	6,09	2,637
22/01/2028	70	5,52	2,390
28/01/2028	70	6,19	2,681
03/02/2028	70	7,38	3,197
05/01/2028	65	8,85	3,835
11/01/2028	65	8,96	3,882
16/01/2028	65	7,62	3,299
22/01/2028	65	7,04	3,049
28/01/2028	65	7,74	3,353
03/02/2028	65	8,97	3,883
05/01/2028	60	11,00	4,765
11/01/2028	60	11,06	4,791
16/01/2028	60	9,60	4,157
22/01/2028	60	9,02	3,906
28/01/2028	60	9,81	4,249
03/02/2028	60	11,11	4,814
05/01/2028	55	14,00	6,065
11/01/2028	55	14,01	6,068
16/01/2028	55	12,30	5,325
22/01/2028	55	11,67	5,052
28/01/2028	55	12,61	5,460
03/02/2028	55	14,11	6,111
05/01/2028	50	18,42	7,979
11/01/2028	50	18,44	7,988
16/01/2028	50	16,28	7,050
22/01/2028	50	15,46	6,696
28/01/2028	50	16,62	7,196
03/02/2028	50	18,51	8,017
05/01/2028	45	26,15	11,325
11/01/2028	45	26,30	11,392
16/01/2028	45	23,06	9,986
22/01/2028	45	21,78	9,433
28/01/2028	45	23,31	10,095
03/02/2028	45	26,20	11,347

Table 6.3: Escape maneuver data for mission's duration under 80 days

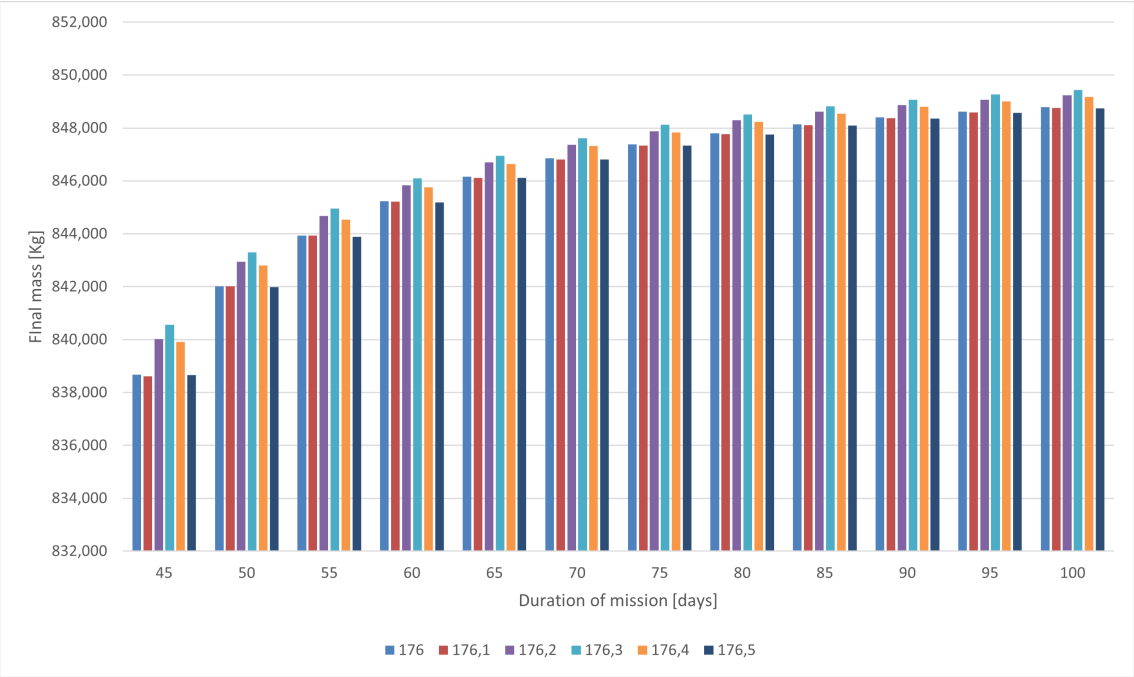

Figure 6.10: Final mass compared in function of the duration of the mission considering different departure time t_0: 176 (blue), 176.1 (red), 176.2 (violet), 176.3 (light blue), 176.4 (orange), 176.5 (dark blue)

Considering Figure 6.10 is important to notice that one of the most important factors that has an impact on the propellant mass consumed is the influence that the Moon has on the spacecraft. This effect is more visible in the first phases of the escape maneuver, where the spacecraft is closer to the Moon. Considering long mission the position of the Moon slightly influence the amount of propellant needed to accomplish the escape maneuver while, for shorter missions, the choice of the departure day is fundamental. In fact, choosing correctly the departure date can allow to reduce the propellant mass The Moon during its revolution around the Earth can push, or pull, the spacecraft. If the spacecraft is in a favourable position will be pushed from the Moon and will gain velocity, on the other hand it will lose velocity. Considering the case where $t_0 = 176.3$, at the beginning the Moon is almost in opposition with the spacecraft, this means that, the spacecraft can take advantage of the position of the Moon nearly for all the first phases of the maneuver, even if in the initial part of the trajectory the spacecraft is not in the best position to be accelerated, while when the effect of the Moon is unfavourable the distance is already grown an thus the negative effect is lower. Considering, for example, the mission with duration of 45 days, during this period the Moon will do almost one and a half rotation around Earth, this mean that the spacecraft will only experience once the push or the pull of the Moon. As a consequence that passage of the Moon will define any gain or loss in term of speed due to the gravity of the Moon. On the other hand if the mission is longer, the spacecraft will experience more time the pull or the push of the Moon and therefore a flattening on the differences previously found on the values of the final mass is found (e.g. 100 days). As is expected the value for $t_0 = 176$ and $t_0 = 176.5$ are almost the same also in terms of final mass.

The influence of the Moon is visible from Fig 6.11 to Fig 6.16. In all of the pictures are present two curves, the blue one is the evolution of c_3 during the evasion maneuver considering the influence of the Moon, the red one, on the other hand, is the evolution

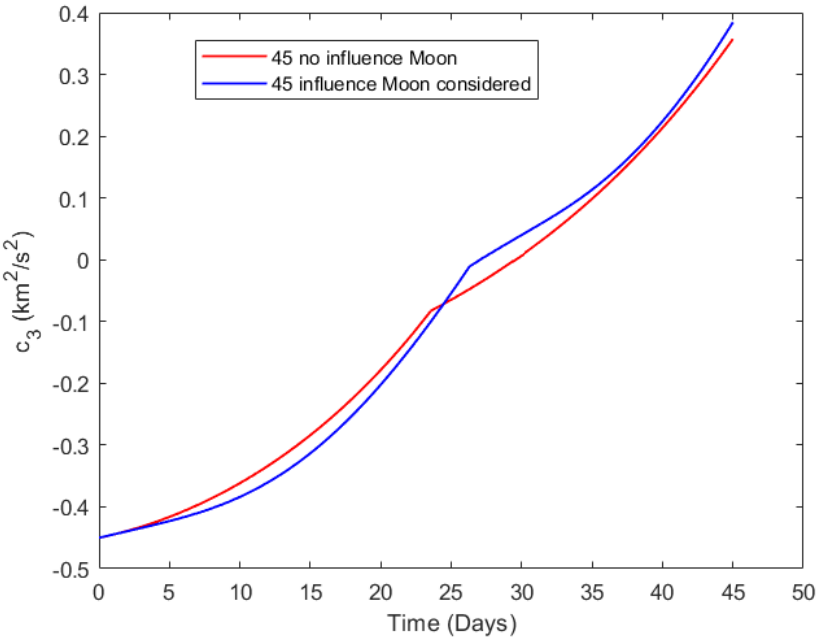

Figure 6.11: Evolution of the value of c_3 during the evasion maneuver considering the perturbation due to the presence (blue case), or the absence (red case) of the Moon. Departure day: 11/01/2028, length of the mission 45 days.

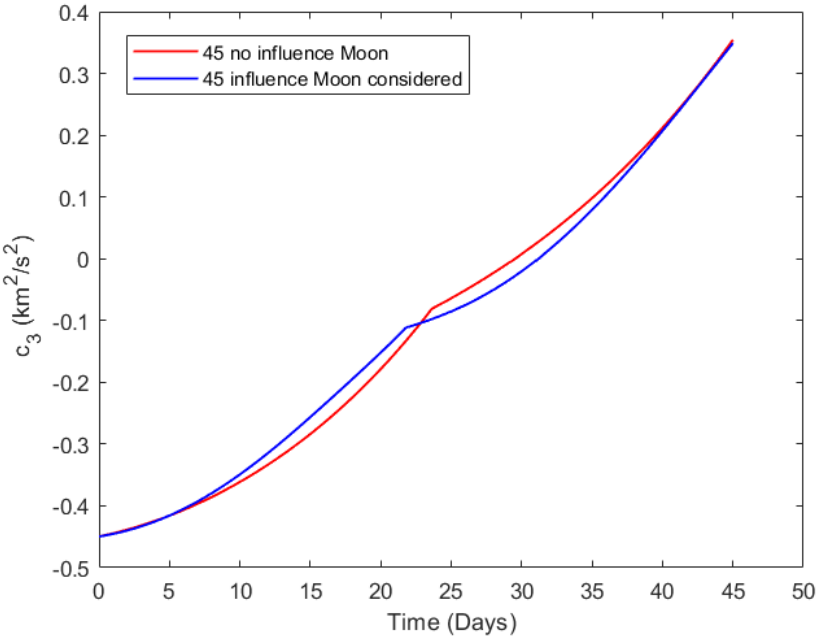

Figure 6.12: Evolution of the value of c_3 during the evasion maneuver considering the perturbation due to the presence (blue case), or the absence (red case) of the Moon. Departure day: 22/01/2028, length of the mission 45 days.

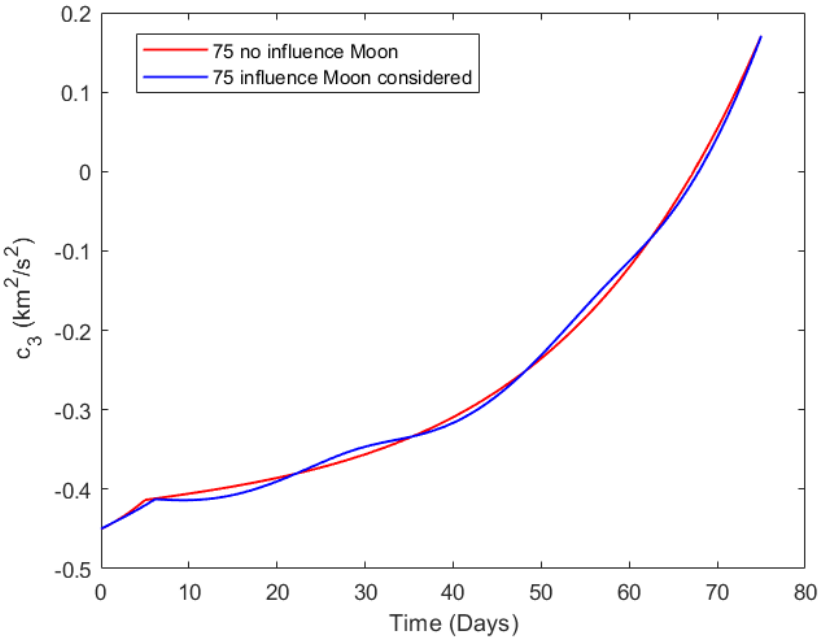

Figure 6.13: Evolution of the value of c_3 during the evasion maneuver considering the perturbation due to the presence (blue case), or the absence (red case) of the Moon. Departure day: 11/01/2028, length of the mission 75 days.

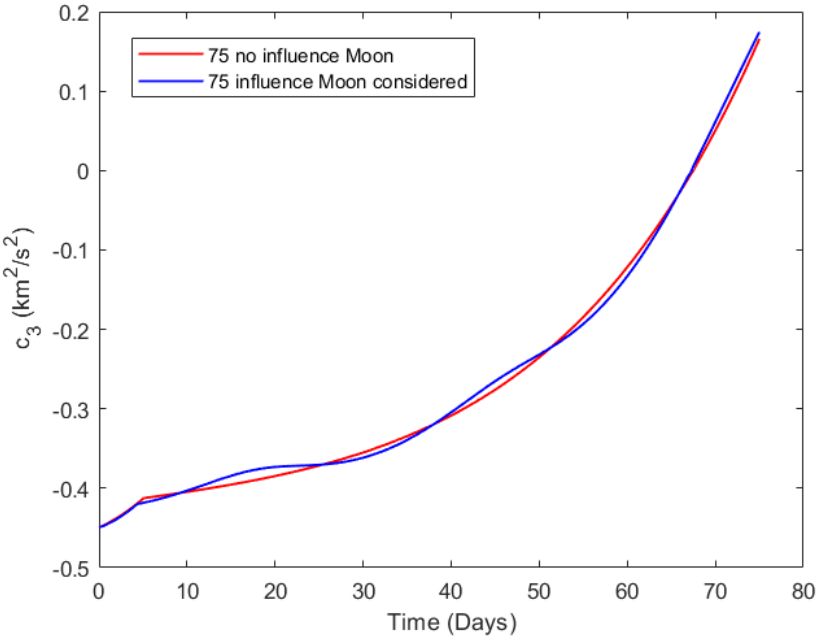

Figure 6.14: Evolution of the value of c_3 during the evasion maneuver considering the perturbation due to the presence (blue case), or the absence (red case) of the Moon. Departure day: 22/01/2028, length of the mission 75 days.

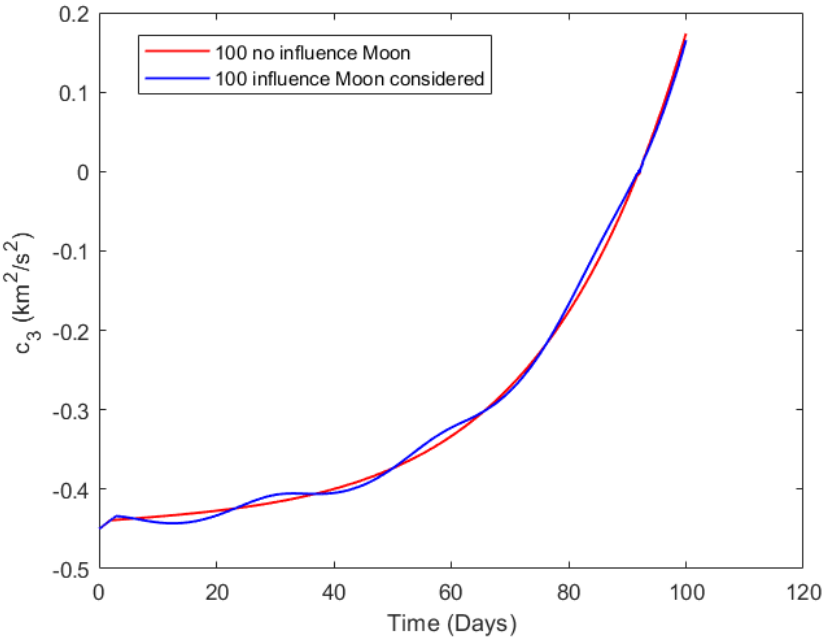

Figure 6.15: Evolution of the value of c_3 during the evasion maneuver considering the perturbation due to the presence (blue case), or the absence (red case) of the Moon. Departure day: 11/01/2028, length of the mission 100 days.

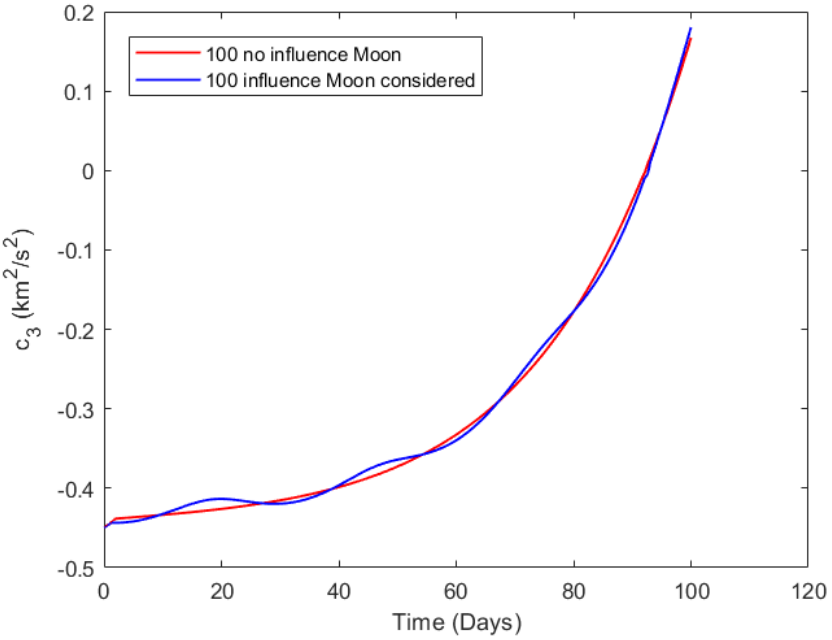

Figure 6.16: Evolution of the value of c_3 during the evasion maneuver considering the perturbation due to the presence (blue case), or the absence (red case) of the Moon. Departure day: 22/01/2028, length of the mission 100 days.

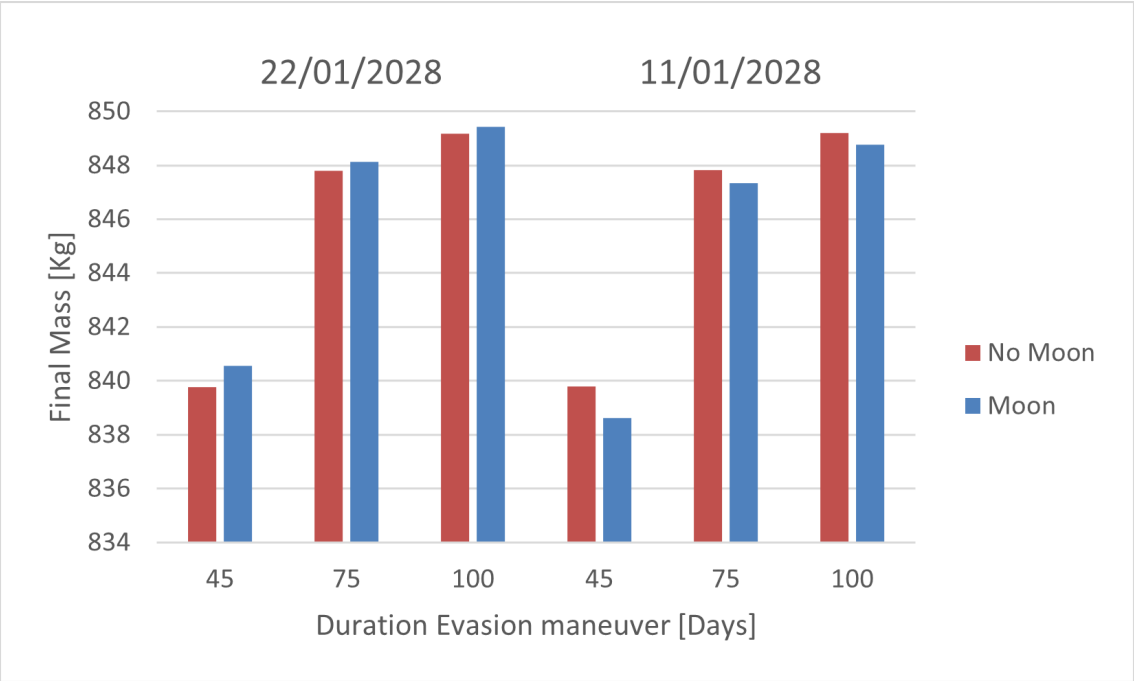

Figure 6.17: Final mass compared in function of the duration of the mission considering different departure date: 22/01/2028, 11/01/2028. Blue case is considering the perturbation of the Moon while red case are the results obtained without consider the Moon

of c_3 in the case of the impact of the Moon is not considered. Two cases are taken into account: in Fig 6.11, Fig. 6.13, Fig 6.15 are considered trajectories that have as a departure day the 11/01/2028, while in Fig 6.12, Fig 6.14, Fig 6.16 the departure day is the 22/01/2028. These two dates are chosen because the Moon in 11 days almost moves 180 degrees around Earth, and so, two different behavior of the spacecraft are deductible, as visible in the following figures. Given a mission of 45 days, different considerations can be deduced from Fig 6.11 and Fig 6.12. In the first case, on a given day, is possible to notice that the value of c_3, where the Moon is present, is slightly lower than where Moon is not considered. This underlines the braking effect that the Moon has on the spacecraft. As a consequence, to fill the gap of c_3 caused by the effect of the Moon, an increase of the propelled arc's time is needed, and therefore an increase of the propellant mass utilized as shown in Fig 6.17. On the other hand, considering 22/01/2028 as the departure date is possible to observe how the position of the Moon influence positively the trajectory. In this case, the influence of the Moon causes an increase of c_3 compared to the case without the influence of the Moon, with a consequent decrease of the propelled arc's length and therefore of the propellant mass. From Fig 6.17 is visible that, leaving the second Lagrangian point on 22/01/2028, causes a decrease of the propellant mass needed of almost 10%. Leaving on 11/01/2028, on contrary, causes an increase of the propellant mass of almost the 10%, which corresponds to an increase of almost 1 Kg.
Given a longer mission, is possible to notice how the impact that the presence of the Moon has, on both characteristic energy and consumption, tends to decrease. Considering the mission that lasts 85 days and so Fig. 6.13 and Fig 6.14 is visible how the Moon causes an oscillation on the value of c_3 that has a periodicity over 27 days; this is heavier when the spacecraft is close to Earth, but, with the increase of the distance, it tends to disappear. Examining the most favorable case, (the one which considers the departure date the 22/01/2028) is possible to notice how the push of the Moon causes not only a decrease of the propellant mass needed but also a soft increase in the final value of c_3.

Same considerations but with opposite results can be made for the trajectory that leaves the second Lagrangian Point the 11/01/2028. The solutions obtained for the 100 days case follow the same trend analyzed for the mission of 85 days, the main difference stays in the number of oscillations, which is increased due to the longer length of the evasion maneuver and on the gain, or loss, in terms of mass.
As can be deduced from the results obtained, leaving L_2 on 22/01/2028 is the best choice in terms of payload mass carriable thanks to the positive influence that the Moon has on the spacecraft.
The energy that the evasion trajectory has at final time is an interesting value to investigate, this value is the energy that the spacecraft has when it leaves the Earth's sphere of influence.
Is therefore necessary to consider not only the influence of the Moon on the spacecraft but also the influence of the Sun. The influence of the Sun is, in fact, one of the main perturbative forces that acts on the spacecraft and the main accelerating source for the spacecraft. Given the model, shown in Chapter 5, adopted in the thesis is possible to notice that there are 2 possible positions where the accelerating effect of the Sun has a maximum positive, and thus the most favourable accelerating effect on the spacecraft, for $\vartheta_b = -135$ and $\vartheta_b = 45$ deg and 2 positions where the accelerating effect of the Sun has a maximum but negative, and thus the most unfavourable accelerating effect on the spacecraft. Considering the escape maneuver to perform, and the initial position, that is the L_2 point of the Sun - Earth system, the initial angle between the Sun and the Spacecraft is $\vartheta_b = -180$ deg. The target is to allow the spacecraft to reach the angle of $\vartheta_b = -135$ deg with respect to the Sun in order to take advantage of the accelerating effect of the Sun. This is possible because, thanks to the propelled arc, the spacecraft move to a more energetic orbit and therefore to a slower orbit. This allow the Sun to reach the wanted position. Obviously the length of the mission influence not only the angle, and thus the perturbation of the Sun, but also the c_3 known as the hyperbolic excess energy or characteristic energy. The characteristic energy is defined as $c_3 = v_\infty^2 = 2E_f = -\frac{1}{a}$.
As it is possible to see from Table 6.4 the values of the hyperbolic excess energy at final time are quite low, the magnitude in fact is in the order of 10^{-1}, this means that the trajectory for the escape maneuver is almost a parabola. The value in Table 6.4 are in the dimensional form, the dimensionless terms, in fact, are multiplied by the square of the first cosmic velocity.

Duration	Departure Date					
(Days)	176	176,1	176,2	176,3	176,4	176,5
100	0,1578	0,1654	0,1801	0,1804	0,1609	0,1426
95	0,1712	0,1618	0,1647	0,1697	0,1703	0,1561
90	0,1834	0,1726	0,1589	0,1547	0,1624	0,1676
85	0,1788	0,1861	0,1677	0,1482	0,1480	0,1624
80	0,1649	0,1837	0,1831	0,1563	0,1410	0,1482
75	0,1554	0,1711	0,1850	0,1747	0,1487	0,1410
70	0,1604	0,1616	0,1751	0,1829	0,1701	0,1487
65	0,1845	0,1669	0,1677	0,1791	0,1862	0,1734
60	0,2109	0,1948	0,1754	0,1772	0,1911	0,1997
55	0,2314	0,2346	0,2095	0,1925	0,2001	0,2193
50	0,2653	0,2807	0,2683	0,2424	0,2351	0,2535
45	0,3699	0,3848	0,3638	0,3494	0,3396	0,3602

Table 6.4: Hyperbolic excess energy at final time in $[\frac{km^2}{s^2}]$

There is no periodicity in the results and also the oscillation that was identified into Table 6.2 and Table 6.3 varying only the duration of the mission and fixing t_0 is not present. This is linked to the relative position between the spacecraft and the Moon but also, and in a greater way, to the position and the influence of the Sun.

6.2 Evasion maneuvre from L2 Sun-Earth system, C_3 fixed

In order to see how quantities vary for a fixed value of final energy, it has been decided to fix c_3 and varying the time of the mission and the departure date. Fixing the final value of c_3 is important because, if the final goal is to reach, an outer or inner, planet is necessary to escape from the Earth's sphere of influence with a well defined value of hyperbolic excess energy and not with a random one. As starting point is decided to use $c_3 = 0.16 \left[\frac{m^2}{s^2}\right]$ and proceed as done before. As first iteration is chosen to analyse the solution with departure at $t_0 = 176$ modifying the duration of the mission from 100 days to the lowest possible, always with 5 days step from one length to the next one.
Also in this case the results obtained follow, for almost the cases, the trend previously found. Is expected that the final mass has to be lower than in the case analysed before, and this is visible from Table 6.5. In this case, in fact, the energy at final time has to be fixed to a certain value, thus is necessary to increase the time of the propelled arc in order to allow the achievement of the chosen c_3. The values of the final mass are not so far from the first case values for long mission but, when mission become shorter, the differences between the two cases begin to increase. Due to the length of the mission and to the fact that the spacecraft has to reach a fixed hyperbolic excess velocity, the shorter is the mission the higher will be the duration of the propelled arc. Thus, in some cases is proved impossible to reach the expected results with mission shorter than 50 days long, in other mission is only possible to reach the limit of 55 days, thus because the duration of the propelled arc will last more than the duration of the evasion maneuver itself and so the results are not taken into account.
Before entering in the analysis of the results of the cases is important to underline that in the case of *95 days* long mission two results are found as possible trajectories, as is possible to see in Table 6.6.

Plotting the evolution of the semi-major axis a in function of time is possible to notice that in case (b), during the propelled arc there is a first phase where the semi-major axis decreases, followed by a phase where a increase. The combination of these two phases lead to an increase of the length of the propelled arc with a decrease of the final mass. Since the goal of the mission is to perform an evasion maneuver maximizing the payload,

Duration (Days)	Duration Propelled Arc (Days)	Final mass (Kg)
100	2,80	848,79
95	3,36	848,55
90	4,53	848,04
85	5,05	847,81
80	5,17	847,76
75	6,23	847,30
70	7,28	846,85
65	14,54	843,70
60	18,19	842,12
55	22,53	840,24

Table 6.5: Escape maneuver result, mission length lower than 100 days, c_3 fixed, Departure day 05/01/2028.

Case	Duration (Days)	End time Propelled Arc	Final mass (Kg)
(a)	95	359,40	848,54
(b)	95	3570,92	835,55

Table 6.6: Case (a) and case (b) results for a 95 days long escape maneuver

this solution will be discarded at the expense of case (a) where only the acceleration phase is present with a reduction of the length of the propelled arc of almost the 90% of time and an increase in terms of final mass of almost 7 Kg. The main difference between these two solutions is the different strategy adopted in the propelled arc. From Fig 6.18 can be easily seen also the discontinuity caused by the end of the propelled arc, this lead to have values of the semi-major axis that does not change a lot but fluctuate. The fluctuation is caused by the interaction of the spacecraft with the Moon while the trend that led to the progressive growing of a is due to the increasing influence of Sun on the spacecraft. The evolution of the trajectory from being elliptical to parabolic, initially, and then hyperbolic can be seen from the evolution of the semi-major axis shown in Figure 6.19. In the last part of Figure 6.19 is also possible to notice the discontinuity in a due to the transition from a parabolic trajectory to a hyperbolic one.
Comparing the results obtained fixing c_3 with the ones where it is free, is possible to notice that; while in the second case with the decrease of the length of the mission an exponential trend is visible in the duration of the propelled arc, in the first case this trend is not visible. Is necessary to underline that the free case is the optimal case, in fact the results take into account the trajectory that maximise the favourable accelerating effect of the presence of the Moon and the Sun, as a consequence the final mass of all the cases with $c_3 = 0.16$ will be lower or at most the same of the free solution.

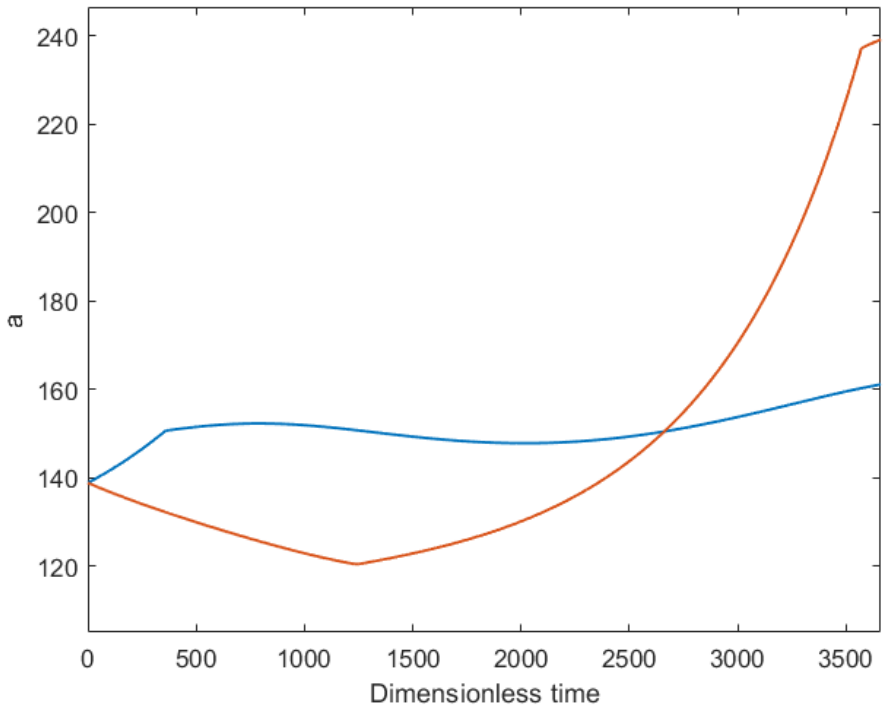

Figure 6.18: Focus on the first part of the evolution of the semi-major axis in function of time for the mission with duration of 95 days, case (a) in blue, case (b) in orange.

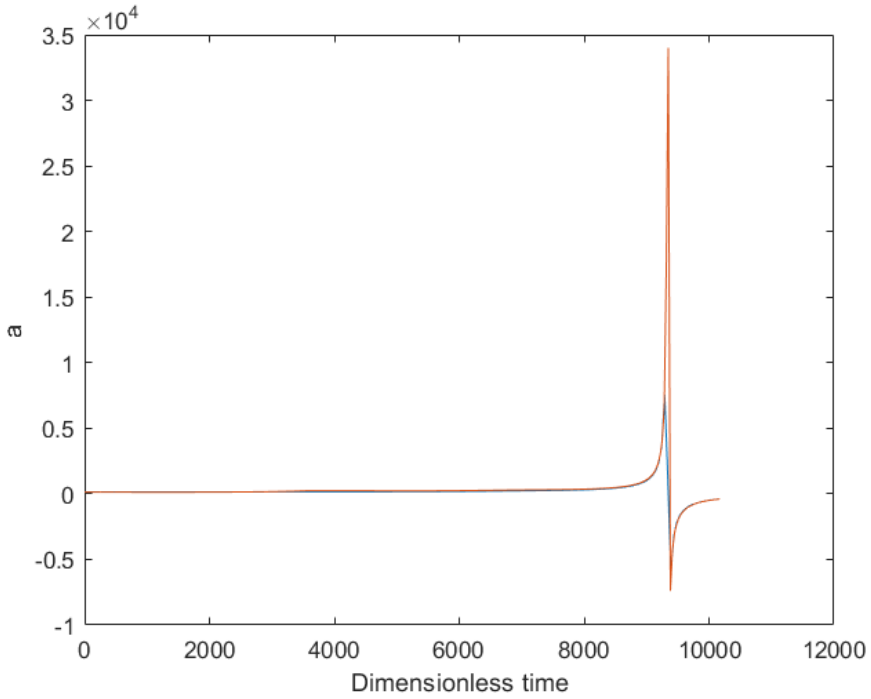

Figure 6.19: Evolution of the semi-major axis in function of time for the mission with duration of 95 days, case (a) in blue, case (b) in orange.

In order to respect the constraint, put over the c_3, the spacecraft has to reduce, or increase, its velocity depending on the value of c_3 reached in the free, and so optimal, case; this lead to a variation of the final mass that is strictly linked to the differences between the two values of c_3. In fact, plotting the final mass of the spacecraft in the free case and in the fixed case (Fig 6.20) in function of the length of the mission, and comparing it with Table 6.7, is visible that the further is the value of c_3 from the free case, the higher will be the loss in terms of final mass.

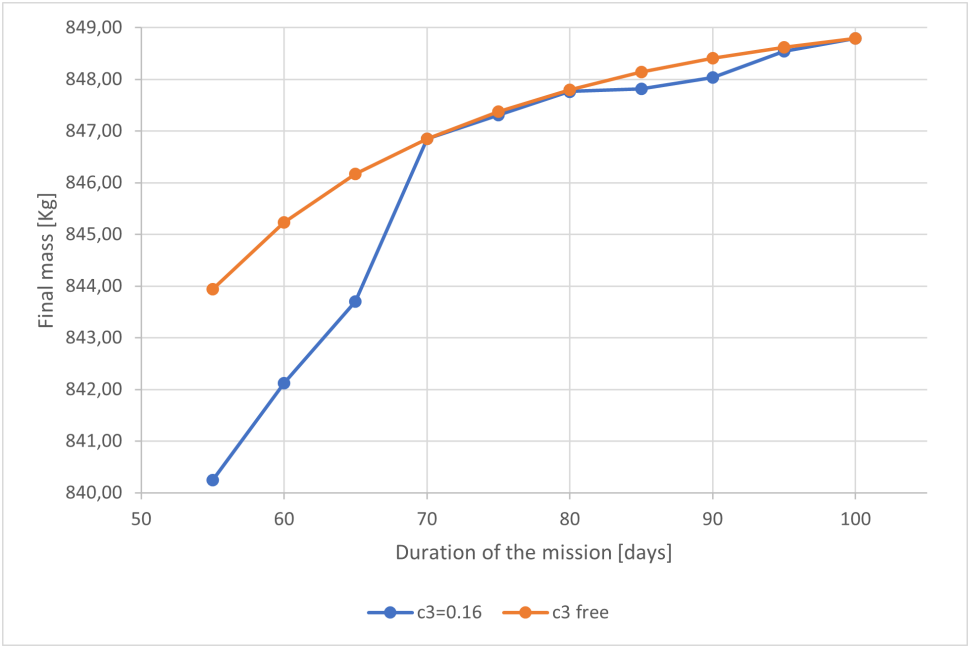

Figure 6.20: Evolution of the final mass in the case of c_3 free and $c_3 = 0.16$, $t_0 = 176$

Duration Escape Maneuver (days)	Final Mass $c_3 = 0.16$	Final Mass c_3 free	Delta Mass	c_3 free	Delta c_3
100	848,79	848,792	0,003	0,1578	0,0022
95	848,55	848,623	0,076	0,1712	0,0112
90	848,04	848,409	0,372	0,1834	0,0234
85	847,81	848,138	0,325	0,1788	0,0188
80	847,76	847,800	0,037	0,1649	0,0049
75	847,30	847,380	0,076	0,1554	0,0046
70	846,85	846,851	0,003	0,1604	0,0004
65	843,70	846,165	2,461	0,1845	0,0245
60	842,12	845,235	3,112	0,2109	0,0509
55	840,24	843,935	3,694	0,2314	0,0714

Table 6.7: Comparison between final masses of c_3 free case and $c_3 = 0.16$ case , $t_0 = 176$

As is possible to see from Figure 6.20, the reduction of the length of the mission from 70 days to 65 days brings to an increase of the duration of the propelled arc, which almost doubled with respect of the 70 days case as is visible in Table 6.5. The increased length of the propelled arc is a consequence of the c_3 value in the free case. The c_3's value in this case is quite far from the imposed value of 0.16 $\frac{Km^2}{s^2}$ thus lead to an increase of the thrust effort in order to satisfy the constraint with consequent reduction of the final mass of almost 3 Kg. Is possible to extend this reasoning to all the cases.
The value of c_3 utilized in Table 6.7 is in the dimensional form, it is obtained by multiplying the dimensionless form of the characteristic energy with the first cosmic velocity squared. In order to understand how the departure date influence the results, different t_0 has been used as initial date for the mission. In the following figures and tables will be shown the results obtained for $t_0 = 176.1,\ 176.2,\ 176.3,\ 176.4$. Also in these cases the initial value for the length of the mission is 100 days. The length will decrease of 5 days' step each time until the propelled arc will last less than the mission itself, when this condition is not true anymore the solution will be discarded.

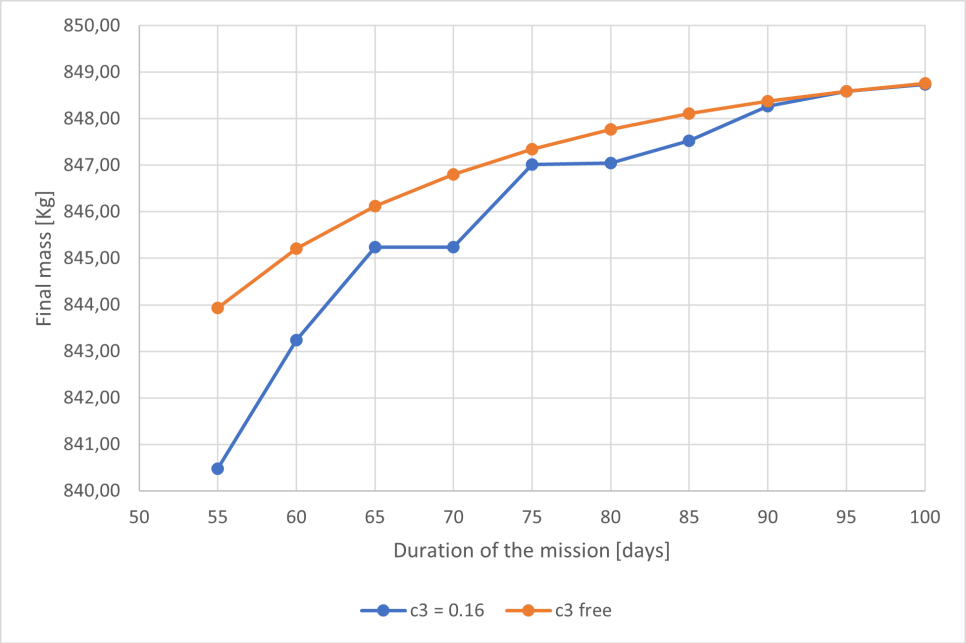

Figure 6.21: Evolution of the final mass in the case of c_3 free and $c_3 = 0.16$, $t_0 = 176.1$

Duration Escape Maneuver (days)	Final Mass $c_3 = 0.16$	Final Mass c_3 free	Delta Mass	c_3 free	Delta c_3
100	848,74	848,762	0,022	0,1654	0,0054
95	848,59	848,590	0,002	0,1618	0,0018
90	848,27	848,378	0,112	0,1726	0,0126
85	847,53	848,111	0,581	0,1861	0,0261
80	847,05	847,770	0,723	0,1837	0,0237
75	847,02	847,341	0,324	0,1711	0,0111
70	845,24	846,803	1,567	0,1616	0,0016
65	845,24	846,118	0,877	0,1669	0,0069
60	843,24	845,209	1,973	0,1948	0,0348
55	840,48	843,932	3,452	0,2346	0,0746

Table 6.8: Comparison between final masses of c_3 free case and $c_3 = 0.16$ case, $t_0 = 176.1$

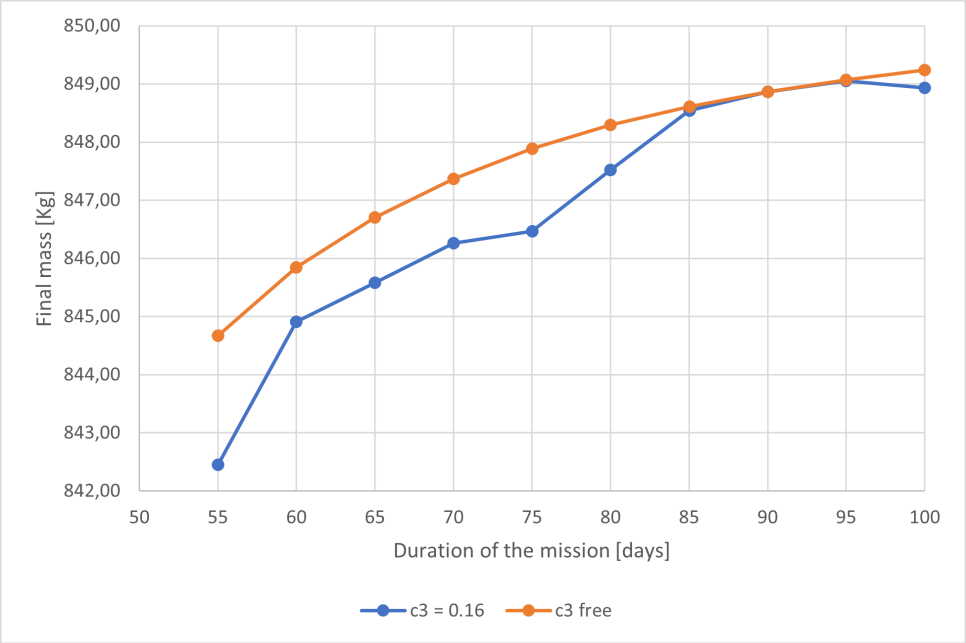

Figure 6.22: Evolution of the final mass in the case of c_3 free and $c_3 = 0.16$, $t_0 = 176.2$

Duration Escape Maneuver (days)	Final Mass $c_3 = 0.16$	Final Mass c_3 free	Delta Mass	c_3 free	Delta c_3
100	848,933	849,237	0,305	0,1801	0,0201
95	849,049	849,069	0,020	0,1647	0,0047
90	848,863	848,864	0,002	0,1589	0,0011
85	848,541	848,612	0,071	0,1677	0,0077
80	847,524	848,293	0,769	0,1831	0,0231
75	846,465	847,884	1,419	0,1850	0,0250
70	846,265	847,363	1,098	0,1751	0,0151
65	845,577	846,701	1,124	0,1677	0,0077
60	844,909	845,842	0,933	0,1754	0,0154
55	842,454	844,674	2,220	0,2095	0,0495

Table 6.9: Comparison between final masses of c_3 free case and $c_3 = 0.16$ case, $t_0 = 176.2$

Duration Escape Maneuver (days)	Final Mass $c_3 = 0.16$	Final Mass c_3 free	Delta Mass	c_3 free	Delta c_3
100	849,057	849,437	0,380	0,1804	0,0204
95	849,166	849,271	0,105	0,1697	0,0097
90	849,027	849,067	0,040	0,1547	0,0053
85	848,602	848,819	0,217	0,1482	0,0118
80	848,478	848,510	0,032	0,1563	0,0037
75	847,546	848,118	0,572	0,1747	0,0147
70	845,406	847,609	2,204	0,1829	0,0229
65	844,523	846,950	2,427	0,1791	0,0191
60	844,773	846,094	1,321	0,1772	0,0172
55	843,339	844,947	1,608	0,1925	0,0325
50	839,476	843,303	3,827	0,2424	0,0824

Table 6.10: Comparison between final masses of c_3 free case and $c_3 = 0.16$ case, $t_0 = 176.3$

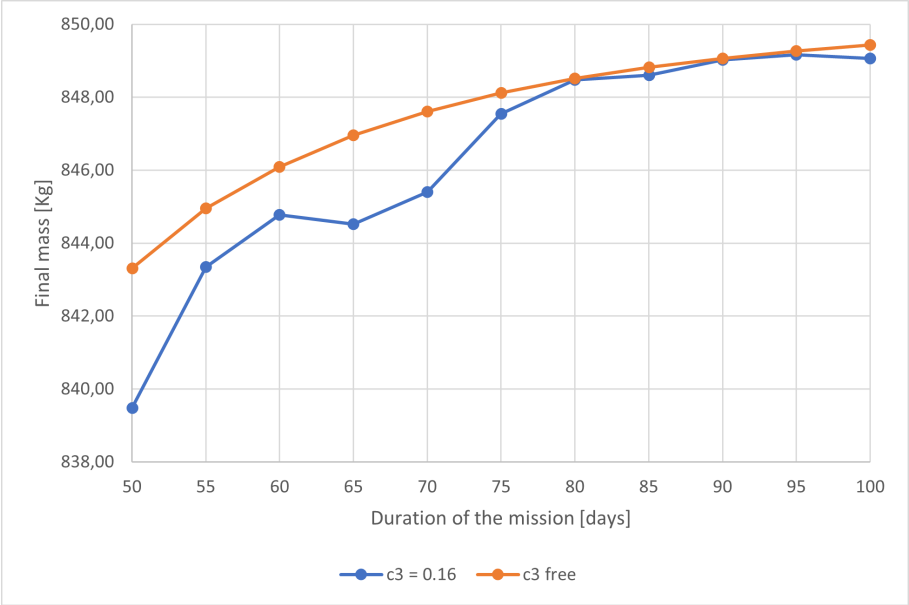

Figure 6.23: Evolution of the final mass in the case of c_3 free and $c_3 = 0.16$, $t_0 = 176.3$

Duration Escape Maneuver (days)	Final Mass $c_3 = 0.16$	Final Mass c_3 free	Delta Mass	c_3 free	Delta c_3
100	849,179	849,180	0,001	0,1609	0,0009
95	848,922	849,013	0,091	0,1703	0,0103
90	848,797	848,803	0,006	0,1624	0,0024
85	848,342	848,544	0,202	0,1480	0,0120
80	847,430	848,225	0,796	0,1410	0,0190
75	847,256	847,828	0,572	0,1487	0,0113
70	844,347	847,319	2,972	0,1701	0,0101
65	843,760	846,646	2,886	0,1862	0,0262
60	843,434	845,751	2,317	0,1911	0,0311
55	842,351	844,539	2,188	0,2001	0,0401
50	838,460	842,803	4,343	0,2351	0,0751

Table 6.11: Comparison between final masses of c_3 free case and $c_3 = 0.16$ case, $t_0 = 176.4$

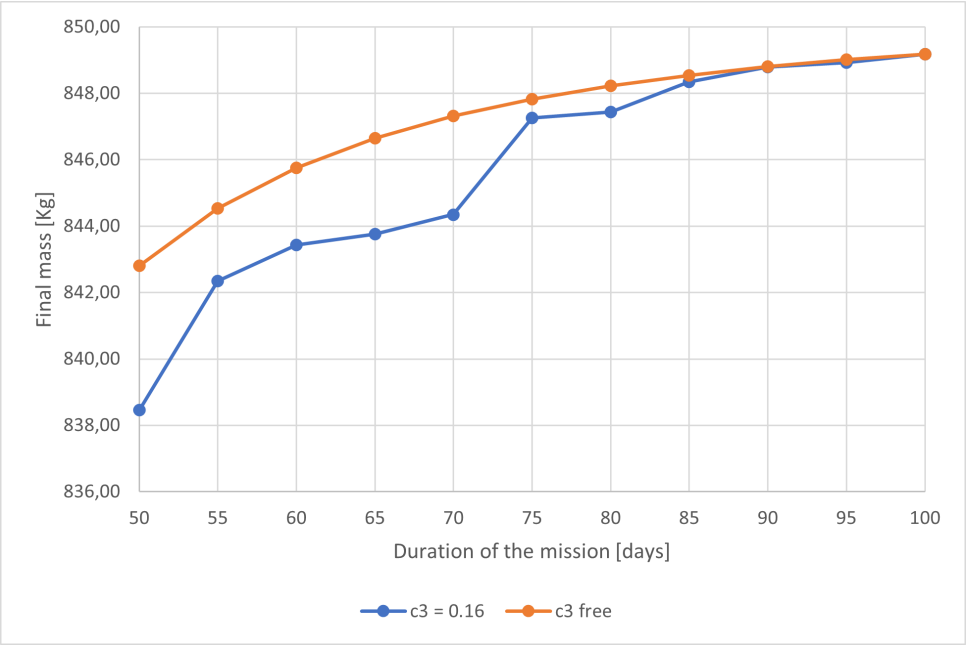

Figure 6.24: Evolution of the final mass in the case of c_3 free and $c_3 = 0.16$, $t_0 = 176.4$

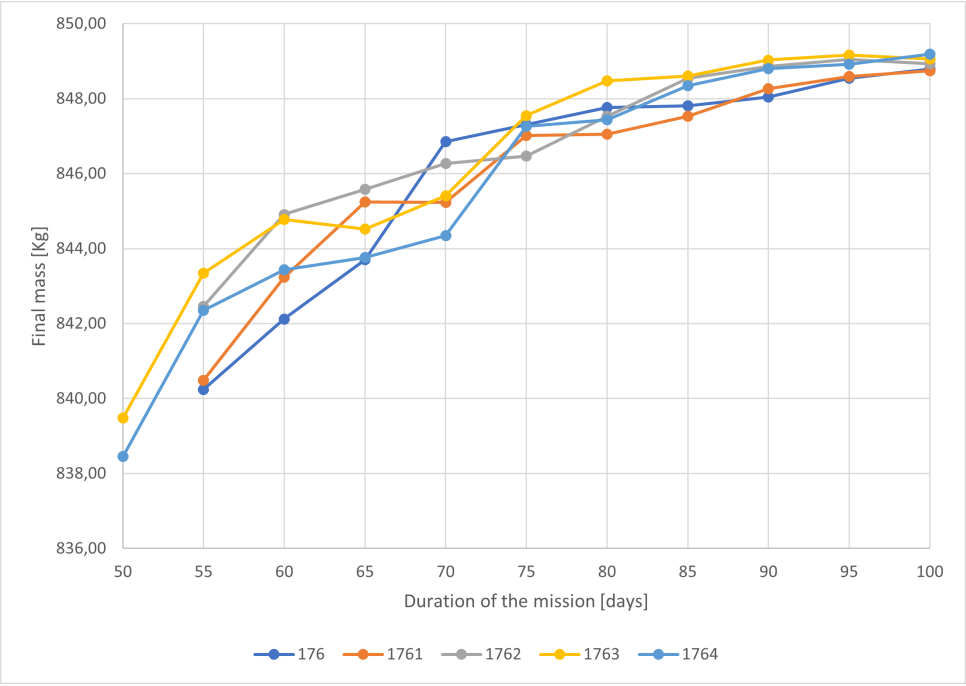

Figure 6.25: Comparison of the final mass in the case of $c_3 = 0.16$, $t_0 = 176$, $t_0 = 176.1$, $t_0 = 176.2$, $t_0 = 176.3$, $t_0 = 176.4$

Comparing the results obtained varying both t_0 and the duration of the mission is visible that for shorter mission the influence of the position of the Moon is higher while for longer mission this have not a great influence on the results. On the other hand, the influence of the Sun is always present and has a great influence in all the cases, it is necessary in fact that the spacecraft take advantage of the presence of the Sun in order to increase its velocity without spending propellant. Also in this case, where c_3 is fixed, 22/01/2028 seems to be the best departure date for almost all the length of the mission, as already found in the free case. Even if the Δc_3 to overcome in the 176.3 case is higher compared to the variation of c_3 observed for different t_0, the value of final mass is still the highest in most of the considered length of mission, as visible in Fig 6.25. From the results obtained is expected to find some correlations between the evolution of the value of the characteristic energy, the angle between the Sun and the spacecraft, and the trajectory followed by the spacecraft. It is important to remember that the goal is to understand how the trajectories change for a given value of c_3. In general, the velocity of the spacecraft is composed of both tangential and radial velocity components.
The maximum accelerating effect, that the Sun has on the spacecraft, is present when the angle ϑ, defined as $\vartheta = \vartheta_{\odot} - \vartheta_{sc}$ is:

- If the tangential component of the velocity is considered ϑ = -135 deg, 45 deg.
- If the radial component of the velocity is considered ϑ = -180 deg, +180 deg, 0 deg.

Considering the departure day most interesting since now, and so the 22/01/2028, is possible to acquire the following figures. In these four figures, three differents behavior can be identified. Fig 6.26 and Fig 6.27 consider short missions, in these cases, the velocity is almost radial for all the maneuver. As a consequence, to maximize the favorable effect of the Sun, the angle between the spacecraft and the Sun, has to be close to -180 deg and this is visible in the free, and so optimal, case. From Table 6.12 is visible how the final value of the characteristic energy in the optimal case is higher than the fixed case, it is therefore necessary that in the fixed case, the angle ϑ, is such to have a slightly unfavorable effect. In Fig 6.26 the differences between the two trends are higher due to the higher difference between the final value of c_3, in fact, the angle ϑ tends to be further from the optimal value, in Fig 6.27 the differences are lower due to the lower differences between the final value of the hyperbolic excess energy in the free and fixed cases and so the values of the angle between the spacecraft and the Sun are closer to the optimal ones.
On the other hand, considering longer missions, the velocity is almost tangential during all the trajectory and so the optimal value, to maximize the favorable effect of the Sun, of ϑ is close to -135 deg.

In Fig 6.28 and Fig 6.29 two long missions, with two different behavior, are shown. In the first figure, the final value of c_3 in the optimal case is lower than the fixed value, as a consequence, the tendency of the spacecraft in the fixed case is to increase the positive accelerating effect that the Sun has on the spacecraft moving closer to the optimal value of $\vartheta = -135 deg$ for increasing the hyperbolic excess energy. The opposite behavior is present in Fig 6.28 where the spacecraft tends to increase the angle Theta in order to place itself in a more unfavorable position and so reduce the characteristic energy.

Maneuver Length [Days]	100	85	55	50
c_3 free case	0,1804	0,1482	0,1925	0,2424
Delta c_3	0,0204	-0,0118	0,0325	0,0824

Table 6.12: Data from Table 6.10 for mission with length 100 days, 85 days, 55 days, 50 days.

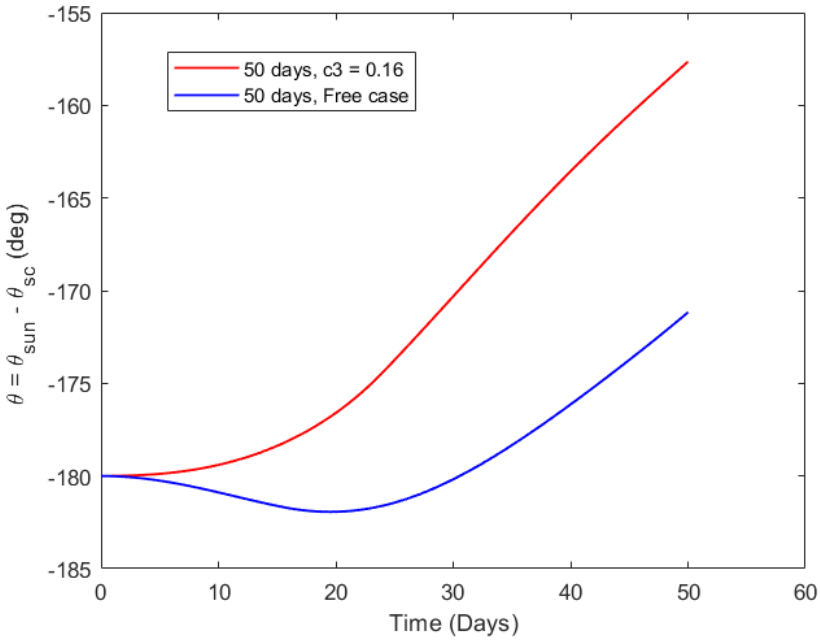

Figure 6.26: Evolution of ϑ during the evasion maneuver in the free and the fixed case; length of the mission 50 days

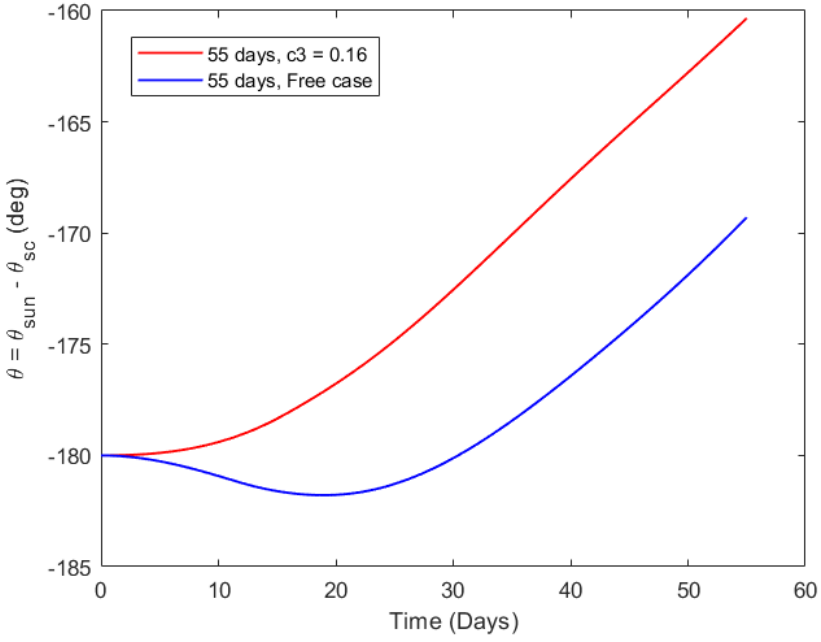

Figure 6.27: Evolution of ϑ during the evasion maneuver in the free and the fixed case; length of the mission 55 days

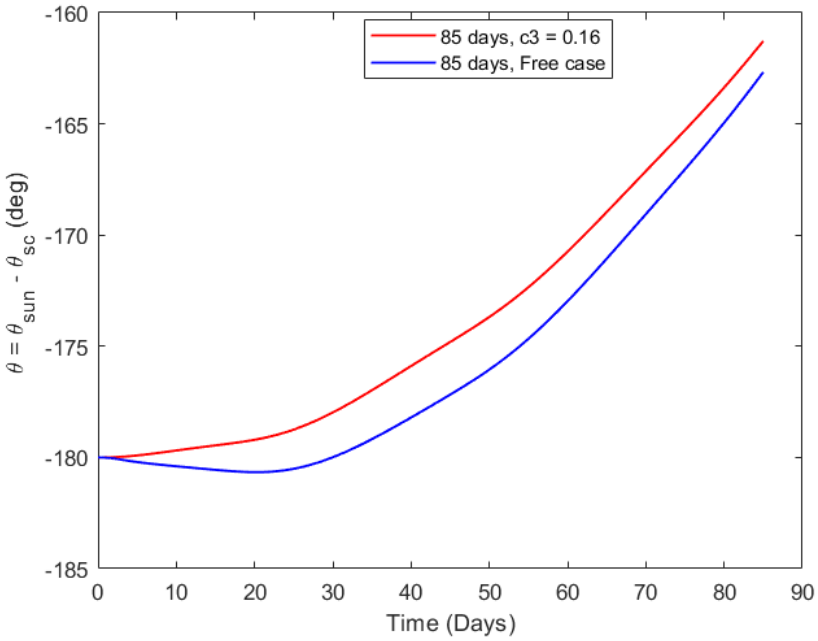

Figure 6.28: Evolution of ϑ during the evasion maneuver in the free and the fixed case; length of the mission 85 days

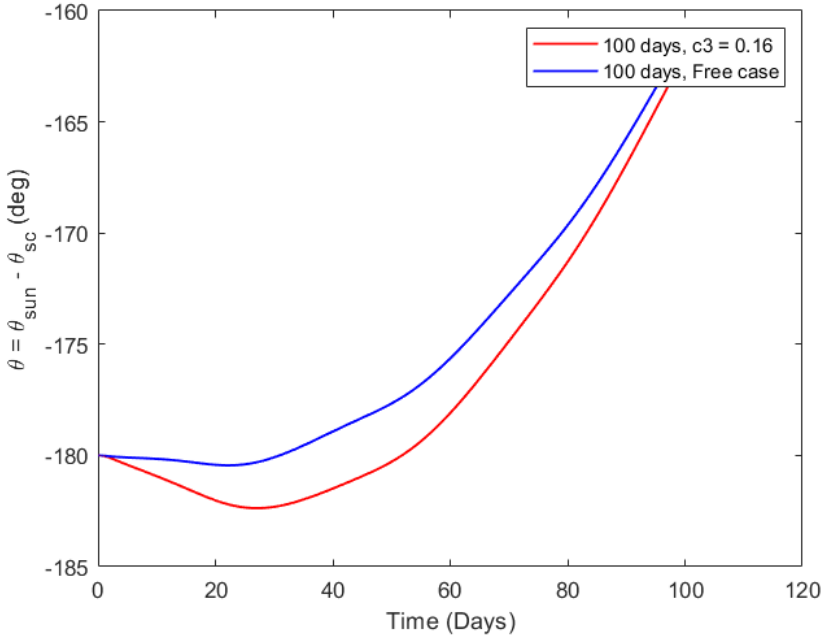

Figure 6.29: Evolution of ϑ during the evasion maneuver in the free and the fixed case; length of the mission 100 days

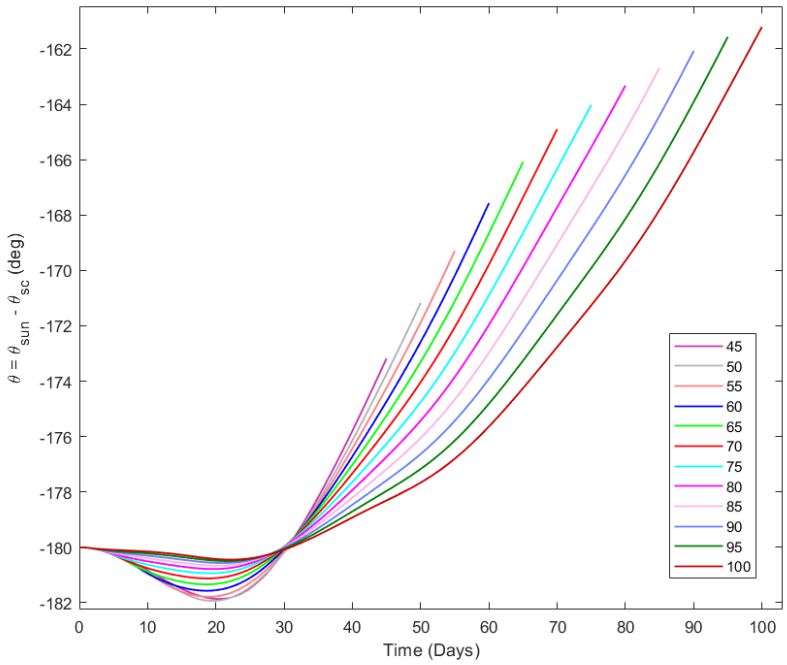

Figure 6.30: Evolution of ϑ during the evasion maneuver, departure day 22/01/2028, length from 100 days to 45 days, optimal case

Obviously, no trajectory has only a component of the velocity, they are a combination of both tangential and radial speed, as a consequence, the maximum favorable accelerating effect of the Sun will not be at -180 deg or -135 deg but it will be between this two values, in case of shorter mission the optimal value will be closer to -180 deg while for longer mission will be closer to -135 deg.
If the trend of ϑ in function of time is plotted, considering the free case and the 22/01/2028 as departure day is possible to obtain Fig 6.30. Considering the mean angle that is present between the Sun and the spacecraft is possible to see what previously anticipated. If 45 days long mission is examined, is possible to see that the mean value of ϑ is close to -180 and is coherent with the fact that the main component of the velocity present is the radial one. With the increase of the length of the mission, the radial component of the velocity decrease while the tangential component increase and consequently the mean value of Theta shifts towards higher values. Comparing the trends obtained from the free case with the ones obtained from the final value of c_3 fixed to 0.16 is possible to notice how the evolution of ϑ does not follow the same sequential scheme. In Fig 6.31 is visible how fixing the final value of the characteristic energy change the strategy adopted. The hyperbolic excess velocity of the missions from 50 days to 65 days have a value that is quite above the one desired. As a consequence, the tendency is to go away from the values where the spacecraft is accelerated more efficiently from the Sun to where the Sun is in a less favorable position. Thus the spacecraft is moved in a slower orbit. Also missions with length 70 days and 75 days have a greater value of c_3 in the final point of the free case but, in contrast with the result obtained for shorter mission, the tendency is to move the spacecraft into faster orbit in order to increase ϑ and so to have a minor accelerating effect on the tangential component of the velocity that is the main component according to the result obtained in the free case.

Looking at Fig 6.36 where the evolution of c_3 is plotted during all the maneuver, is possible to identify the two strategies. The family A's one is characterized by an initial

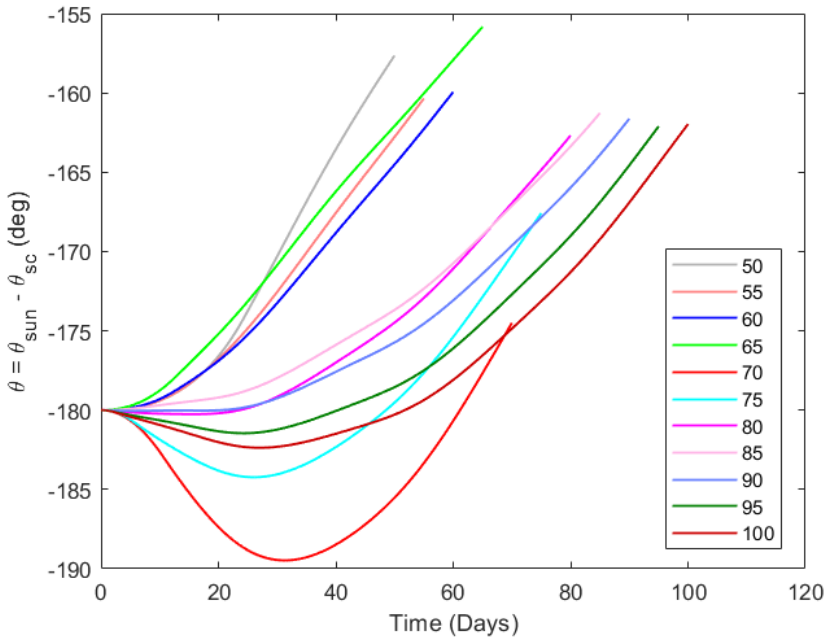

Figure 6.31: Evolution of ϑ during the evasion maneuver, departure day 22/01/2028, length from 100 days to 45 days, c_3 fixed

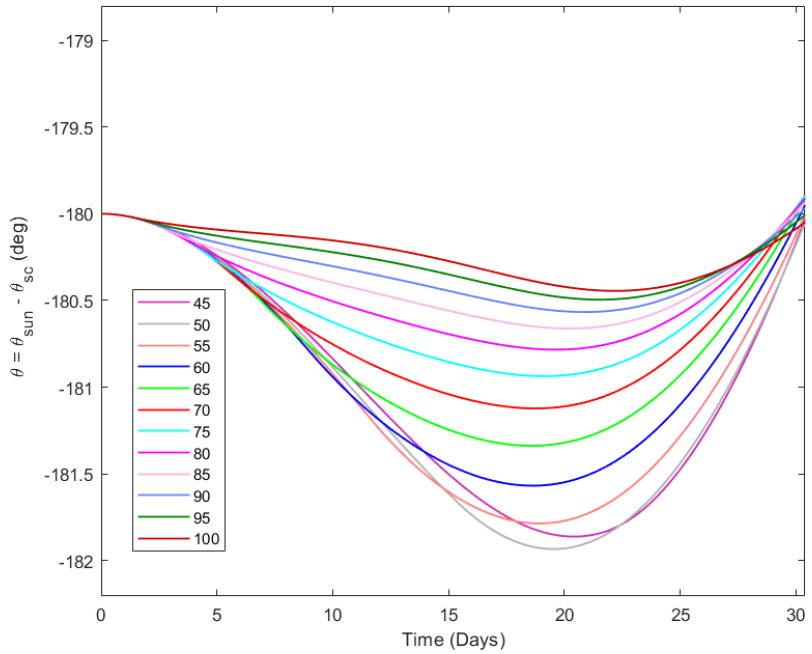

Figure 6.32: Zoom on the initial part of the evolution of ϑ during the evasion maneuver, departure day 22/01/2028, length from 100 days to 45 days, free case

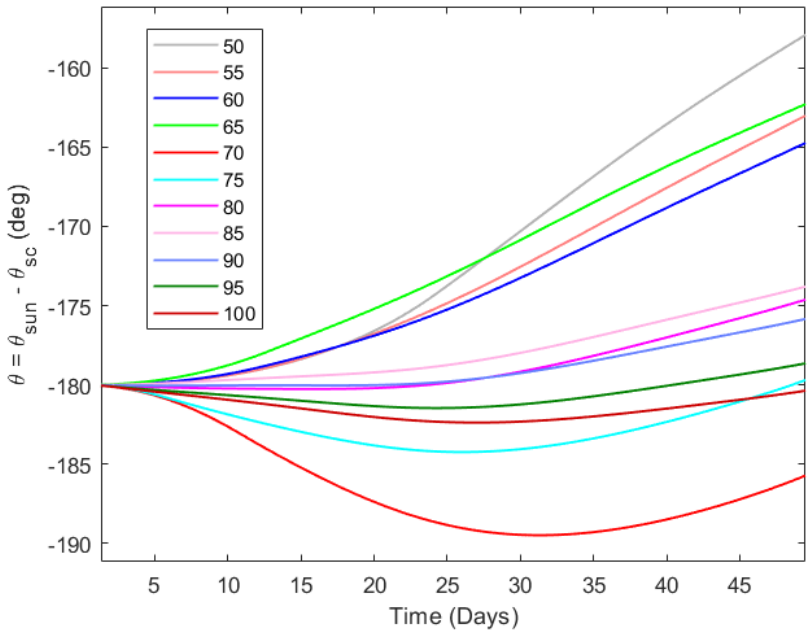

Figure 6.33: Zoom on the initial part of the evolution of ϑ during the evasion maneuver, departure day 22/01/2028, length from 100 days to 45 days, fixed case

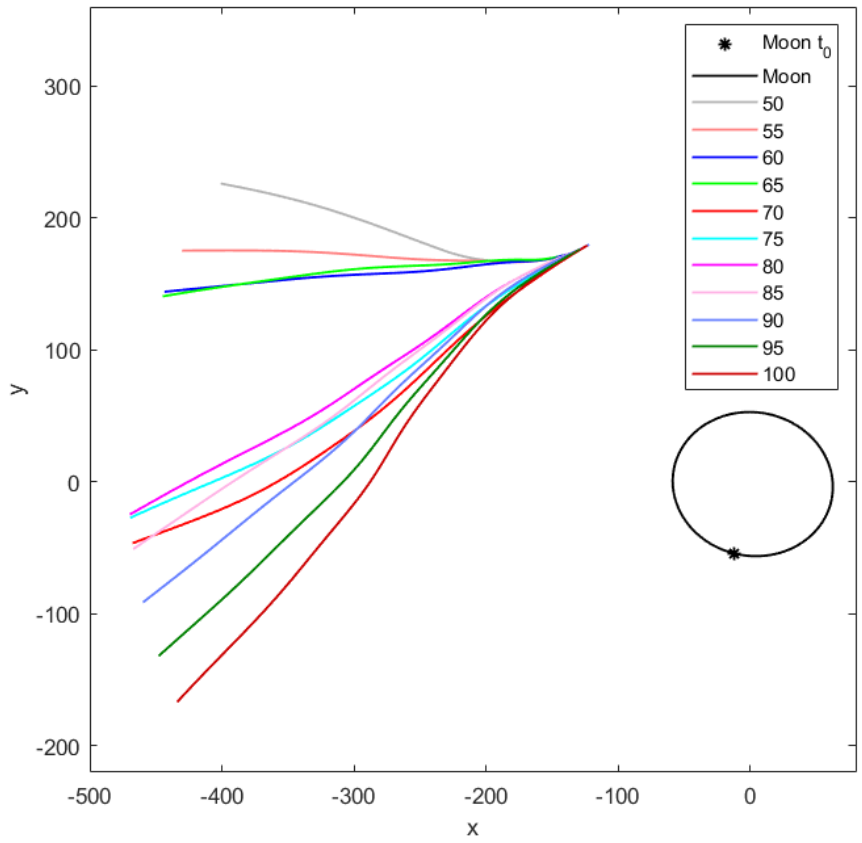

Figure 6.34: Trajectory of the evasion maneuver in the xy plane for all the length of the mission, $t_0 = 176.3$

trend that is almost flat or slightly decrescent. This underlines a 'waiting' phase where the spacecraft accelerated not in a tangential way but mostly radial, causing the slowdown of the spacecraft, and therefore, the value of the characteristic energy does not increase. On the contrary, if family B is considered, is visible how the trend is similar to the optimal case where no constraint over the hyperbolic excess velocity was utilized, the only difference is that in some cases the propelled arc last more than in the free case and, as a consequence, the spacecraft tends to be in a faster orbit, with a resultant crush towards Earth. This behavior can causes also a switch between the trajectory with respect to the free case as can be seen from Fig 6.34 where 70 days' trajectory lies closer to Earth than 75's one.
The trajectory resultant from the 65 days case can be considered as an extreme case of 'A' Family's trajectory, in fact, with mission longer than 65 days, the strategy has to be changed to achieve the goal. The same strategy of family A can not be followed from family B trajectory's for a simple reason: considered that Sun almost does 1 deg/day, after 100 days the Sun would have been in the first quadrant and, as a consequence, ϑ would be too small and thus the effect of the Sun would be too unfavorable. Considering the propellant mass utilized is possible to identify how the strategy influences the results, the results of family A seems to be more expensive in terms of mass but it is necessary to consider that in these cases the final value of c_3 in the free case is higher due to the more favorable effect of the Sun in the optimal case and thus, the effort in order to decrease the characteristic energy has to be higher.
From Fig 6.35 can be easily identified the propelled arc, which is, in fact, visible in the first part of the evolution of c_3 until a discontinuity is found. In that point the propelled arc finish and the coasting arc begin, during this phase, the spacecraft take advantage of the presence of the Sun to accelerate itself. As is visible from Figure 6.35 the propelled arc gives only a little amount of the energy needed to perform the escape maneuver (if mission longer than 50 days are considered), the greatest amount of energy is given from the Sun and is, therefore, necessary to maximize the positive effect that the influence of the Sun has on the spacecraft.

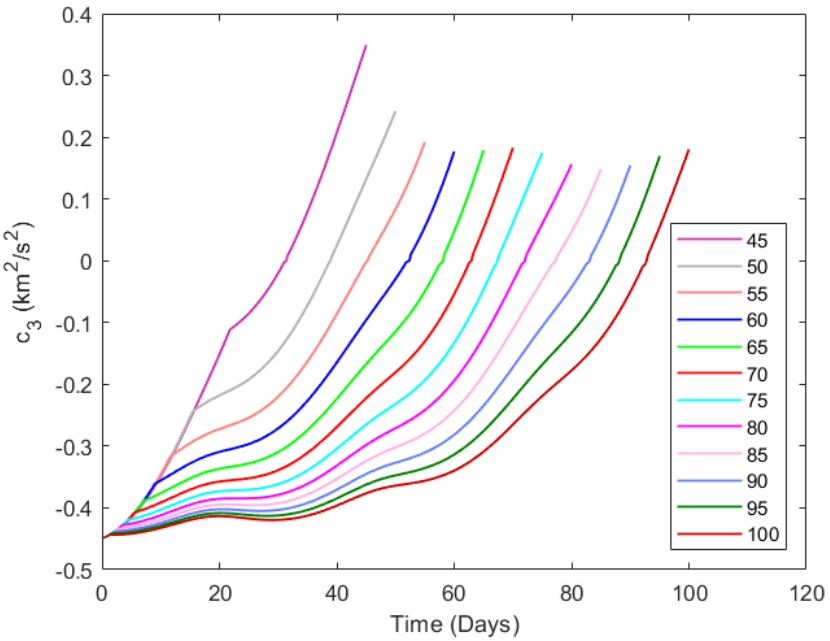

Figure 6.35: Complete trend of the c_3 during the evasion maneuver for all the length of the mission, free case, departure date 22/01/2028

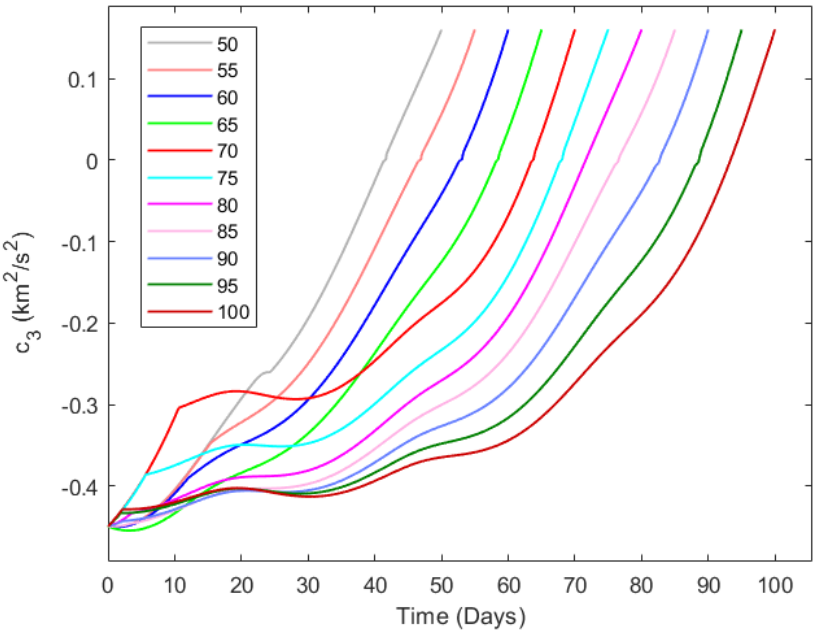

Figure 6.36: Complete trend of the c_3 during the evasion maneuver for all the length of the mission, c_3 fixed, departure date 22/01/2028

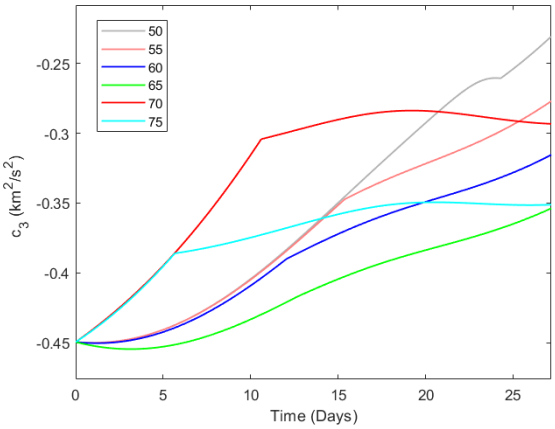

Figure 6.37: Focus on the c_3 trend, $t_0 = 176.3$, duration lower than 80 days

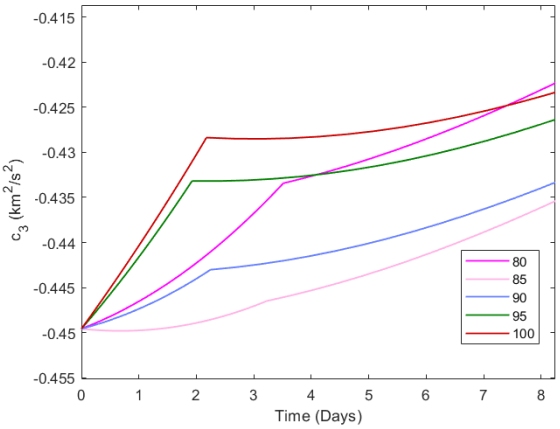

Figure 6.38: Focus on the c_3 trend, $t_0 = 176.3$, duration higher than 80 days

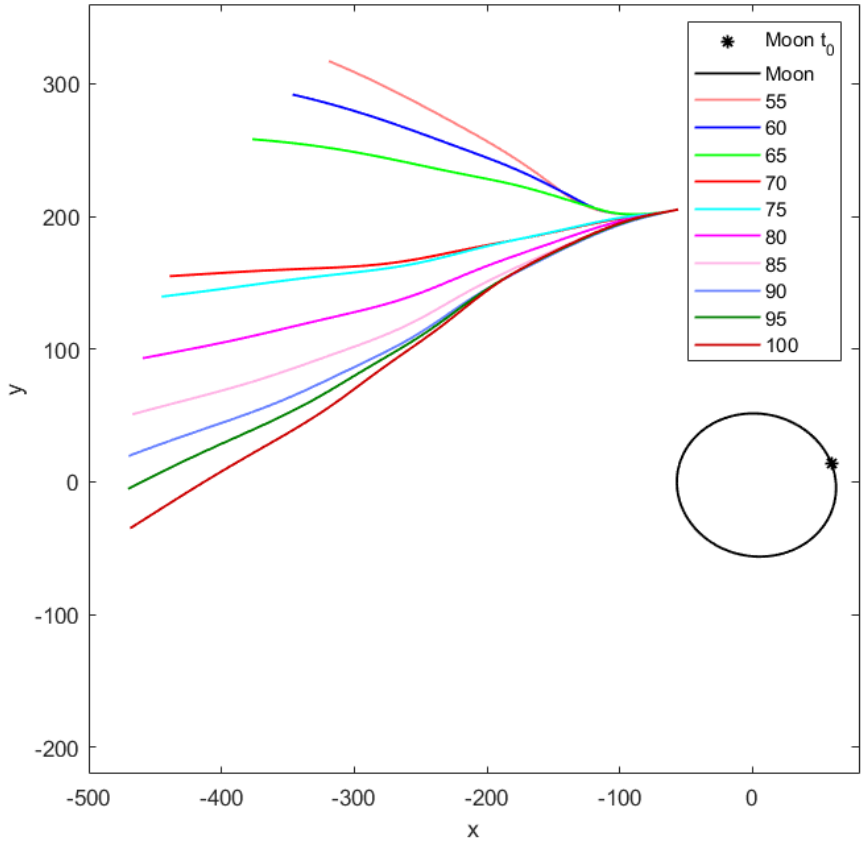

Figure 6.39: Trajectory of the evasion maneuver in the xy plane for all the length of the mission, $t_0 = 176$

In the following pages, and in the figure above, the results obtained for different departure days from 22/01/2028 will be shown. In particular, the dates chosen are:

- t_0= 176,0 ⇒ 05/01/2028
- t_0= 176,1 ⇒ 11/01/2028
- t_0= 176,2 ⇒ 16/01/2028
- t_0= 176,4 ⇒ 28/01/2028
- t_0= 176,5 ⇒ 03/02/2028

For the sake of simplicity each case will be shown in 4 different figures, the first represents the trajectory followed by the spacecraft in order to accomplish the maneuver, the second is the evolution of c_3 varying the length of the mission and, last but not least, two figures will show two focus on the first phase of the maneuver, where the propelled arc is visible, one for missions longer than 80 days the other one for missions shorter than 75 days.
All the considerations done for the mission with the departure on 22/01/2028 can be extended to the following cases. Obviously, since the behavior of the spacecraft is strictly linked to the final value of c_3 in the free case; the trajectories followed, the strategies adopted and the trend of ϑ will be different from one case to the other.
As can be visible from Fig 6.43 and Fig 6.52 the trajectory of the mission 70 days long, that in Fig 6.34 belong to Family B, in these two cases belong to Family A.

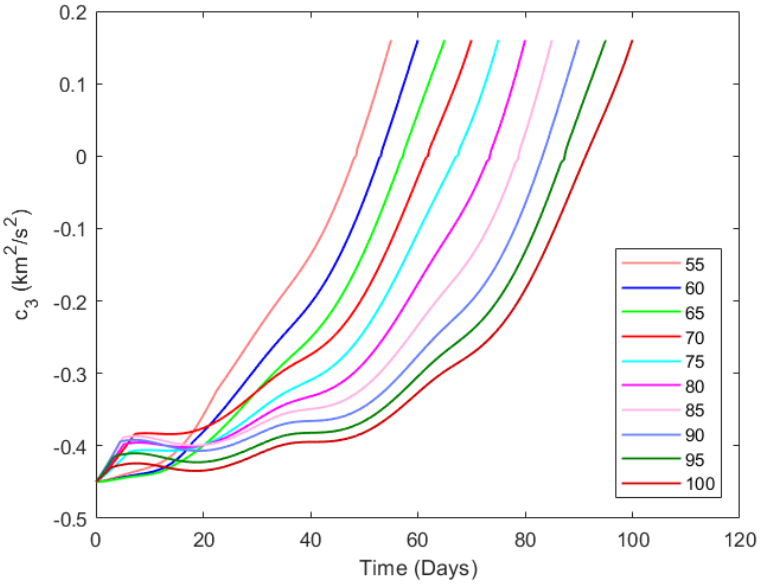

Figure 6.40: Complete trend of the c_3 during the evasion maneuver for all the length of the mission, $t_0 = 176$

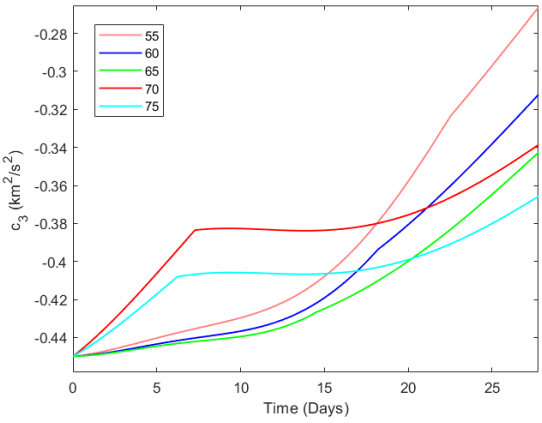

Figure 6.41: Focus on the c_3 trend, $t_0 = 176$, duration lower than 80 days

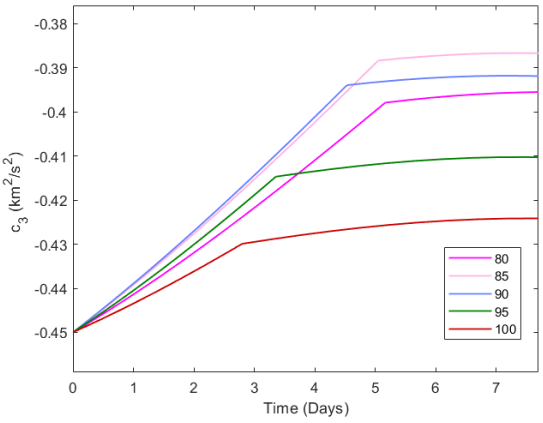

Figure 6.42: Focus on the c_3 trend, $t_0 = 176$, duration higher than 80 days

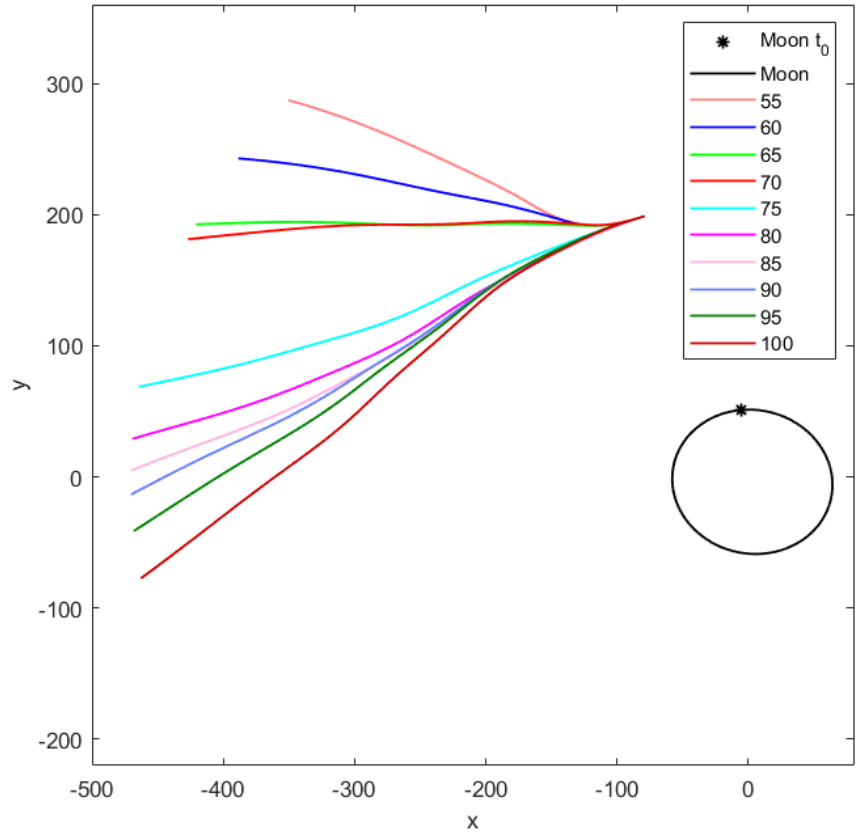

Figure 6.43: Trajectory of the evasion maneuver in the xy plane for all the length of the mission, $t_0 = 176.1$

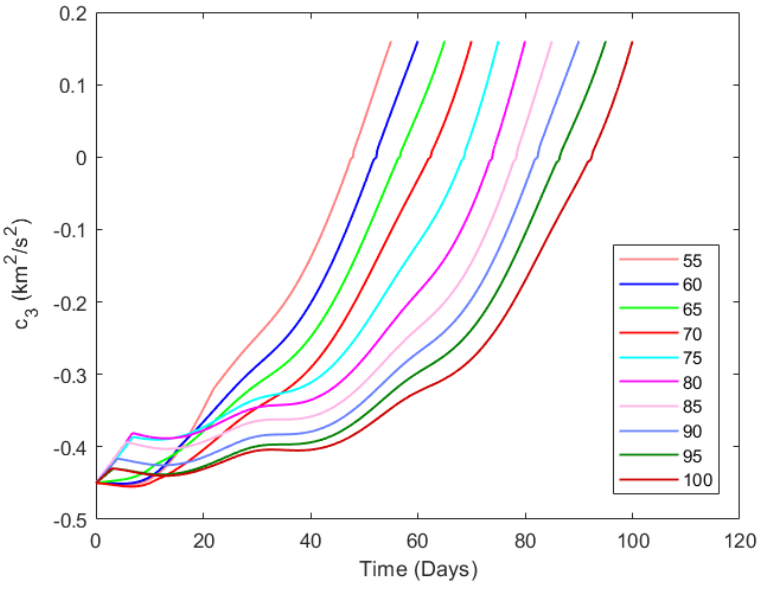

Figure 6.44: Complete trend of the c_3 during the evasion maneuver for all the length of the mission, $t_0 = 176.1$

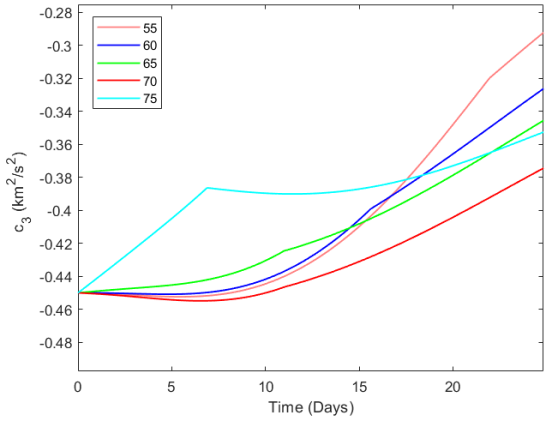

Figure 6.45: Focus on the c_3 trend, $t_0 = 176.1$, duration lower than 80 days

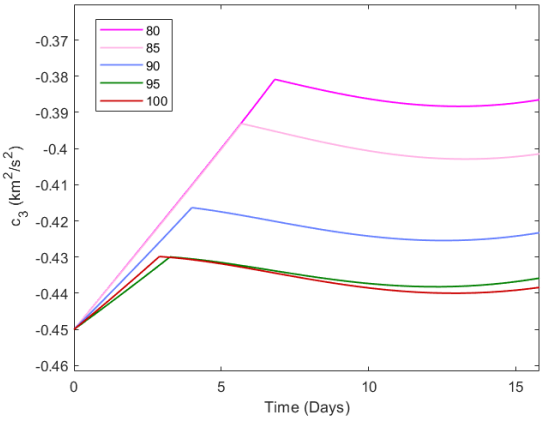

Figure 6.46: Focus on the c_3 trend, $t_0 = 176.1$, duration higher than 80 days

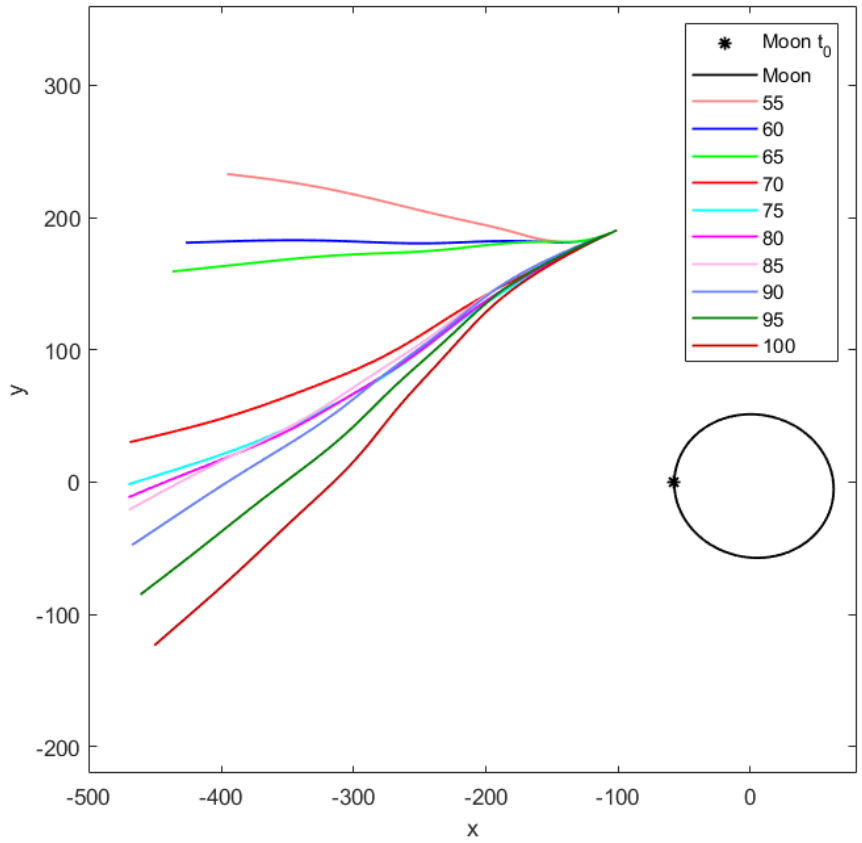

Figure 6.47: Trajectory of the evasion maneuver in the xy plane for all the length of the mission, $t_0 = 176.2$

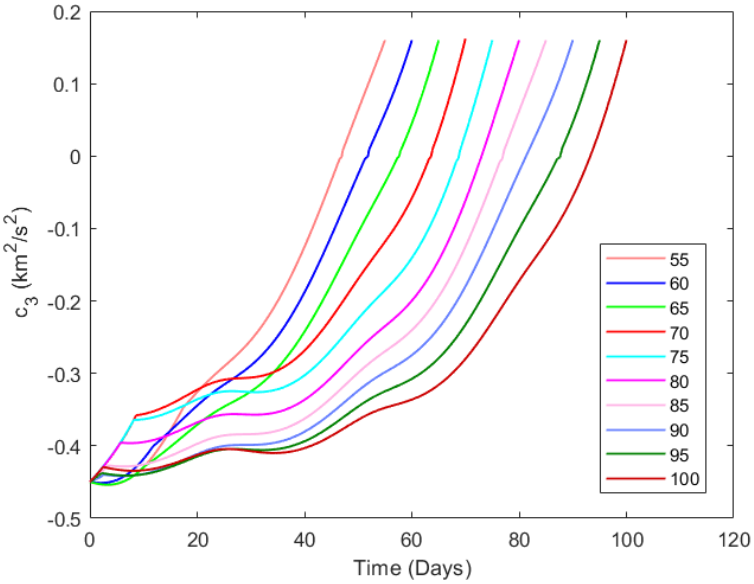

Figure 6.48: Complete trend of c_3 during the evasion maneuver for all the length of the mission, $t_0 = 176.2$

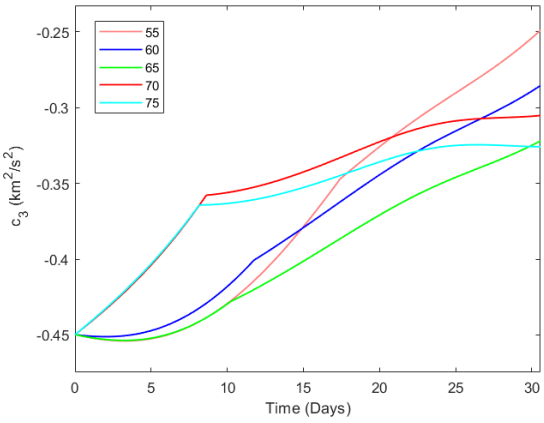

Figure 6.49: Focus on the c_3 trend, $t_0 = 176.2$, duration lower than 80 days

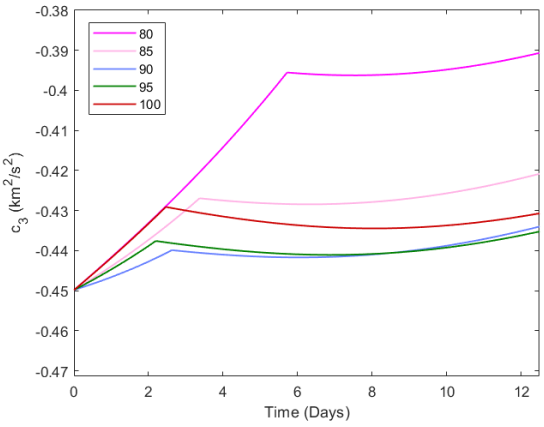

Figure 6.50: Focus on the c_3 trend, $t_0 = 176.2$, duration higher than 80 days

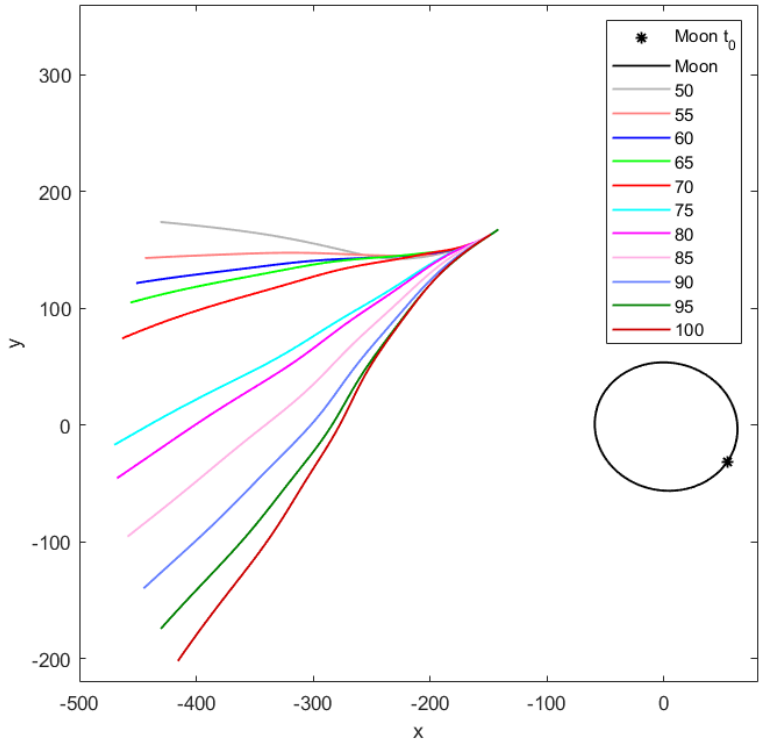

Figure 6.51: Trajectory of the evasion maneuver in the xy plane for all the length of the mission, $t_0 = 176.4$

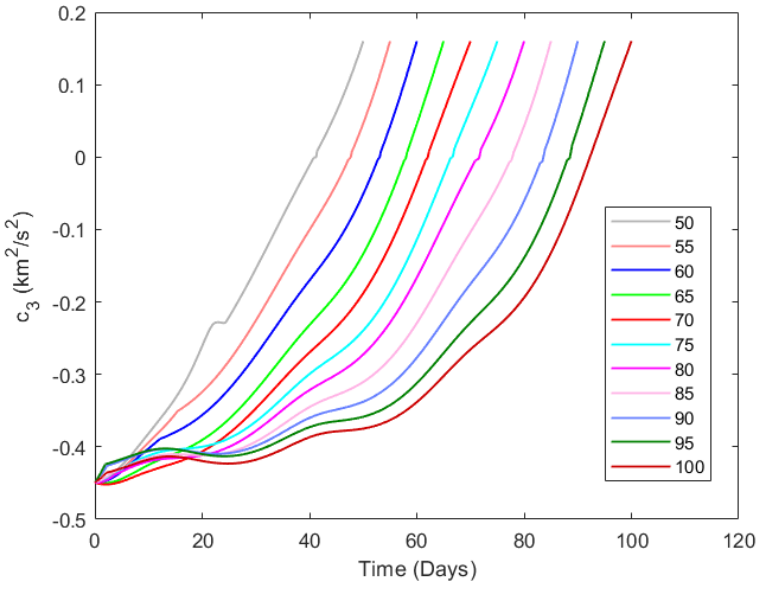

Figure 6.52: Complete trend of c_3 during the evasion maneuver for all the length of the mission, $t_0 = 176.4$

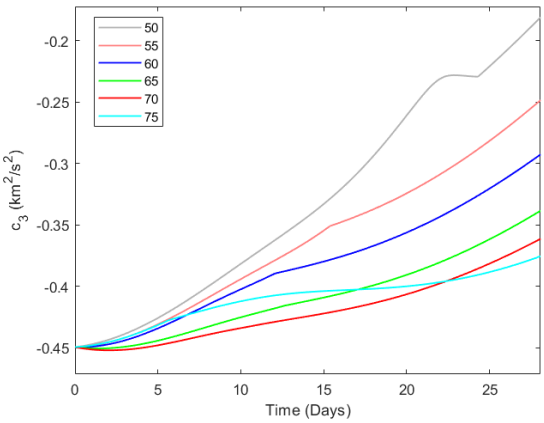

Figure 6.53: Focus on c_3 trend,
$t_0 = 176.4$, duration lower than 80 days

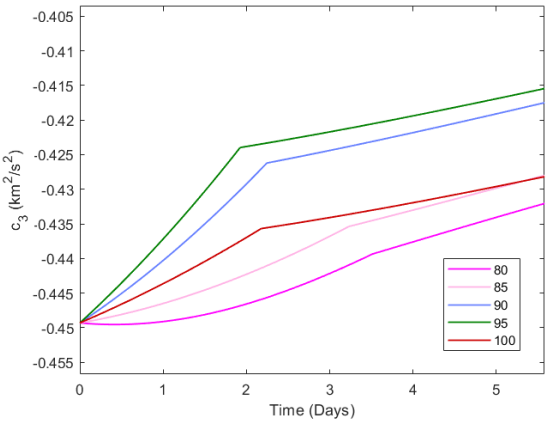

Figure 6.54: Focus on the c_3 trend,
$t_0 = 176.4$, duration higher than 80 days

Chapter 7

Conclusion

The results obtained by the utilization of an indirect method of optimization for escape maneuver from the Sun-Earth L_2 Lagrangian point have been presented and discussed in the previous chapters. In this chapter, a summary of the fundamental concepts, which are previously analyzed will be given, with a final focus on future developments of the present work.

The mission refers to a satellite left in the L_2 Lagrangian point as a piggyback of a primary larger spacecraft, as Comet Interceptor's mission. Even if this point is not characterized by a stable equilibrium, only a little amount of propellant is needed to perform the station-keeping maneuver that allows the spacecraft to maintain the orbit around this point, waiting for the most favorable target and departure time. Evasion maneuver from this point became more and more important with the increasing value that is being given to L_2, this point can be used as a starting point for an interplanetary mission, mission towards interstellar objects, or comets. The maneuver studied in here, is always divided into two different arcs, the first one is always a propelled arc and it aims to position correctly the spacecraft for the second phase. The second arc is always a coasting arc where the spacecraft takes advantage of the influence of the Sun to accelerate itself until the end Earth's sphere of influence.

The solutions obtained, using an indirect method based on the Optimal Control Theory, are precise and reliable but are very sensitive to the precision of the first guess solution, the solution, in fact, has to be varied by very little from one case to the other one to allow the convergence of the system.

The results obtained underlined how both Moon and Sun influence the evasion maneuver. Moon has a bigger effort in the first phase of the trajectory while Sun increases its influence with the decrease of the distance between the spacecraft and itself. The influence of the position of the Moon is mostly visible in missions with a duration lower than 55 days while for a longer mission the effect tends to vanish in a sinusoidal oscillation of the energy during the maneuver. A favorable position of the Moon can allow a reduction of the propellant needed, considering the same length of the mission but different departure dates. Sun's influence on the other hand has the task of speeding up the spacecraft and the maximization of this effect is visible in the results obtained for the free case.

In the second part of this thesis, the final value of c_3 has been fixed to 0.16 in order to understand how the trajectories and the strategies change with a constraint over the characteristic energy.

Obviously, the best solution for an escape maneuver is the one found in the free case, as a consequence if the escape velocity needed for a given mission is closer to the 80 days escape maneuver this will be chosen as the one to follow. For both the free case and the fixed case, the 22/01/2028 departure date seems to be the best considering the propellant mass utilized and the excess hyperbolic velocity reached at the edge of the Earth sphere

of influence even if in some cases of the c_3 fixed case the 16/01/2028 departure date seems better.
The results show the feasibility of the evasion maneuver from the second Lagrangian point of the Sun-Earth system, possible future developments and refinements of the work here discussed may include:

- Analyze deeply how the Moon influences the first phase of the evasion maneuver by considering a denser range of dates during the same month. This would be necessary to minimize the loss due to the unfavorable position of the Moon in missions shorter than 55 days,
- Analyze how the trajectory and the propellant consumption change, modifying the hyperbolic excess energy to a value closer to the one characteristic for interplanetary missions or a mission towards NEA.
- Investigate how future technologies could help to achieve the escape maneuver in lower time than the solutions found.
- Set the direction that the spacecraft need to have once it has reached the Earth's sphere of influence. The value of the hyperbolic excess velocity, in fact, is not the only important parameters to satisfy in order to perform an interplanetary mission, the direction is foundamental for the correct execution of the heliocentric phase and the capture from the target planet.

Bibliography

[1] ESA, SCIENCE and EXPLORATION, *L2, the second Lagrangian Point* https://www.esa.int/Science_Exploration/Space_Science/Herschel/L2_the_second_Lagrangian_Point

[2] Eoportal, *Satellite Missions Database* https://directory.eoportal.org/web/eoportal/satellite-missions

[3] Snodgrass, C., Jones, G.H. *The European Space Agency's Comet Interceptor lies in wait*, Nat Commun 10, 2019.

[4] ESA, *Comet Interceptor* https://www.cometinterceptor.space/

[5] SPACE, *European Comet Interceptor Could Visit an Interstellar Object*

[6] ESA, SCIENCE and EXPLORATION, *ESA's new mission to intercept a comet* http://www.esa.int/Science_Exploration/Space_Science/ESA_s_new_mission_to_intercept_a_comet

[7] ESA, SCIENCE and EXPLORATION, *Herschel overview* https://www.esa.int/Science_Exploration/Space_Science/Herschel_overview

[8] NASA, WMAP Wilkinson Microwave Anisotropy Probe, *WMAP News* https://wmap.gsfc.nasa.gov/news/facts.html

[9] ESA, ENABLING and SUPPORT, *Planck* https://www.esa.int/Enabling_Support/Operations/Planck

[10] ESA,*Gaia* https://sci.esa.int/web/gaia

[11] NASA, James Webb Space Telescope, *Engineering Webb Space Telescope* https://www.jwst.nasa.gov/

[12] ESA, *Athena* https://sci.esa.int/web/athena/-/59896-mission-summary

[13] ESA, *Plato* https://sci.esa.int/web/plato/-/42276-summaryhttps://sci.esa.int/web/euclid

[14] ESA, *Euclid* https://sci.esa.int/web/euclid

[15] Curtis H., *Orbital Mechanics for Engineering Students*, Elsevier, Oxford, 2005.

[16] Bate Roger, Donald D. Mueller, and Jerry E. White. *Fundamentals of Astrodynamics*, Dover Publications, New York, 1971.

[17] NASA, Solar system exploration, *Lagrangian points.*, `https://solarsystem.nasa.gov/resources/754/what-is-a-lagrange-point/`

[18] Jahn, R. G., *Physics of Electric Propulsion*, McGraw-Hill, New York, 1968

[19] Nasa, Glenn Research Centre, *Ion Propulsion: Farther, Faster, Cheaper.*, `https://www.nasa.gov/centers/glenn/technology/Ion_Propulsion1.html`

[20] NASA, NASA Ames Research Center, *State of the Art of Small Spacecraft Technology - In space propulsion.*, `https://www.nasa.gov/smallsat-institute/sst-soa-2020/in-space-propulsion`

[21] Casalino L., Simeoni F., Zavoli A., Colasurdo G., *Indirect Optimization of Satellite Deployment into a Highly Elliptic Orbit*, International Journal of Aerospace Engineering, Hindawi Publishing Corporation

[22] Casalino L., *Ottimizzazione Indiretta di traiettorie Spaziali*

[23] Casalino L., *Equazioni in coordinate sferiche*

[24] Casalino L., *Dispense corso di Propulsione spaziale*